ADVANCED FIBRE BRAGG GRATINGS: DESIGN AND APPLICATIONS

Elena Turitsyna

Doctor of Philosophy

ASTON UNIVERSITY

June 2007

Abstract

Advanced Fibre Bragg Gratings: Design and Applications

Elena Turitsyna

Doctor of Philosophy

June 2007

ASTON UNIVERSITY

This thesis describes the study of advanced fibre Bragg gratings (FBG); methods of synthesising, modelling and characterising them. A number of FBG-based devices for application in optical communications and signal processing are proposed and examined in the thesis.

The theoretical background of the presented research work is based on the application of the coupled-mode equations and the transfer matrix method to design and modelling of FBGs. The layer peeling algorithm was used in the grating synthesis problem. Computing simulations programs based on these method were developed, which enable to design advanced FBGs with desired spectra and to characterise the designed gratings in terms of reflectivity, group delay and dispersion. Good agreements have been achieved between spectra of designed and experimentally fabricated gratings.

The designed FBGs are considered for applications in wavelength-division multiplexing, demultiplexing and dispersion compensation in optical fibre links. The FBG-based ultra-narrow optical filters in dense WDM (wavelength division multiplexing) systems and optical filters based on FBGs operated in transmission have been proposed. A number of C++ and MATLAB codes have been developed to evaluate performance of the proposed devices in fibre transmission lines.

The performance of advanced FBGs in optical pulse manipulations has been also examined. A new type of the FBG with a V-shaped dispersion characteristic has been proposed and investigated. It has been demonstrated that V-shaped FBG used as a pre-chirping device can offer interesting opportunities for signal shaping and chirping. A new type of FBG with a "zigzag" dispersion profile and single reflection band has been designed and fabricated aiming applications in dispersion compensation in WDM telecommunication systems.

Key words: fibre Bragg grating, WDM transmission systems, optical filters.

Acknowledgements

I would like to use this opportunity to express my gratitude to my supervisor Prof. Keith Blow for his advice, valuable suggestions and his constant readiness to help.

I would like to thank Prof. Ian Bennion who offered me a great opportunity to carry out research in the Photonics Research Group at Aston University, who encouraged me to join the PhD program and was always highly supportive during these research years.

I would like to express my gratitude to Dr. Xuewen Shu, who fabricated the gratings I designed, who helped me to improve my understanding of the gratings fabrication process. Based on his ideas and discussions, we designed and fabricated novel types of multi-channel FBGs, which form an important part of this thesis.

I would like to thank my collaborators Dr. Vladimir Mezentsev and Ranjeet Bhamber for their advice and kind assistance in solving some numerical problems.

I would like to thank Mykhaylo Dubov for helping me to understand many physical phenomena during our daily morning coffee breaks.

I would like to use this chance to thank all the past and present colleagues in the Photonics Research Group for their support, useful discussions and their friendliness.

I would like to thank my family for always being supportive and encouraging, for always believing in me, convincing me that it is possible to return to research after a long break due to a growing family. Most of all I would like to thank my son Konstantin Turitsyn, who helped me to recover my programming skills and to learn the C++ programming language. Useful discussions with him helped me to implement codes used in this research. I would like to thank my husband and my children for their understanding and continued encouragement that helped me to accomplish this research.

Contents

List of Figures

List of Tables

Introduction

1.1 Background

Modern fibre optic communication is one of the exciting research and development fields. We are witnessing explosive growth of the Internet and corresponding increase in the amount of transported information data. Fibre optic communication plays an important role in providing this traffic. There are many experimental results demonstrating transmission of optical data over thousands of kilometres, at many wavelengths simultaneously, at rates over tens of gigabit per second (Gbit/s) per channel.

Optical fibre communication systems exploit high carrier frequency (about 190 THz) in the near infrared region of the electromagnetic spectrum [1]. Optical signal transmission along the fibre link is mostly affected by effects of fibre loss, chromatic dispersion, and nonlinearity. Understanding of nonlinear effects such as Raman and Brillouin scattering, self-phase modulation (SPM) (the nonlinear shift introduced by the optical field itself) is essential for the design of long-haul transmission systems. The invention of erbium-doped fibre amplifiers (EDFAs) in 1987 [2] made it possible for the light to propagate within a fibre links over thousands of kilometres using periodic amplification. After worldwide deployment of optical amplifiers the system performance is limited not by the fibre loss, but mostly by nonlinearity, noise introduced by optical amplifier and dispersion. In-line optical amplifiers cannot be installed too close to each other because of the high cost of such schemes. In most WDM systems, erbium-doped amplifiers are placed periodically every 60-80km to compensate fibre losses. To provide optical signal with enough power to travel for longer distances before the next amplification, the launch power should be high enough. The launched power level for semiconductor lasers, which are employed as optical sources in most lightwave systems, can be ~10 dBm. dBm units are typically used to express the launched power with the definition:

$$power\ (dBm) = 10\log_{10}\left(\frac{power}{1\,mW}\right) \tag{1.1}$$

High level of launched power leads to nonlinear effects that can degrade signal and impact overall system performance. There are different techniques to combat the nonlinear transmission impairments. Here, however, only a few of them that are relevant to the thesis are discussed.

In addition to dispersion management, the application of different signal modulation formats was proven to be a very attractive technique to reduce nonlinear impairments. In particular, formats based on return-to-zero (RZ) signal modulation format have shown better resistance against nonlinear impairments compared to non-return-to-zero (NRZ) and similar formats. In the NRZ format, the optical pulse occupies the entire bit slot, whereas in the RZ-based format the pulse is on for only a portion of the bit slot. The main advantage of the NRZ format is that signal bandwidth is smaller compared to RZ format. However, because the pulse occupies the entire bit slot, the NRZ format is less tolerant to carrier pulse broadening, which can be caused by a combined action of dispersive and nonlinear effects during transmission. It has been shown that the RZ format can improve the performance of high capacity lightwave systems [3]. There are different variants of RZ formats such as chirped RZ (CRZ), when the pulses in each bit are chirped before launching into fibre; RZ-DPSK (differential phase shift keying) format, when the pulse is present in all bit slots, but the information is coded in the phase difference of neighbouring bits; carrier-suppressed RZ (CS-RZ), when the carrier frequency is suppressed, e.g. by alternation of the phases of neighbouring pulses. Many new modulation formats are being proposed continuously to enhance the spectral efficiency of communication systems; to increase the bit rate of each wavelength division multiplexing (WDM) channel. Note that transmission capacity can be increased by raising the single-channel bit rate in an optical time-division multiplexing (OTDM) approach and/or by increasing a number of channels using the WDM technique.

Optical WDM systems are based on the ability of optical fibre to carry many different wavelengths of light simultaneously without mutual interference. Optical fibre WDM systems are continuously progressing, using techniques such as dispersion management, distributed Raman amplification, new modulation formats along with a number of others fibre-based technologies (like fibre Bragg gratings), which help reduce the cost of devices, making them

economically viable. In particular, fibre Bragg gratings (FBGs) are rapidly developing in mature technology with applications both in telecom, lasers and in other areas. I will discuss FBG technology in more detail, because its applications are in the core of this thesis.

Using photosensitive effect of silica fibres (which can be achieved, for xample, by adding some dopants like germanium, phosphorous or boron or by hydrogen loading [4]) it is possible to modulate the refractive index of the core along the length of the fibre, resulting in the formation of Bragg grating. This can be done by exposing the core of the fibre with a pair of interfering beams of ultraviolet (UV) light. The first in-fibre Bragg grating was discovered quite by accident by Ken Hill and his colleagues in 1978, while they were studying nonlinear effects in specially designed optical fibre, when intense visible light was launched from an argon ion laser into the core of the fibre [5]. It was determined that with the increase of the exposure the intensity of the back-reflected light from the fibre was increased significantly, with almost all of the incident radiation back-reflected out of the fibre. The fibre was exposed to 514.5 nm light, and the reflectivity of the grating was only 44%. The gratings bandwidth was very narrow (<200 MHz) with the grating length of approximately 1m. At that time it was not clear what the potential applications could be. The technology had to wait almost a decade until Bill Morey and Gerry Meltz were successful in forming a controlled, finite length grating in a fibre [6]. They applied more versatile technique using interferometric superposition of ultraviolet beams which come from the side of the fibre. Morey and Meltz transverse inscription allowed for different gratings periodicities, whilst Hill experiments produced only fixed periodicity depending on the writing wavelength. The gratings they produced were essentially filters. With broadband light incident on the grating within the fibre, the grating will reflect light with a wavelength corresponding to twice the grating period Λ multiplied by the effective refractive index of the refraction n_{eff} (so called the Bragg condition), and all the other present wavelengths pass through the grating without significant attenuation. The grating acts like a mirror for that wavelength. In other words, the grating operates as a narrow-band reflection filter (Fig.1.1).

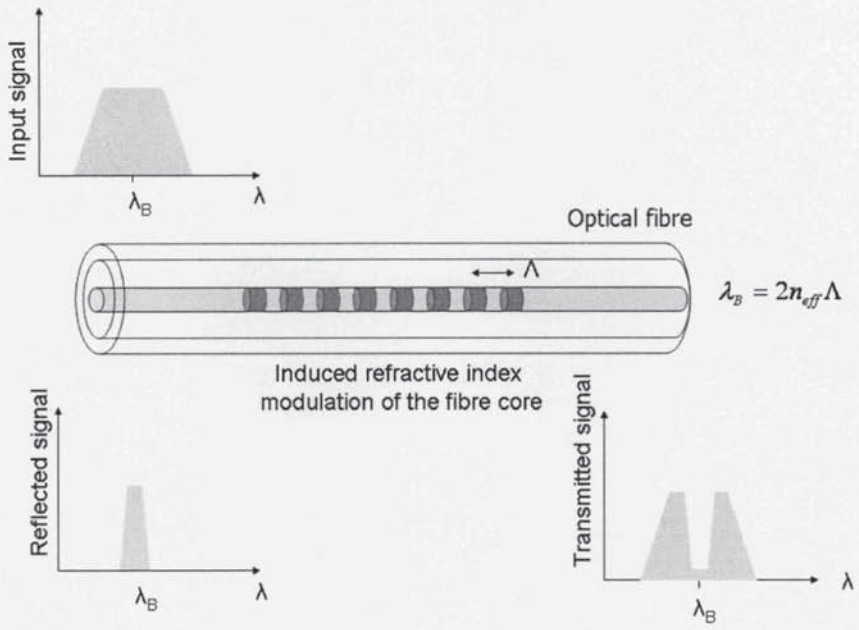

Fig.1.1 Fibre Bragg gratings operate as narrow-band reflection filters for the Bragg wavelength.

Since then, interest and activity in the field of fabrication FBGs have increased rapidly providing different fabrication techniques [7, 8] that enable the making of advanced fibre Bragg gratings for different applications [9] in telecommunications.

Continues works on using FBGs to produce WDM demultiplexers have shown great potential of this approach [10,11]. One of the proposed approaches is based on using optical circulators and gratings (see Fig.1.2).

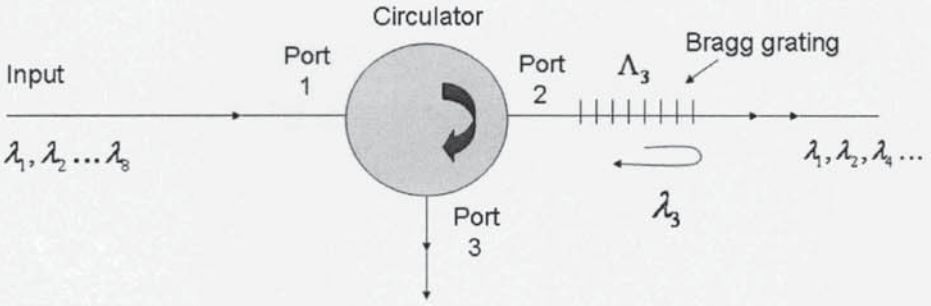

Fig.1.2 Optical circulator. Bragg grating attached to the Port 2 redirects one wavelength of the multiple-wavelength signal to the "drop" Port 3.

Typically a circulator is a three-port device, which operation principle is based on the optical Faraday effect. When the multiplexed signal is input to port 1 of circulator it flows through port 2 to a fibre Bragg grating that reflects only certain wavelengths. The signal light reflected from the FBG is returned to port 2 of circulator and output (or dropped) from port 3. Scheme in the Fig.1.2 demonstrates how the Bragg grating connected to the port 2 reflects the corresponding wavelength, which will exit through the port 3. Two or more such devices placed back to back enable both drop and add functions. Optical circulators have an insertion loss of ~1-3 dB. Several gratings with different Bragg wavelengths may be cascaded to form an add-drop multiplexer. Due to the low polarization sensitivity, stability in operation and despite their insertion loss, optical circulators are an attractive solution for amplified long-haul fibre communication systems.

The other method incorporates fibre Bragg gratings in Mach-Zender (MZ) interferometer configuration (Fig. 1.3). MZ interferometer is a basic waveguide interference device. Two identical FBGs are formed in the centre of each arm of the device.

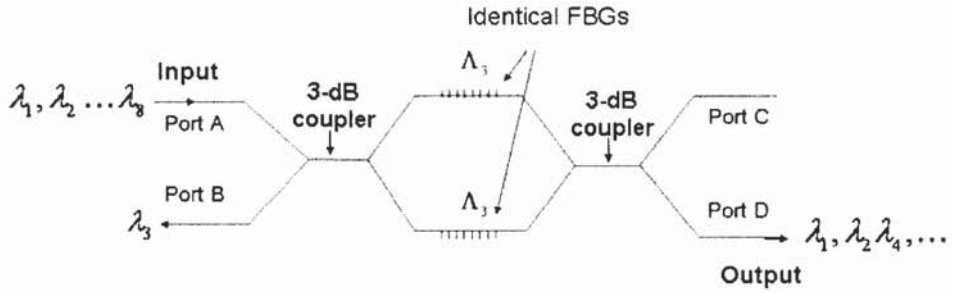

Fig.1.3 Mach-Zender interferometer configuration using FBGs

Consider for example a stream of several wavelengths $\lambda_1, \lambda_2 \ldots \lambda_8$ entering the port A. The first coupler splits the signal into two parts equally between two arms of the coupler. As there are FBGs with reflection wavelength λ_3, then λ_3 will be reflected by the two identical gratings. On reaching the coupling region with a π phase different between them all of the signal at the λ_3 wavelength will exit through port B. The remaining wavelengths leave through the port D after adjusting their phase for maximising the output. When necessary, it's

possible to add the wavelength λ_3 from port C (when using as Add / Drop device), then it will be reflected by both gratings and will exit with other wavelengths through port D. In practice, using the cascaded configuration of described devices (one for each wavelength) it is possible to form a complete WDM device. However, the MZ scheme has drawbacks in terms of its practicality. First, both arms in the MZ have to be identical to allow for the state of polarization of the reflected λ_3 wave to be the same at the input of 3 dB coupler. This means that the two FBG's have to have identical Johns matrix, which is possible but difficult to achieve due to the residual birefringence in the FBG's. Second, the phase difference between two MZ arms has to be controlled. If one finds a practical solution of the last two problems, then the whole MZ scheme may become practical, although they are less expensive than optical circulators.

Another telecommunication application in which fibre gratings can be very useful is dispersion compensation [12,13]. The effective refractive index of the fibre depends on the frequency of light launched into it. As the result, different wavelength components of the signal travel at different group velocities due to a dependence of the wave's speed on its wavelength, the phenomenon referred to as group velocity dispersion (GVD) or chromatic dispersion. This leads to signal degradation because the varying delay in arrival time between different components of a signal spreads the signal, increasing bit-error rates. When light propagates along the fibre, the group velocity is dependant on the light wavelength, which is described by the dispersion. The simplified linear transfer function $H(\omega)$ of a fibre with the length L is :

$$H(\omega) = \exp(-(\alpha + i\beta(\omega))L) \qquad (1.1)$$

where α is the attenuation constant and β(ω) is the phase constant, which is usually expressed by using Taylor series:

$$\beta(\omega) = \sum_0^\infty \frac{1}{n!}\left[\frac{d^n\beta(\omega)}{d\omega^n}\right]_{\omega=\omega_0} (\omega-\omega_0)^n \qquad (1.2)$$

Here ω_0 is the angular carrier frequency, $\omega = \frac{2\pi c}{\lambda}$ is the angular frequency, c is the speed of light in vacuum. Specific spectral component at the frequency ω, propagated through the fibre of the length L, will arrive at the end of the

fibre in a time $T = L / v_{group}$, where $v_{group} = (d\beta / d\omega)^{-1}$ is the group velocity. In the absence of second and higher order dispersions the optical pulse propagates without any change in its shape, and the delay equals $\beta_1 L$ ($\beta_1 > 0$ to satisfy causality). The impulse response to the second-order dispersion $D = \frac{d}{d\lambda}(\frac{1}{v_{group}}) = -\frac{2\pi c}{\lambda^2_0}\beta_2$ (and the corresponding pulse broadening factor) can be obtained analytically [1]. If a light pulse is propagated through a normally dispersive medium (D>0), then the higher frequency components travel slower than the lower frequency components. The response to a Gaussian input pulse in a fibre with third-order dispersion can be expressed using the Airy function [14]. The impact of higher order dispersions on the pulse broadening has been shown in [15].

As network data rates increase, chromatic dispersion in standard single mode fibre becomes the main factor limiting performance. A chirped fibre Bragg grating is an attractive way to recompress pulses back to their original states. The optical period of the chirped FBG is non constant and changes along the grating length. Since the resonant frequency $\lambda_B = 2n_{eff}\Lambda$ varies along the grating, so different frequencies are reflected with different delays at different points. In application, such gratings can be placed periodically along the fibre link to compensate for the fibre's chromatic dispersion.

The alternative solution is to put into the link a few kilometres of Dispersion Compensating Fibre (DCF) with negative (normal) dispersion to compensate for the positive (anomalous) dispersion of the standard telecom fibre. This type of fibre has a specially designed cross sectional refractive index profile and the reduced core size. The fundamental mode of the fibre is weakly confined. A large fraction of the mode propagates inside the cladding region, and the wave guiding contribution to the total dispersion is enhanced considerably, resulting in large negative values of the dispersion *D* [16]. Due to a relatively narrow core diameter, DCF's suffer from high losses (0.4-0.6 dB/km) (because of much higher Germanium concentration in the core) and from nonlinear effects, which occur because the nonlinear parameter is four times larger for DCF's than for standard fibres. The typical length of DCF required for compensating a span of standard single mode fibre is about of

one sixth of the SMF span length. In most WDM systems, fibre losses are compensated periodically using erbium doped amplifiers spaced apart by 60-80 km. DCFs compensate for dispersion, while the amplifier compensates fibre losses. The disadvantage of using DCF is high additional losses that requires additional amplifiers to compensate this additional signal attenuation, and in turn leads to increasing amplified spontaneous emission (ASE) noise. To avoid nonlinear effects, the launched power typically is kept relatively low and the system performance then is limited by ASE noise [17]. DCF solution has the advantage of full band and channel plan independent compensation, although it cannot compensate for each individual constituent wavelength, and it is limited by its power handling capability and intrinsic high loss characteristics.

With chirped FBGs, dispersion slope of each individual wavelength can be very accurately compensated at the receiver end, which enables higher data rates and more channels over longer distances, but because the fibre Bragg gratings operate as reflectors, the insertion of optical circulators causes additional losses. It is too early to conclude what will be the optimal design of future dispersion compensating modules. It could be that a combination of dispersion compensating fibre and tuneable post-compensation using FBGs will be the right solution.

Tunability features in dispersion compensation devices play an important role in developments of optical networks. There are different reasons, like environmental fluctuations and cable movements that might cause dispersion changes. As the result of the aging, fibre links can be replaced/ upgraded. Newly installed fibres may have different dispersion characteristics. It is a common practice to reconfigure the existing networks by adding / dropping of multiplexed channels, which also causes dispersion changes.

The gratings are compact, passive and commercially available at a reasonable cost. There are a few good manufacturers (like Teraxion, for example) providing commercial FBG-based devices. Their products include tunable dispersion compensators that allow making real-time wideband adjustments of chromatic dispersion, to tune over a large dispersion range, to generate positive and/or negative dispersion.

Among other products there are pump laser stabilizers [18], where the gratings can be used to stabilize the wavelength and intensity of optical amplifier pump lasers; also they can be used as fibre laser reflectors to create reliable fibre-based lasers. The idea first introduced in [19], when a tunable erbium-doped fibre with an external grating was reported by Reekie et al in 1986). Since then the number of works with different laser configuration with two or more intracavity gratings is increasing continuously [20-21].

Fibre Bragg gratings have also become popular as sensors since they are sensitive to stress, strain and temperature. Any change in the fibre properties, such as strain, temperature, or polarization which varies the modal index or grating pitch, will change the Bragg wavelength. Thus, by determining the peak reflectivity wavelength of the grating, we will get information about the sensing parameters. FBGs can be easily embedded into composite materials, or surface mounted which widens the field of applications of FBG sensors, which ranges from structural monitoring to chemical sensing [22].

The use of fibre Bragg gratings, as passive devices for optical pulse manipulation and control, has received an increasing attention as well, especially for their potential in pulse control for optical communication [9, 23-26]. With achievements in FBG writing techniques [27-29] in conjunction with powerful design methods it has become possible to model and fabricate complex grating structures with precise control of both amplitude and phase of the gratings. The synthesis problem of gratings amounts to finding the grating structure (grating amplitude and phase) from a specified, complex spectrum.

The methods such as integral (GLM) [30, 31, 33-35] or differential (layer-peeling) [32, 34], or genetic algorithm [36-38] allow to design high-reflectivity pass-band gratings with ultra-low sidelobe suppression [39], with complete control over the grating dispersion characteristics [40-43], complex spectral profiles for signal shaping [44, 45], which were not only designed, but also experimentally demonstrated.

Recently developed methods make it possible to design multi-channel FBGs [46-51], which provide wavelength filtering and dispersion management simultaneously. Recently, a sampling method was used for the design of multi-channel FBGs, when a seed grating envelope is imposed periodically in the spatial domain. Such period modulation then results in channel

multiplication in the spectrum domain. Recently the design of a multi-channel FBG based on a discrete layer peeling algorithm has been presented [55]. These powerful design methods allow the modelling of more advanced super-structured FBGs for numerous applications in the field of lightwave communications.

To summarise, fibre Bragg gratings already play and will play an even more significant role not only in the telecommunications, but also in lasers, sensing and other applications. Therefore, there is an increasing demand for improved FBG modelling and design techniques and methods. I'm convinced that this work will bring a useful and reasonable contribution to this field.

1.2 Thesis overview

This thesis is mostly devoted to the study of advanced fibre Bragg gratings, methods of synthesising and characterising them and their novel applications.

Part I describes the theoretical background of the grating theory and lightwave thechnology. The most common mathematical model that governs wave propagation in gratings is the coupled-mode theory, which is detailed in Chapter 2. It also contains the most convenient methods for solving the coupled-mode equations numerically: the numerical integration method (Runge-Kutta) and the common transfer-matrix method, which are described in addition to the transfer-matrix method (when the grating is approximated with a number N of uniform gratings) that is the counterpart to the discrete layer-peeling method for the corresponding inverse problem. Chapter 3 is devoted to the synthesis problem of gratings. It presents the direct design method, the layer-peeling algorithm. Section 3.3 demonstrates some numerical examples of the FBGs designed by using the layer-peeling algorithm. A flat-top dispersionless bandpass FBG-based filter was modelled. An impact of simplified apodisation profiles on the grating performance in transmission has been investigated. Section 3.4 presents the models of advanced chirped FBGs for a third- and fourth-order dispersion compensation. A number of C++ programs have been implemented to solve "direct" and "inverse" (synthesis) problems of the grating theory, which allowed to model desired gratings and to characterise their properties.
Part II consists of chapters 4,5,6 and 7 that are devoted to the novel applications of fibre Bragg gratings. Chapter 4 presents another approach of ultra-narrow optical filtering based on a specially designed slightly asymmetric filter, which can be fabricated using fibre Bragg gratings. The performance of this FBG-based device has been evaluated and compared with the performance of specially designed symmetrical FBG filter. A C++ programming code has been implemented as a part of GNLS (Generalised NonLinear Schrödinger) code (that belongs to the Photonics Research Group

for numerical simulations of transmission lines). This code uses the standard split-step fast Fourier transform method for solving nonlinear Schrödinger equation. This method uses small steps, applying separately linear steps (in frequency domain to treat dispersive effects) and nonlinear steps in time domain. The modules I have prepared for the GNLS code (ReadFilter.cc and ReadFilter.h) allows to read data from a file with the grating transfer function. Numerous Perl and MATLAB scripts have been implemented for running optimisation and data sorting tasks. As a result, a feasibility of 8x40Gbit/s DWDM RZ transmission with 0.8 bit/s/Hz spectral efficiency (without polarization multiplexing and FEC) over 1287km of SMF/DCF link has been confirmed by numerical modelling.

Chapter 5 is about the design of ultra-narrow optical Vestigial Side Band (VSB) filtering based on a specially designed FBGs operating in transmission. Different types of FBGs have been considered, including Gaussian, super-Gaussian and raised cosine profiles of the transmission function trying to achieve a compromise between steepness of the transfer function and the group delay response. Firstly, an 8 x 40 Gbit/s DWDM transmission system, employing VSB filtering along with square MUX/DEMUX filters of 42 GHz bandwidth and using an RZ signal with 80% spectral efficiency (channel spacing of 50 GHz) has been examined. After the optimisation of the filters detuning and input signal duty cycle, error-free transmission over 500 km SMF/DCF link has been demonstrated. An FBG-based double-notch filter has been introduced afterwards. The proposed design presents a composite VSB filter that comprised a pair of FBG's operating in transmission. The proposed filtering method has an advantage of low cost, and the flexibility of tuneability provided by FBG devices that could be especially important for large channel count DWDM systems. Using the proposed VSB filter a feasibility of 8 x 40 Gbit/s DWDM RZ transmission with 0.8 bit/s /Hz spectral efficiency (without polarisation multiplexing and FEC (forward error correction)) has been demonstrated over 500 km of the same SMF/DCF link.

Chapter 6 describes FBGs used for filtering and pulse manipulation purposes. Starting with the properties of the Gaussian pulse propagating along the fibre,

considering its broadening and chirping factor, I investigate how the propagation through different types of FBGs (with different second-order dispersion compensation) will affect the broadening and chirping of the pulses. A new type of fibre Bragg grating with a V-shaped dispersion profile, which can produce signal with the phase having different (controllable) behaviors at the center and at the pulse tails has been introduced. It has been demonstrated that the V-shaped FBGs have superior properties for optical signal manipulation and chirping compared to conventional FBGs with constant dispersion or with the dispersion slope. Application of the proposed V-shaped FBGs for a signal pre-chirping in fibre transmission has been examined. We have observed an operational regime in which V-shaped grating outperforms a conventional FBG with constant dispersion. A good agreement between designed and fabricated V-shaped FBG has been demonstrated.

Chapter 7 presents a novel design of multi-channel gratings with a "zigzag" dispersion profile (as symmetric as asymmetric) and a single (nonchannelised) reflection band. Gratings like this have an advantage over the gratings with both channelised reflection and dispersion, because although channelised reflection bands can add a filtering function, in some cases their presence also reduces the efficiency of the usage of the spectrum. The "inverse" C++ program has been modified for designing gratings with multi-channel dispersion profile.

Lastly, Part III presents overall conclusions of the thesis and suggestions for future work. A listing of publications and some of the most significant implemented programs in C++ and MATLAB are contained in the Appendix.

PART I
Fibre Bragg Grating model

The fibre Bragg grating model that is used in this thesis is described in this chapter.

2 Coupled-Mode Theory

2.1 Coupled-Mode equations

Coupled-mode theory (CMT) is used for analysis of fibre Bragg gratings: for describing the dependence of a fibre grating spectral response and the corresponding grating structure. Description and detailed analysis of CMT can be found in a number of books, articles and reviews [24-25, 56-61]. CMT is a general tool developed to model interaction between fields in periodically perturbed structures [62-63]. According to this approach the propagation of light is analysed by using the eigenmodes of the unperturbed guiding medium. Here we consider a single mode, lossless fibres only. In other words, we consider only one forward- and backward-propagating mode. Also we assume that the fibre is weakly guiding (the difference between the refractive index in the core and in the cladding is very small). Considering the field propagation along *z*-axis and that the electric field is *x*-polarised, we can write the total electric field as a superposition of the forward and backward propagation modes:

$$E_x(x,y,z) = b_1(z)\psi(z) + b_{-1}(z)\psi(z) \tag{2.1}$$

Here $b_{\pm 1}$ contain all *z*-dependence of the modes and are dependent on frequency, because they contain the harmonic propagation factor $exp(\pm i\beta z)$ with $\beta=\beta(\omega)=n_{eff}\,\omega/c= n_{eff}k$ as a scalar propagation constant. We treat the grating as a perturbation on the fibre. The unperturbed fibre has a refractive index $\bar{n}(x,y)$, and the perturbed fibre- $n(x,y,z)$. Due to the fact that both fibres are weakly guided we assume that $\bar{n} \cong n \cong n_{cl} \cong n_{eff}$, where n_{cl} is the refractive index in the cladding and n_{eff} is the refractive index of the supported

mode in the absence of the grating. The function ψ in (2.1) is responsible for transverse dependence and satisfies the scalar wave equation for the unperturbed fibre:

$$\left\{\nabla_t^2 + k^2\bar{n}^2(x,y) - \beta^2\right\}\psi = 0, \tag{2.2}$$

where $\nabla_t^2 = \partial^2/\partial x^2 + \partial^2/\partial y^2$, and $k = \omega/c$ is the vacuum wavenumber. The total electric field E_x in the perturbed fibre must satisfy the scalar wave equation:

$$\left\{\nabla_t^2 + k^2 n^2(x,y,z) + \partial^2/\partial z^2\right\}E_x = 0 \tag{2.3}$$

After substituting (2.1) into (2.3) and taking into account (2.2) we get:

$$\frac{d^2}{dz^2}(b_1 + b_{-1})\psi + [\beta^2 + k^2(n^2 - \bar{n}^2)](b_1 + b_{-1})\psi = 0 \tag{2.4}$$

After multiplication by ψ and integration over the x-y plane, we obtain:

$$\frac{d^2 b_1}{dz^2} + \frac{d^2 b_{-1}}{dz^2} + (\beta^2 + 2kn_{co}D_{11}(z))(b_1 + b_{-1}) = 0 \tag{2.5}$$

where

$$D_{11}(z) = \frac{\frac{2}{kn_{co}}\int(n^2 - \bar{n}^2)\psi^2 dA}{\int\psi^2 dA} \tag{2.6}$$

Here $n_{co} \approx n_{eff}$ is an approximate value of the refractive index in the fibre core. Equation (2.5) can be written as a set of ordinary differential equations [52]:

$$\begin{aligned}\frac{db_1}{dz} - i(\beta + D_{11})b_1 &= iD_{11}b_{-1}\\ \frac{db_{-1}}{dz} + i(\beta + D_{11})b_{-1} &= -iD_{11}b_1\end{aligned} \tag{2.7}$$

This system of equations presents the same composition of forward and backward propagating fields, as (2.1) In the absence of the grating (when $n = \bar{n}$), the solution of (2.7) is $b_{\pm 1}(z) = B_{\pm 1}\exp(\pm i\beta z)$; forward and backward propagating modes don't interact with each other. Otherwise, they couple to each other through the coefficient $D_{11}(z)$. A quasi-sinusoidal form of the index perturbation for a fibre grating can be written in the form:

$$n^2 - \bar{n}^2 = \Delta\varepsilon_{r,ac}(z)\cos\left(\frac{2\pi}{\Lambda} + \theta(z)\right) + \Delta\varepsilon_{r,dc}(z) \tag{2.8}$$

where Λ is the chosen grating period and $\theta(z)$ is the slow variation compared with the period Λ. $\Delta\varepsilon_{r,ac}(z)$ and $\Delta\varepsilon_{r,dc}(z)$ are real and slowly varying functions, which satisfy the condition: $|\Delta\varepsilon_{r,ac}(z)| << n_{co}^2, |\Delta\varepsilon_{r,dc}(z)| << n_{co}^2$. We can express $D_{11}(z)$ as a quasi-sinusoidal function:

$$D_{11}(z) = h(z)\exp(i\frac{2\pi}{\Lambda}z) + h^*(z)\exp(-i\frac{2\pi}{\Lambda}z) + \sigma(z) \tag{2.9}$$

where $h(z)$ is a complex slow varying function. $\sigma(z)$ is a real slow varying function that is related to the average refractive index change. Now we introduce the new field amplitude $u(z)$ and $v(z)$ via $b_{\pm 1}(z)$:

$$b_1(z) = u(z)\exp(+i\frac{2\pi}{\Lambda}z)\exp(+i\int_0^z \sigma(z')dz')$$

$$b_{-1}(z) = v(z)\exp(-i\frac{2\pi}{\Lambda}z)\exp(-i\int_0^z \sigma(z')dz') \tag{2.10}$$

After substituting (2.10) and (2.9) into (2.7) and after ignoring rapidly oscillating terms, we will get the coupled-mode equations:

$$\frac{du}{dz} = +i\delta u + q(z)v$$

$$\frac{dv}{dz} = -i\delta v + q^*(z)u \tag{2.11}$$

here $\delta = \beta - \frac{\pi}{\Lambda} = 2\pi n_{eff}(\frac{1}{\lambda} - \frac{1}{\lambda_B})$ is the wavelength detuning ($\lambda_B = 2n_{eff}\Lambda$ is the Bragg wavelength) and $q(z)$ is the coupling coefficient:

$$q(z) = ih(z)\exp(-2i\int_0^z \sigma(z')dz') \tag{2.12}$$

We can note the phase factors in (2.10) are independent of the propagation constant β and therefore are independent of frequency. Now we can consider u and v variables as the fields themselves for a fixed z_0. Hence, the reflection coefficient $b_{-1}(z_0)/b_1(z_0)$ can be computed by $v(z_0)/u(z_0)$. The functions u, v and q are slowly varying with z compared to the period Λ, because $\beta \approx \frac{\pi}{\Lambda}$ when the wavelength is close to the Bragg wavelength λ_B. Considering that the induced index change for a fibre Bragg grating happens in the core only (i.e. $n = \bar{n}$ in the cladding) and that it is uniform, we obtain

$$D_{11} = \frac{k}{2n_{co}}(n^2 - \bar{n}^2)\eta \tag{2.13}$$

where η is the fraction of the modal power contained in the fibre core. After substituting (2.8) into (2.13) and after comparing with (2.9) we obtain $2|h(z)| = \eta k \Delta\varepsilon_{r,ac}(z)/2n_{co}$, $\theta = \arg h$, $\sigma = \eta k \Delta\varepsilon_{r,dc}(z)/2n_{co}$. Due to the assumption of a small index change (~10^{-3}-10^{-4}) we can set $\Delta\varepsilon_r = \Delta(n_{co}^2) = 2n_{co}\Delta n$, and after using (2.12) we get the following dependence of the coupling coefficient and the grating parameters: $|q(z)| = \frac{\eta\pi\Delta n_{ac}(z)}{\lambda_B}$

$$\frac{d\arg q}{dz} = \frac{d\theta}{dz} + 2\eta k_B \Delta n_{dc}(z) \tag{2.14}$$

where k_B is the reference Bragg wave number. Since the index perturbation is small we can write (2.8) in the form:

$$n - \bar{n} = \Delta n_{ac}(z)\cos(\frac{2\pi}{\Lambda} + \theta(z)) + \Delta n_{dc}(z) \tag{2.15}$$

Here we used the approximation $n^2 - \bar{n}^2 \approx 2n_{co}(n - \bar{n})$. (2.15) leads to the effective grating period represented as:

$$\Lambda_{eff}(z) = \Lambda_B\left(1 + \frac{\Lambda_B}{2\pi}\frac{d\theta}{dz} - \eta\frac{\Delta n_{dc}(z)}{n_{eff}}\right)^{-1} \tag{2.16}$$

We can summarise that the coupling coefficient amplitude corresponds to the amplitude of the perturbations, and the phase determines the grating phase envelope.

2.2 Solutions to the coupled-mode equations

The calculation of the grating response from equation (2.11), given the refractive index perturbation, is known as the *direct* problem. It is also possible to ask what the index perturbation should be given the grating response, and this is known as the *indirect* (inverse) problem. Any solution *u(z,δ)* and *v(z, δ)* of the equation (2.11) must be obtained by applying the following boundary conditions: *u(0,δ)=1 and v(L,δ)=0* at the back *z=L* of the grating. We can consider the partial grating reflection spectrum as *r(z, δ)= v(z, δ)/ u(z,δ)*. The final complex reflection spectrum of the grating at the front *z=0* can be

represented as $r(\delta)=v(0, \delta)$, and the transmission spectrum of the grating as $t(\delta)=u(L, \delta)$. Here we will consider analytical solutions of the coupled-mode equation in the case of uniform gratings (when $q(z)$=const) and numerical solutions for nonuniform gratings.

2.2.1 Uniform FBGs

The grating is uniform if the coupling coefficient is a constant value over the grating length $0 \le z \le L$. Then the equation (2.11) can be solved analytically. By differentiating it over z and substituting the coefficients from the original equations we obtain $d^2u/dz^2 = (|q|^2 - \delta^2)u$; $d^2v/dz^2 = (|q|^2 - \delta^2)v$. By solving these equations and after applying the appropriate boundary conditions we get the reflection coefficient of the grating:

$$r(\delta) = \frac{-q^* \sinh(\gamma L)}{\gamma \cosh(\gamma L) - i\delta \sinh(\gamma L)} \tag{2.15}$$

where $\gamma^2 = |q|^2 - \delta^2$. The transmission coefficient is

$$t(\delta) = \frac{\gamma}{\gamma \cosh(\gamma L) - i\delta \sinh(\gamma L)} \tag{2.16}$$

Maximum reflectivity occurs when $\delta=0$, which is

$$R_{\max} = |r(\delta)|^2 = \tanh^2(\gamma L) \tag{2.17}$$

For example, for $\gamma L = 2$, reflectivity is $R=0.93$.

2.2.2. Numerical solutions for nonuniform FBGs

There is a variety of procedures for solving differential equations like (2.11), which include the Runge-Kutta method and a transfer matrix method. If we define $r(z,\delta) = v(z,\delta)/u(z,\delta)$, then we can substitute the equations (2.11) with the following Ricatti equation:

$$\frac{dr(z,\delta)}{dz} = -2i\delta r - q(z)r^2 + q^*(z) \tag{2.17}$$

Applying the boundary conditions $r(L,\delta) = 0$ we can solve it using the Runge-Kutta method when starting at the end of the grating and calculating backwards to z=0. The reflection coefficient of the grating is $r(\delta) = r(0,\delta)$.

This method is simple, but numerical computations can require a large number of steps to ensure the convergence of the method, and can be quite slow.

Another method of solving the equation (2.11) is the transfer matrix method (TMM) proposed by Yamada and Sakuda in [87], when the grating is approximated with a number *N* of uniform gratings. Each section is described by a transfer matrix corresponding to a uniform grating by calculating the input and output fields of this section. Then the outputs of the first matrix are used as the inputs for the second matrix and so on, until the entire structure of the grating is covered. The final matrix is obtained as a product of individual matrixes. We should be careful when choosing the number of sections of the gratings to apply the TTM in order to provide good results and to avoid long computational time. It should be taken into account, that each section of the grating must have an integer number of grating periods in order to achieve a smooth transition between sections. The number of sections also depends on the chirp of the grating. In the original work of Yamada and Sakuda the number *N* of divisions for most types of considered gratings (except for phase-shifted gratings) was chosen as small as *N=50*. Typically, the number N=500 is enough to achieve accurate results of the transfer matrix method. We can state that the transfer matrix approach is faster and more versatile than the direct integration using the numerical methods such as Runge-Kutta. Some examples of the number of layers chosen in my designs and the corresponding gratings characteristics are demonstrated and discussed in Section 3.3.2.

Suppose, the section length of each grating is $\Delta=L/N$, where L is the total grating length. After applying the appropriate boundary conditions and solving the coupled-mode equations (like described in 2.2.1) for each section, we get the following fields relations at z and $z+\Delta$:

$$\begin{bmatrix} u(z+\Delta) \\ v(z+\Delta) \end{bmatrix} = \begin{bmatrix} \cosh(\gamma\Delta) + i\frac{\delta}{\gamma}\sinh(\gamma\Delta) & \frac{q}{\gamma}\sinh(\gamma\Delta) \\ \frac{q^*}{\gamma}\sinh(\gamma\Delta) & \cosh(\gamma\Delta) - i\frac{\delta}{\gamma}\sinh(\gamma\Delta) \end{bmatrix} \begin{bmatrix} u(z) \\ v(z) \end{bmatrix} \tag{2.18}$$

Now we can represent the whole structure through the grating in the form of:

$$\begin{bmatrix} u(L,\delta) \\ v(L,\delta) \end{bmatrix} = \mathrm{M}(\delta) \begin{bmatrix} u(0,\delta) \\ v(0,\delta) \end{bmatrix} \tag{2.19}$$

where $M(\delta) = M_N \cdot M_{N-1} \cdot \ldots \cdot M_1$ is the overall transfer matrix obtained from M_j matrixes written in (2.18). The resulting M matrix is a 2x2 matrix, which satisfies the conditions $M_{22} = M_{11}^*, M_{21} = M_{12}^*$ and det *M*=1. Taking into account the boundary conditions, the reflection and the transmission coefficients can be calculated as

$$\begin{aligned} r(\delta) &= -M_{21} / M_{22}; \\ t(\delta) &= 1 / M_{22}. \end{aligned} \tag{2.20}$$

This method is stable and efficient. A relatively small number of sections can provide an accurate analysis of the whole grating structure. Numerical examples confirming the accuracy and stability of the transfer matrix method are presented in Section 3.3.2.

2.2.3 Properties of the reflection and transmission spectra and their group delays.

The most detailed analysis of the relationships between the amplitudes of the reflected and the transmitted waves and their group delays of FBGs is presented in [64]. In many applications these characteristics are very important. In this work we will widely use them in the characterisation of the gratings.

Here we assume that the grating doesn't exhibit any gain or loss and that it satisfies the standard conditions of the coupled-mode theory. We consider the solution of the coupled-mode theory $r^{\pm}(\omega)$ (reflection coefficient at the front and at the back of the grating respectively), and the transmission coefficient $t(\omega)$, which is independent of the light incident side. They are related by

$$r^{-}(\omega) = -r^{+}(\omega)^* \frac{t(\omega)}{t(\omega)^*} \tag{2.21}$$

where asterisks denote the complex conjugate. We consider reflectivity $R(\omega) = \mid r^{\pm}(\omega) \mid^2$ and transmissivity $T(\omega) = \mid t(\omega) \mid^2$, their group delays as the

phase derivative of $r^{\pm}(\omega)$ and $t(\omega)$ respectively: $D_T(\omega) = \partial\phi_t(\omega)/\partial\omega$, $D_R^{\pm}(\omega) = \partial\phi_r^{\pm}(\omega)/\partial\omega$. All these five quantities satisfy the following:

$$\begin{aligned} &R(\omega) + T(\omega) = 1 \\ &1/2\,[D_R^{+}(\omega) + D_R^{-}(\omega)] = D_T(\omega) \end{aligned} \tag{2.22}$$

For a symmetric grating $D_R^{+}(\omega) = D_R^{-}(\omega) = D_T(\omega)$ the group delays in reflection are equal to the group delay in transmission. In general, the reflectivity doesn't characterise the grating completely as there are different possible group delays with the same reflection profile. Meanwhile, the group delay in transmission is uniquely determined by $T(\omega)$ by the Hilbert transform as the following:

$$D_T(\omega) - D_0 = -\frac{1}{\pi}\int_{-\infty}^{\infty} \frac{\partial \log\sqrt{T(\omega')}}{\partial\omega'} \frac{d\omega'}{\omega' - \omega} \tag{2.23}$$

where the constant D_0 is the propagation delay in the absence of the grating (i.e., the time taken to propagate a distance equal to the grating length).

3 Synthesis of Fibre Bragg Gratings

In this chapter we consider one of the methods of synthesising fibre Bragg gratings – a discrete layer peeling algorithm. We show the numerical results of different gratings designed using this algorithm.

3.1. Introduction

The idea of reconstruction of the grating structure (phase and amplitude) from a specified (complex) spectral response attracted a great deal of attention [30-38]. The synthesis algorithms can be used not only as a powerful designing tool, but also for characterising of already fabricated gratings with complex profiles. For a long time a synthesis problem was considered as too difficult to tackle one until the layer peeling (LP) ("inverse-scattering") algorithm was applied for synthesis of fibre gratings [32, 34]. The principle of the method is to consider the whole grating structure as a number of layers consisting of uniform gratings. However, there are different types of LP algorithms: continuous (CLP) [33] and discrete (DLP) [32, 34]. Both classes use the fact, when the coupling coefficient at the front of the grating is determined by leading edge of the impulse response due to the fact, that the reflection function is a causal function, otherwise there is no physical grating that can produce the spectrum [60]. After computing the coupling coefficient of the first layer, the field propagates to the second layer. Solving this direct problem we get the first layer "peeled off". The iteration process of peeling continues until the entire grating structure is reconstructed.

CLP method uses the coupled mode equations to propagate the fields. Thus it has some advantage in terms of flexibility, but it is slower due to expensive numerical integration routines required for solving the coupled mode equations, also for the convergence of the method smaller layer steps are required, which significantly increases computation time. DLP method represents the grating as a series of discrete reflectors using the TMM to calculate the fields, which also limits the degree of approximation. However, it is significantly faster and often proves being more stable, when given a

realisable target spectrum [34]. Both CLP and DLP methods allow accurately reconstruct most of practical gratings. However, when the grating's reflectivity is very high, when light propagates too deep into the grating, the errors (that accumulate during the layer peeling process) can increase significantly and can prevent the accurate reconstruction of the grating structure.

3.2. Discrete Layer Peeling (DLP) Method

Although the DLP methods proposed by Feced *et al* [32] and Skaar *et al* [34] are both discrete layer peeling methods, Skaar's algorithm is more simple and numerically faster, when the whole grating is represented as a series of discrete reflectors, separated by free-space regions. In Feced's approach the reference plane is always at the beginning of the grating (at $z=0$), whereas In Skaars there is a so-called [28] "moving reference plane". Here I give a detailed description of the discrete layer peeling algorithm as it was provided in [28] and which I used for implementing my program.

Consider a fibre Bragg grating of the length L with a constant average effective refractive index n_0. The effective index profile along the grating can be written as $n(z) = n_0\{1 + 2h(z)\cos[2\pi z/\Lambda_0 + \phi(z)]\}$ for $0<z<L$, where Λ_0 is a nominal grating period, $h(z)$ is a slow variation of the amplitude, and $\phi(z)$ is a slow variation of the phase of the grating structure, compared with the grating period Λ_0. If we consider a light propagating through the FBG, there are two counterpropagating fields - the forward propagating field $u(z,\delta)$ and backward propagating field $v(z,\delta)$. δ is the detuning from the Bragg wavelength. Using a transfer matrix T_i, which connects the fields at the point $z+\Delta$ with the fields at z, we can write:

$$\begin{bmatrix} u(z+\Delta,\delta) \\ v(z+\Delta,\delta) \end{bmatrix} = \begin{bmatrix} \cosh(\gamma\Delta) + i\frac{\delta}{\gamma}\sinh(\gamma\Delta) & \frac{q}{\gamma}\sinh(\gamma\Delta) \\ \frac{q^*}{\gamma}\sinh(\gamma\Delta) & \cosh(\gamma\Delta) - i\frac{\delta}{\gamma}\sinh(\gamma\Delta) \end{bmatrix} \begin{bmatrix} u(z,\delta) \\ v(z,\delta) \end{bmatrix} \qquad (3.1)$$

Here $\gamma^2 = |q|^2 - \delta^2$, where $q = q(z) = k_B h(z)\exp[i\phi(z)]$ is the coupling coefficient after assuming that the grating is uniform in the interval $[z,\ z+\Delta]$. We can

represent the matrix T_i, as the product of propagation matrix T_i^{Δ} and discrete reflector matrix T_i^{ρ}.

$$T_i^{\rho} = (1-|\rho_i|^2)^{-1/2}\begin{bmatrix} 1 & -\rho_i^* \\ -\rho_i & 1 \end{bmatrix} \tag{3.2}$$

$$T_i^{\Delta} = \begin{bmatrix} \exp(i\delta\Delta) & 0 \\ 0 & \exp(-i\delta\Delta) \end{bmatrix} \tag{3.3}$$

where $\rho = -\tanh(|q|\Delta)q^*/|q|$ is the complex reflection coefficient. The matrix T_i^{ρ} can be obtained from the matrix T_i from (3.1) by letting $|q_i| \to \infty$ and holding the product $q_i\Delta_i$ constant, as if the coupling takes place in a single point. T_i^{Δ} matrix can be obtained from (3.1) by letting $|q_i| \to 0$. Then the coupling function $q(i\Delta)$ can be found from ρ_i using the relation:

$$q(i\Delta) = -\frac{1}{\Delta}\frac{\rho_i^*}{|\rho_i|}\arctan|\rho_i| \tag{3.4}$$

The idea is to consider each subgrating as discrete complex reflector, then the entire grating is represented as a series of N discrete complex reflectors ρ_j with forward- and backward-propagating fields $u_j(\delta)$ and $v_j(\delta)$ correspondingly (see Fig. 3.1).

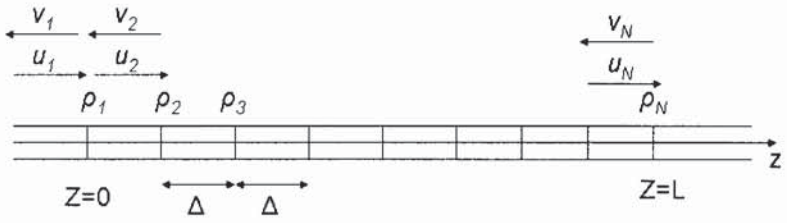

Fig.3.1 Discrete model of a FBG with N sections; u_j and v_j are forward and backward propagating waves of reflector ρ_i.

Now we want to reconstruct the reflector amplitudes ρ_j from known (or realisable) reflection spectrum $r_1(\delta)$. If we look at the reflector for time t=0, we note that the reflector is independent of other reflectors as the light doesn't have enough time to propagate to and from next reflectors. Thus we can obtain a structure for the first layer directly from the impulse response. Using the inverse Fourier transform we calculate ρ_1 from $r_1(\delta) = v_1(\delta)/u_1(\delta)$, where

$$r_1(\delta) = \sum_{\tau=0}^{\infty} h_1(\tau)\exp(i\delta\tau 2\Delta) \tag{3.5}$$

From (3.5) we can see that the sample period of the discrete impulse response is 2Δ, which is the time, required for propagation through one layer. Due to assumption that there is present only one reflector at the time $\tau=0$, we can treat ρ_1 is a 0^{th} Fourier coefficient in (3.5), we obtain

$$\rho_1 = h_1(0) = \frac{\Delta}{\pi}\int_{-\pi/2\Delta}^{\pi/2\Delta} r_1(\delta)d\delta = \frac{1}{M}\sum_{m=1}^{M} r_1(m) \tag{3.6}$$

Here M is the number of wavelengths in the spectrum, which should be greater or equal to the number of layers N, δ is in the range $|\delta| \leq \pi/2\Delta$.

Now using (3.4) we can calculate $q_1(z)$. Since we have the first layer "peeled off", we can calculate the fields at the beginning of the next layer using the TTM method.

$$r_2(\delta) = \exp(-i2\delta\Delta)\frac{r_1(\delta) - \rho_1}{1 - \rho_1^* r_1(\delta)} \tag{3.7}$$

We repeat the procedure until the whole grating structure is revealed.

This method is exact and extremely efficient for gratings reconstruction, but it is important to provide a realisable target spectrum, which will be applied as input for grating synthesis problem.

3.3. Numerical Design Example

Using C++ programming language a "direct" program to calculate the spectrum of a given fibre Bragg grating has been implemented. It is based on the transfer matrix method, described in Section 2.2.2. The "inverse" (synthesis) program has also been designed, based on the discrete layer peeling algorithm. Here I demonstrate the design of different gratings of interest in telecommunication applications, designed using the "inverse" program. This includes dispersionless band-pass filters along with second-, and higher-dispersion compensators.

3.3.1 Construction of an ideal target spectral response

Before applying the layer peeling algorithm, we have to ensure that our ideal target spectral response function $r(\delta)$ is a causal function with a causal and physically realisable impulse response $h(\tau)$. To achieve all these requirements we have to apply the windowing procedure, which is common in digital finite-impulse-response filter design. We calculate both functions as

$$h(\tau) = h^{id}(\tau - \tau_0) \cdot w(\tau - \tau_0) \tag{3.8}$$

$$r(\delta) = [r^{id}(\delta) \otimes W(\delta)] \cdot \exp(i\delta\tau_0) \tag{3.9}$$

Here $\otimes$ stands for the convolution operation and $W(\delta)$ is the Fourier transform of the window function $w(\tau)$ [26]. The detuning window δ_w is related to the layer thickness by

$$\delta_w = \pi/\Delta. \tag{3.10}$$

The apodising windowing procedure is required to reduce the undesirable oscillations in the spectrum due to the finite length of the desired impulse response that is represented in the computer [34]. Performing analysis over a range wider than bandwidths yields better numerical accuracy and stability [33].

3.3.2 Example of flat-top dispersionless bandpass filter.

Our target was a flat-top, nearly rectangular, dispersionless bandpass filter described by the super-Gaussian function:

$$r^{id}(\delta) = \sqrt{0.95}\exp(-(\delta/\delta_{PB})^8) \tag{3.11}$$

Here the maximum reflectivity is 95%, the width is determined by $\delta_{PB}=7.9cm^{-1}$, which corresponds to 50 GHz in frequency at -3 dB level, or to approximately 0.4 nm in wavelength at the centre wavelength of 1550 nm. We chose the length of the grating to be L=5 cm with the number of layers N=1000, which therefore determines the layer thickness Δ=0.005cm and the detuning window δ_w = 628 cm^{-1} according to (3.10). Using the "inverse" program, the coupling coefficient was reconstructed. Fig. 3.2 demonstrates the real part of the coupling coefficient. The imaginary part is close to zero.

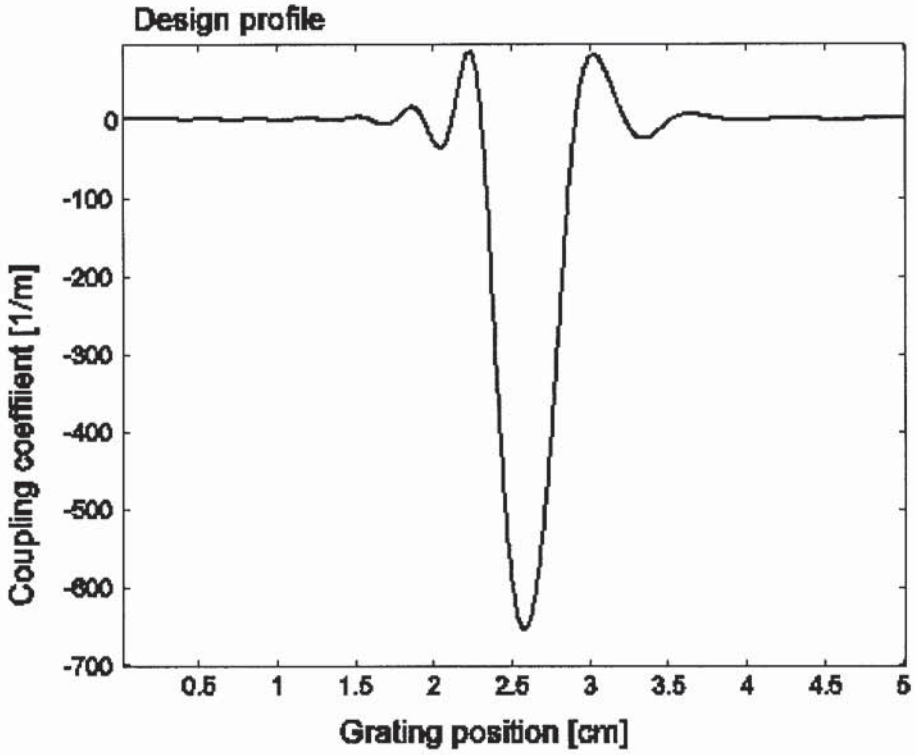

Fig.3.2 Real part of the coupling coefficient reconstructed from ideal, flat-top, dispersionless reflection spectrum using the discrete layer peeling algorithm.

For the fabrication of this kind of grating only positive index modulation is used. Alternative regions of a positive and negative refractive index, as required in this design, can be obtained by insertion of a π phase shift every time the sign of the index modulation changes [43] as shown on Fig. 3.3

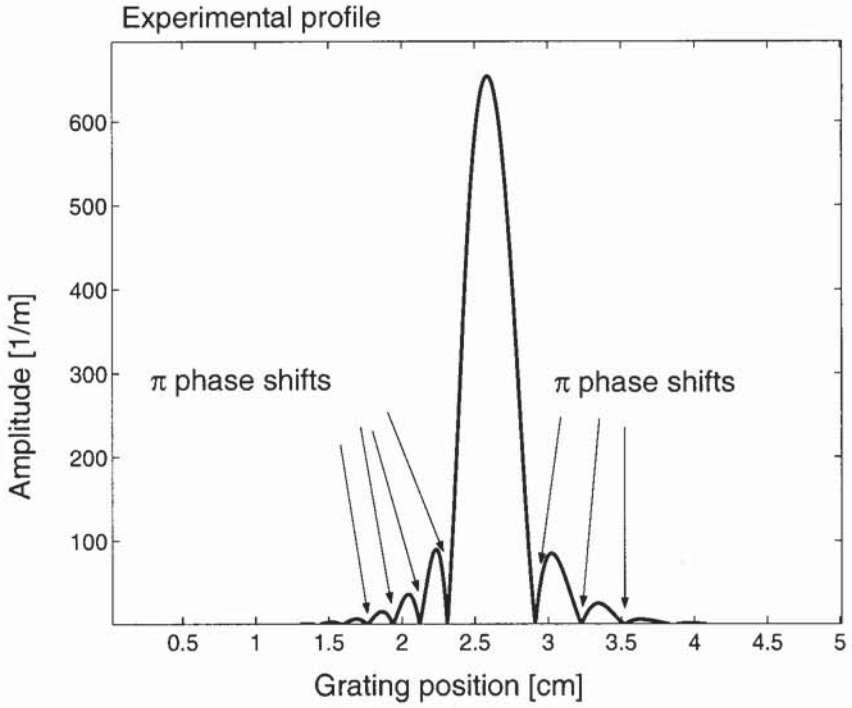

Fig.3.3 Experimental profile as imposed on the grating from Fig. 3.2.

To investigate the importance of the layer thickness for the grating reconstruction and how it determines the grating response spectrum, four gratings have been reconstructed (using the "inverse" program) with the layer thickness of 0.05 cm (N=100), 0.025 cm (N=200), 0.01 cm (N=500) and 0.005 cm (N=1000).

To verify whether we have achieved the desired spectrum, we run the "direct" program to compute the spectra response of the designed gratings. Fig.3.4. demonstrates the top-flat super-Gaussian reflection response with the bandwidth of 50 GHz and the constant in-band group delay. From the power reflectivity curves (Fig.3.4a) we can observe how the layer thickness of the reconstructed grating affects its reflection spectra. Figure 3.4b shows the group delay profiles of the gratings and we can see that with increasing number of layers increases the flatness in the group delay profiles. Figure 3.4 show that a relatively small number of sections (as small as 500) can provide and accurate analysis of the whole grating structure, which also confirms the stability and accuracy of the transfer matrix method.

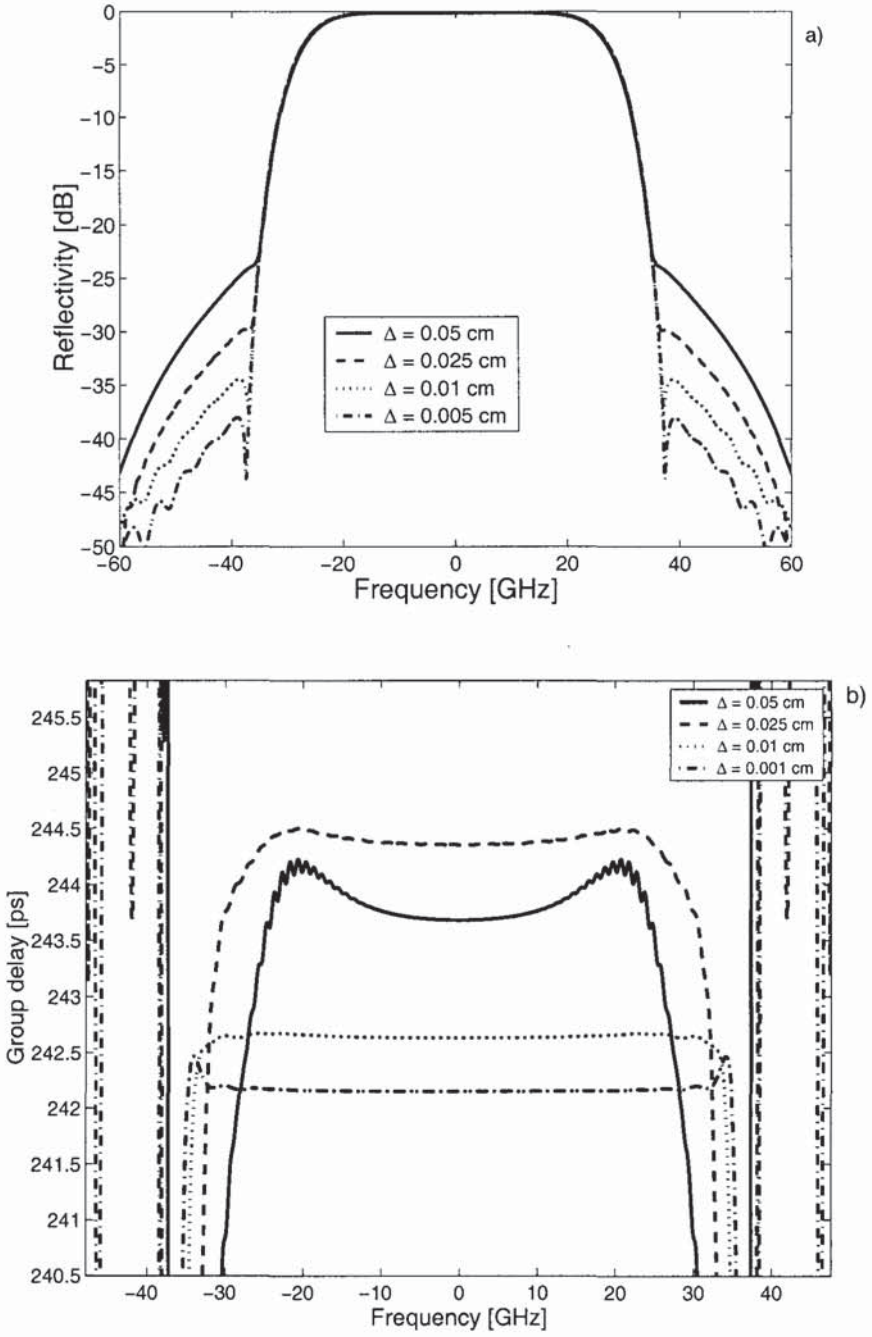

Fig.3.4 Spectrum response of the reconstructed gratings with different layer thickness and with the target as in (3.11): a) reflectivity, b) group delay.

3.3.3 Impact of simplified apodisation profiles on the grating performance

Consider the dispersionless square-filter grating with the target response function described as

$$r(\delta) = \sqrt{0.9995 \exp(-(\delta / \delta_{PB})^{10})} \tag{3.12}$$

where δ_{PB} = *6.07 cm*$^{-1}$. The filter bandwidth of this grating is 33GHz at -1 dB level and 46 GHz at -30 dB level, which corresponds to a bandwidth utilisation ($BW_{-1\,dB} / BW_{-30\,dB}$) of ~72%.

We decided to verify whether it is possible to simplify the apodisation profile of the grating in order to minimize the number of π phase shifts, and how it will affect the grating performance.

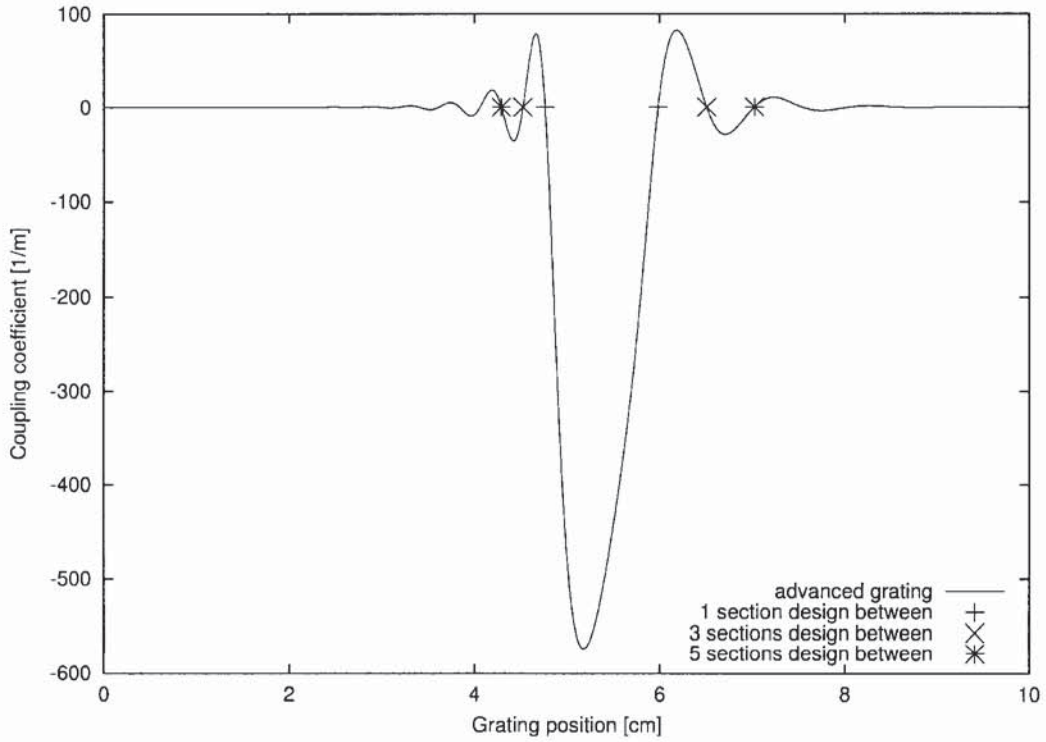

Fig. 3.5 Apodisation profiles for the different degrees of approximation.

Aside from the ideal device structure, three proposed simplified apodisation profiles have been studied (Fig. 3.5); each of them including an increasing number of phase shifts and therefore containing information closer to the

original, with the "squareness" of the filter (in terms of bandwidth utilisation BU) increasing with the number of sections covered.

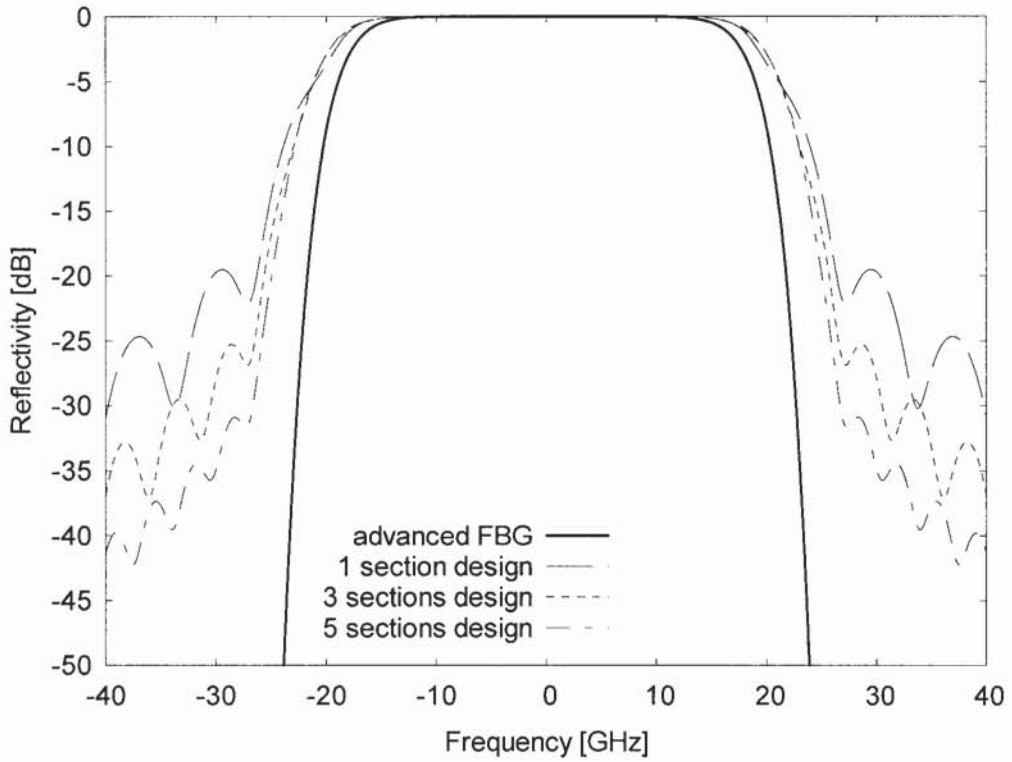

Fig. 3.6. Reflection profiles of the gratings described in Fig. 3.5.

Figure 3.6 demonstrates the reflection profiles of the described gratings. We can calculate a half BU factor (bandwidth at -1dB level over the bandwidth at -15 dB level), because it's impossible to calculate the standard BU factor for the one- and three-sections gratings due to the presence of ripples of the reflection function at -30 dB level. Half BU factor for the advanced grating is 76% (32 GHz @-1 dB and 42 GHz @ -15 dB), for 1-section design - 70% (35 GHz @ -1 dB and 50 GHz @ -15 dB), for 3 section design – 71.5% (35 GHz @ -1 dB and 49 GHz @ -15 dB), and for the 5 sections grating the half BU factor is ~ 75% (36 GHz @ -1 dB level and 48 GHz @ -15 dB level).

Note that a fabrication of one-section design grating requires no phase shifts at all. There were one-, three- and five-sections designs' gratings fabricated. The comparison between designed and fabricated 5-section design grating is demonstrated in the Fig. 3.7, which shows a good agreement between the model and experiment. [67] The advanced grating wasn't fabricated that time

due to different technical problems that appeared in "Indigo Photonics", where the gratings were fabricated.

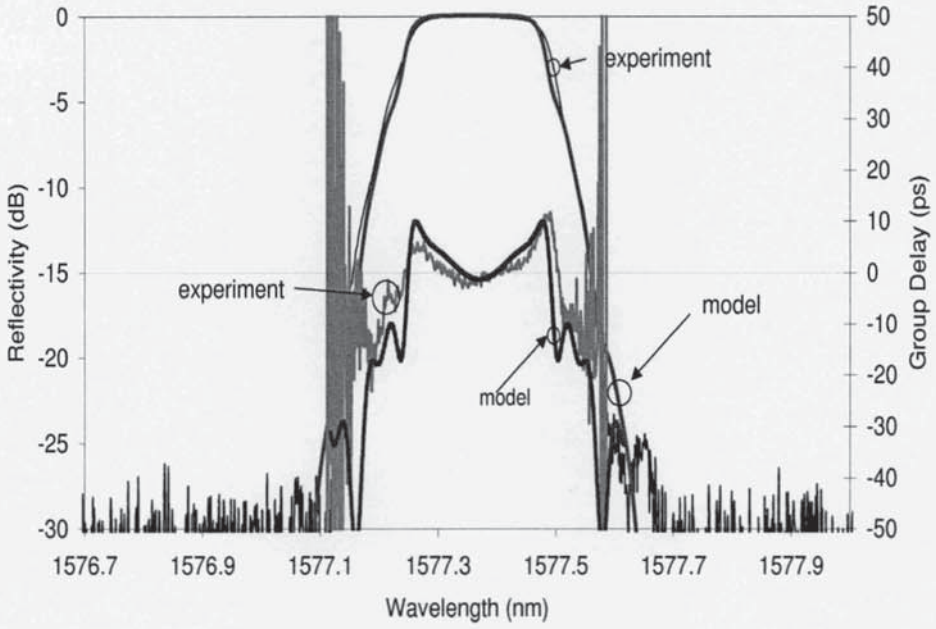

Fig.3.7 Comparison of spectra of the designed and fabricated gratings

At first glance the transition between the simplest one-section design and an ideal advanced FBG should be monotonically reflected in the performance of such gratings. As we show below this transition is actually not monotonic in terms of performance, and the one-section design FBG can offer smaller penalties (compared with 3-5 section design gratings) in some applications. In order to study the performance of the different designs, first the gratings were inserted as inline filters at the end of a symmetric periodic span composed of 100 km of single mode fibre (SMF with dispersion 17ps/(km-nm), dispersion slope 0.07 ps/(km-nm$^{2)}$ and the fibre loss 0.2dB/km in the wavelength region near 1.55 μm) and 17 km of dispersion compensating fibre (DCF with dispersion -100ps/(km-nm), dispersion slope -0.41 ps/(km-nm$^{2)}$) and the fibre loss 0.65 dB/km in the wavelength region near 1.55 μm) specially designed to compensate for both dispersion and dispersion slope from the transmission through SMF. Amplification with erbium doped amplifiers (EDFA) with a noise figure of 4.5dB was included in the middle and at the end of the symmetric map (50 km SMF + 8.5 km DCF + EDFA (gain 25.5 dB)+ 8.5 km DCF + 50 km

SMF + EDFA (gain 25.5 dB) + FBG) meant to compensate the loss in the span. I have chosen of a symmetrical map for diminishing pulse distortions due to Kerr nonlinearity. As it was shown in [71], a symmetrical ordering of the compensation sections could be beneficial in comparison with conventional maps, when the total number of pre-compensation and post-compensation sections is equal. The selected bit rate of RZ signal was 10 Gbit/s with the duty cycle of 50% and the pattern length of 2^9 -1. A system performance was analysed in terms of Q-factor (Q-factor >6 for BER< 10^{-9}) averaging after 6 runs to reduce the pattering effects. The obtained Q-value vs. distance for each of the gratings is depicted in Fig. 3.8. For numerical simulations the "VPI Transmission maker" software have been used.

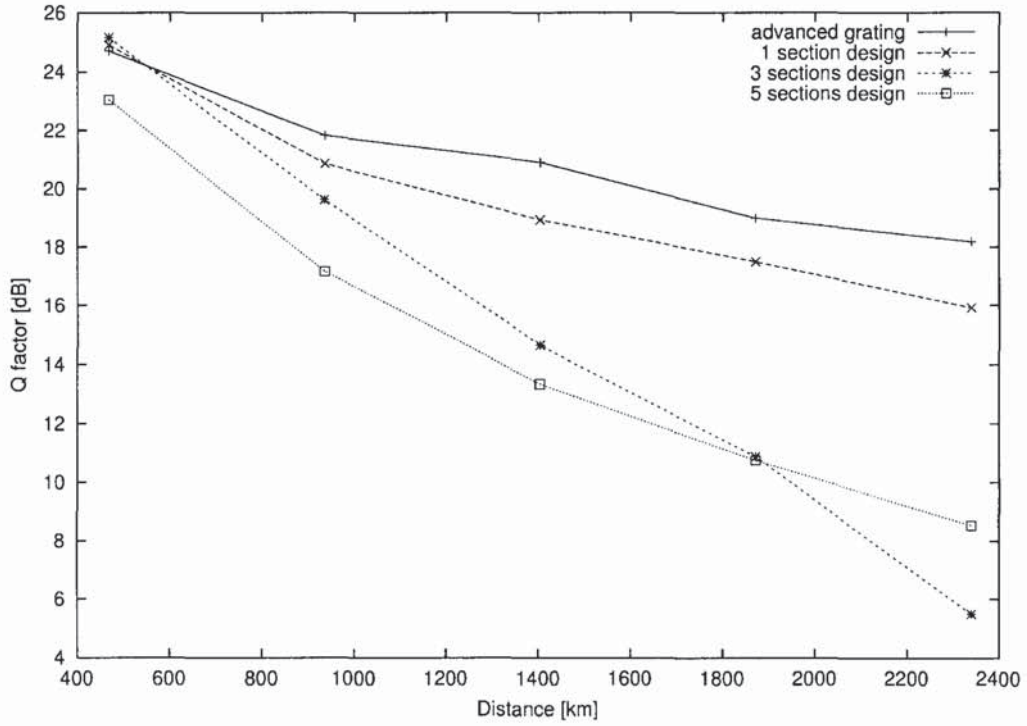

Fig.3.8 Q-value vs distance for each of the gratings in the dispersion-managed single-channel system.

One can observe that for very short distances, the simplest one-section approximation and the 3-sections one offer even a slightly better result than the original "ideal" grating. This is due to our particular single-channel testing conditions, in which a broader filter bandwidth (see Fig. 3.6) can be initially beneficial. However, after a few loops the ideal grating presents the best performance. What is more surprising, at first glance, is the fact that the

gratings obtained with the improved approximation with 3 and 5-sections perform worse than the simplest one. This behaviour, however, can be explained by the analysis of the dispersion profiles of each of the gratings, depicted in Fig. 3.9.

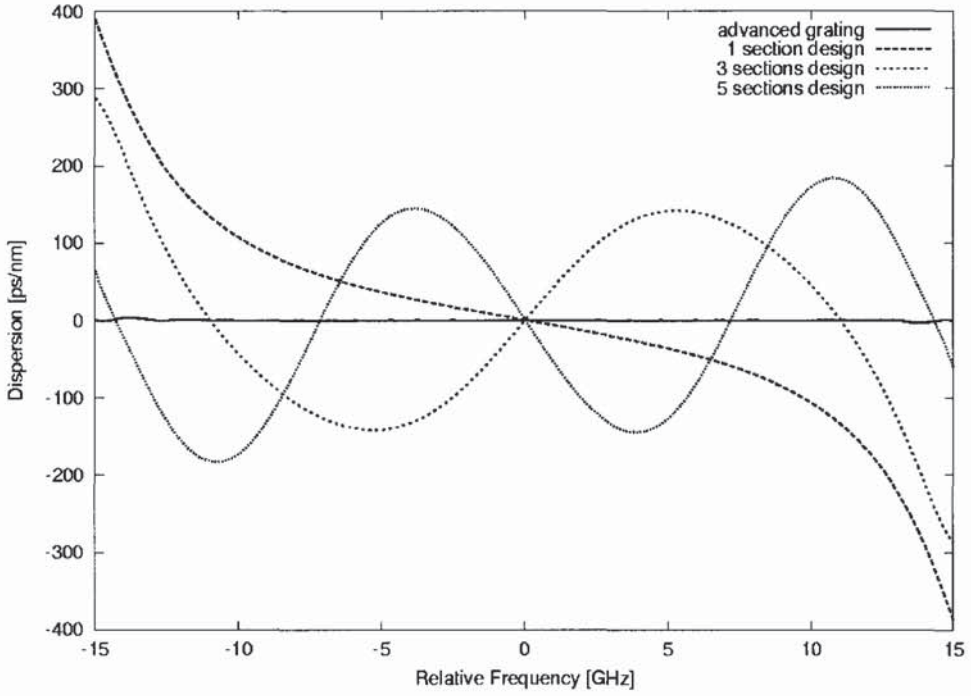

Fig.3.9 Dispersion profile of each of the gratings.

Both higher order approximations present larger local deviations from zero dispersion in the vicinities of the central frequency of the signal, which eventually leads to signal distortion. The one-section roughest approximation to the ideal grating will therefore always outperform the other two in any situation in which the spectral 'squareness' – that can be defined as a sharpness of the decrease of the filter response function at the edges of the utilised bandwidth - is not the main concern. These results suggest that, in order to apply approximated flat-dispersion gratings as inline filters in a periodic system, some post-compensation must be included to account for the extra dispersion introduced by the gratings.

For the performance of the gratings to be tested under a situation in which both high BU factor and dispersion flatness play an important role, they must

be used in a multi-channel system. Next, starting from the same basic span as in the previous test, we used the gratings to perform periodical demultiplexing of 4 WDM channels at the end of the span. The channel spacing was set to 60 GHz, with 10 Gbit/s channels and a 4.5dB noise figure from the EDFAs. The signal was then recombined and inserted again into the loop. One can say that the considered channel spacing doesn't satisfy ITU (International Telecommunication Union) standards, but the purpose of these simulations was to demonstrate gratings performances, avoiding any complex optimisation.

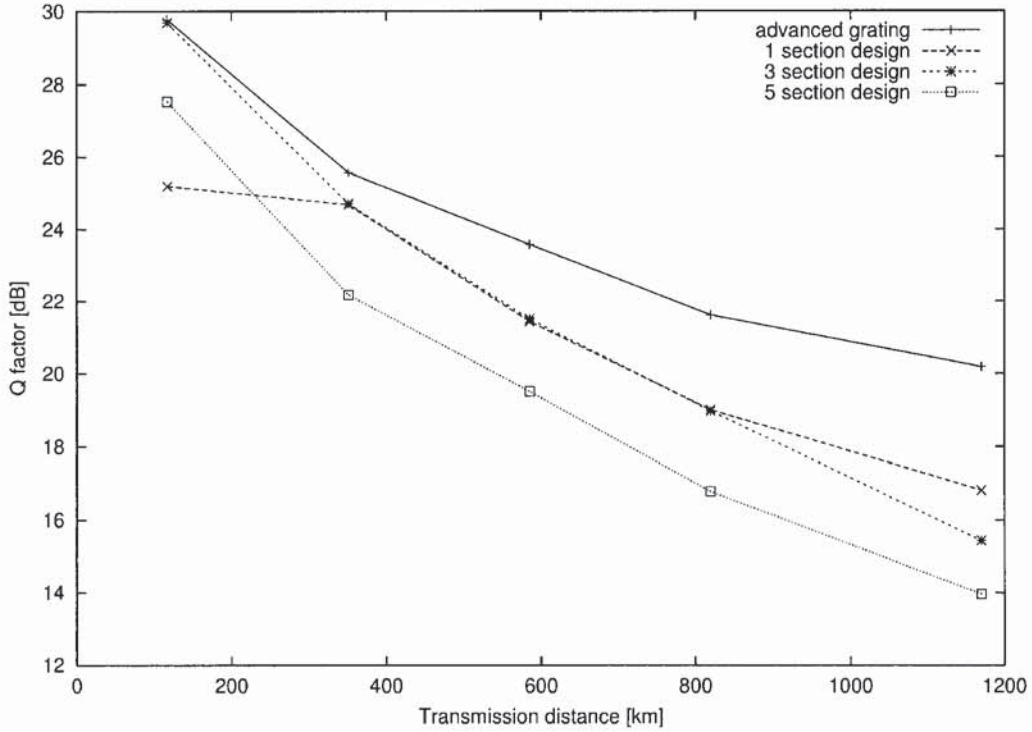

Fig.3.10 Q-value (in the worst channel) vs distance for each of the gratings in the multi-channel system.

The evolution of the Q-value of the worst channel vs. the propagation distance for this scheme is depicted in Fig. 3.10. As we can see from the figure, the performance of the one-section approximation is in this case initially the worst, due to not sharp decrease of its response function at the edges of the filtering band (reduced "squareness"). It is only after seven loops that the 1-section grating gives better results than the 3-sections one. The performance of the 5-sections approximation grating, on the other hand, drops fast, due to its bigger

deviation from dispersion flatness, displaying the worst Q-values after just three loops. In all cases, the original advanced grating shows the best performance.

I would like to point out that with these simulations we didn't try to achieve an optimised error-free transmission distance, but just to demonstrate a simplified grating structure in some telecom applications.

3.4. Chirped Gratings for Higher-Order Dispersion Compensation

Many existing submarine and terrestrial fibre links are non-slope matched; and dispersion slope compensation is required. The average group velocity dispersion can be reduced to zero for the central channel of WDM systems, but remains nonzero for all other channels. In long haul transmission systems the total cumulative dispersion for the boundary channels may exceed 1000 ps/nm. One of the solutions is to add DCF fibres of different lengths at the transmitter or receiver ends, using so-called pre- or postcompensation technique. Another solution is in designing and fabrication of fibre Bragg gratings that can be used as dispersion slope compensators.

3.4.1 Dispersion slope compensation

We examine now the design of a grating, which will compensate the dispersion slope of 550 ps/nm^2 over >1 nm usable bandwidth. The desired spectrum is as following: the reflectivity is similar to any rectangular-like profile with -3 dB level bandwidths of about 1.5nm. The grating strength has to be greater than 10 dB, with linear dispersion variation $D(\lambda)=550\ \lambda$, or with the group delay $T(\lambda)=275\ \lambda^2$. Practical requirements on the target grating have been proposed by the optical communication group from Fraunhofer-Institut für Nachrichtentechnik - Heinrich-Hertz Institut, Germany for the purposes of slope compensation in a typical fibre transmission link. Note that, for instance, accumulation of the typical slope of SMF (+0.07 ps / km / nm^2) over 7500 km leads to 0.07*7500 = 525 ps / nm^2.

I consider the ideal reflection profile described by

$$r(\delta) = \sqrt{0.93}\exp(-(\delta/\delta_{PB})^8)\exp(-i(\beta'''/3!)L((c/n_o)\delta)^3) \quad (3.12)$$

Here the grating bandwidth is determined by δ_{PB}=34.16 cm^{-1}, which corresponds to 1.5 nm in wavelength, c is the speed of light and n_0 is the effective refractive index. To achieve the required dispersion profile we take $\beta'''L \approx 901 ps^2$, which corresponds to the dispersion slope of -550 ps/nm^2.

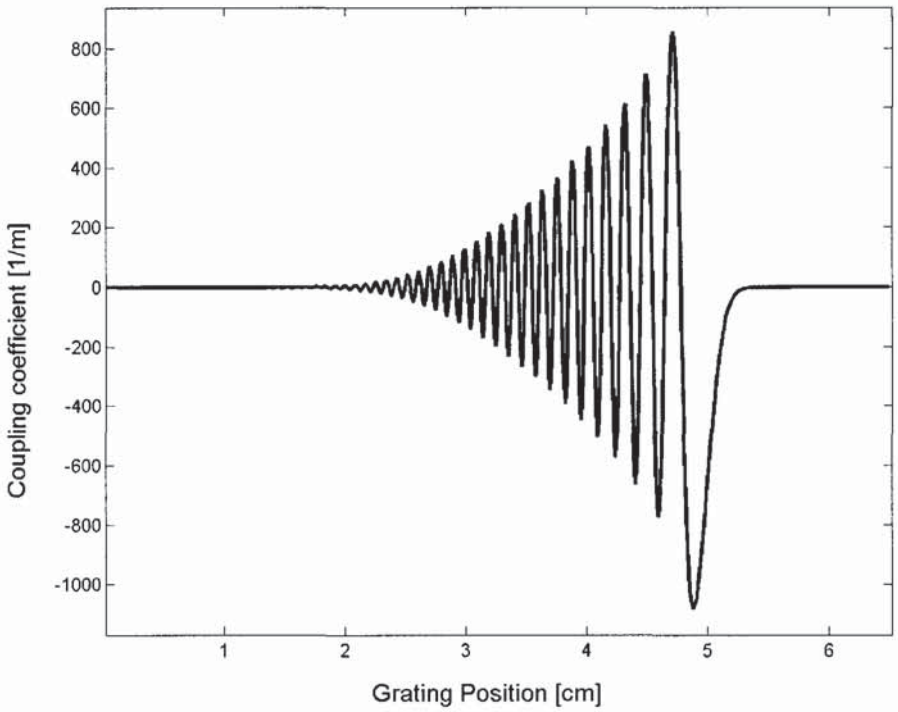

Fig.3.11 Real part of the coupling coefficient of the reconstructed grating for dispersion slope compensation

The reconstructed grating has the coupling coefficient like in Fig.3.11. It has a zero imaginary part, therefore for the fabrication of the grating a π phase shift has to be inserted every time the sign of the index modulation changes. The refractive index changes for this grating are of the order of $7 \cdot 10^{-4}$.

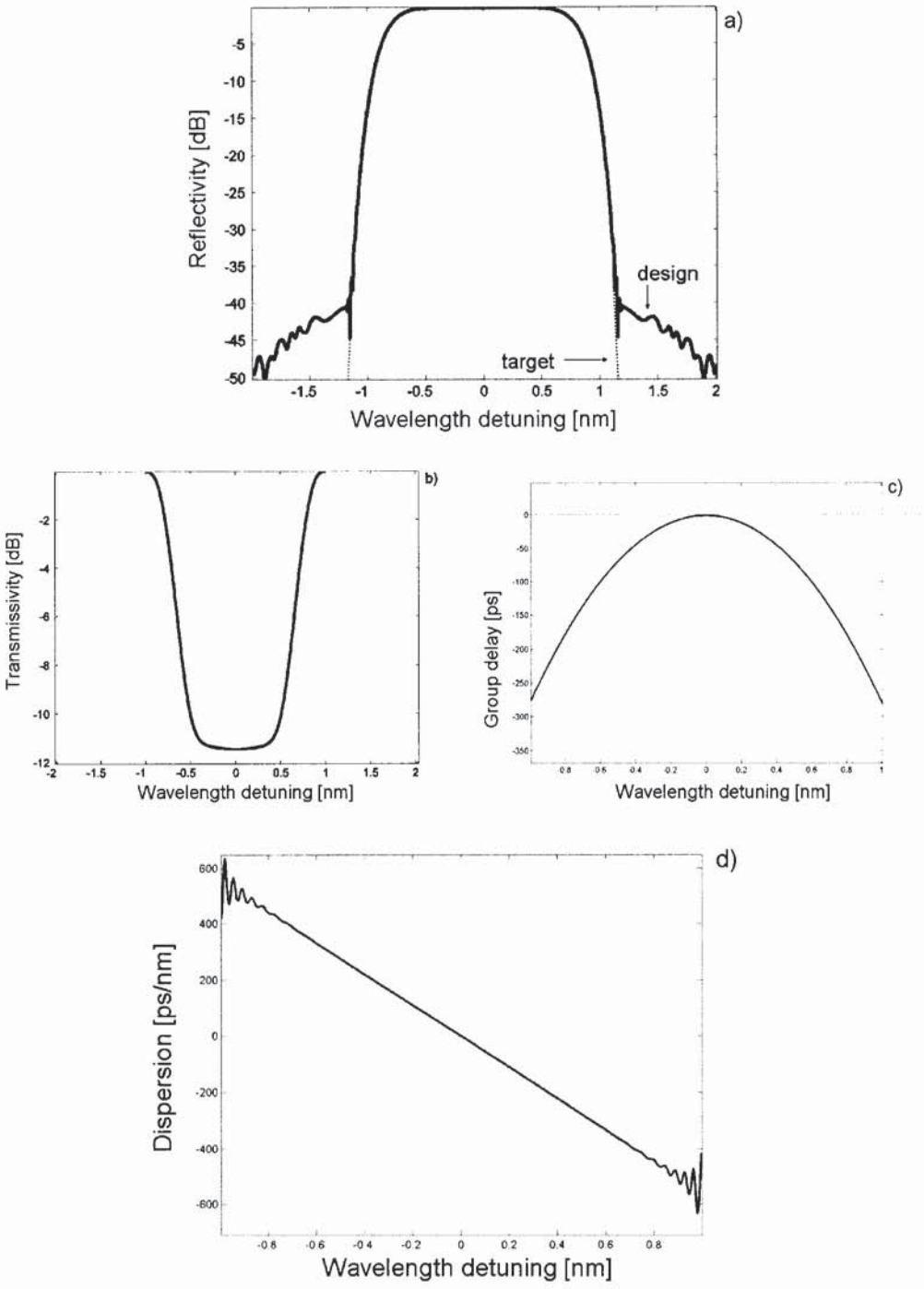

Fig.3.12 Grating response: a) reflectivity of the design grating - solid line and target response as in (3.12) –dotted line, b) transmissivity, c) group delay, d) dispersion.

To verify the spectrum of the designed grating we run the "direct" program. Fig. 3.12 demonstrates that the desired spectrum requirements have been achieved.

3.4.2 Tunable dispersion slope compensator

Another request from Heinrich-Hertz Institut was to fabricate a grating, which can be used for intra-channel dispersion compensation in 40 Gb/s and beyond transmission systems. As it was mentioned earlier, in WDM transmission systems it's important to compensate not only accumulated dispersion, but also dispersion slope. There are lots of works devoted to dispersion slope compensators, including the usage of fibre Bragg gratings, but mostly these approaches cover fixed value dispersion slopes. There is a demand in tunable dispersion slope compensators (TDSC), as the dispersion slope itself changes due to different factors, like environmental changes, network reconfigurations and many others. One of possible solutions is to design tunable dispersion slope compensators using FBGs. There are reports of designing multi-channel dispersion compensators [68], also using broadband nonchannelised third-order fibre Bragg gratings [69]. Here we present a design of TDSC for compensating a dispersion slope within a single channel in 40 Gb/s (and higher) WDM transmission systems.

Consider a grating with a third-order group delay variations against wavelengths and second-order dispersion curve. A second grating has an inversed dispersion profile, which can be obtained by launching the light from another end of the grating. The combination of two inversed gratings cascaded, using a 4-port optical circulator, provide a tunable dispersion slope compensator. The resulting group delay of two inversed FBGs (used as described) is quadratic and the resulting dispersion curve is linear and tunable. The wavelength change can be achieved by applying strain or using heating elements.

The grating I have been asked to design, has the same reflection and transmission profile as in 3.4.1 (Fig. 3.14a, dotted line), but with a quadratic dispersion variation $D(\lambda)=600\ \lambda^2$, or the cubic group delay profile: $T(\lambda)=200\ \lambda^3$. The target reflection function used for this grating is

$$r(\delta) = \sqrt{0.93}\exp(-(\delta/\delta_{PB})^8)\exp(-i(\beta^{IV}/4!)L((c/n_o)\delta)^4) \qquad (3.13)$$

Here δ_{PB} is the same as in (3.12), the value of $\beta^{IV}L$=2489 ps^4 is set to obtain the required dispersion profile. The coupling coefficient of the reconstructed grating is shown in Fig. 3.13.

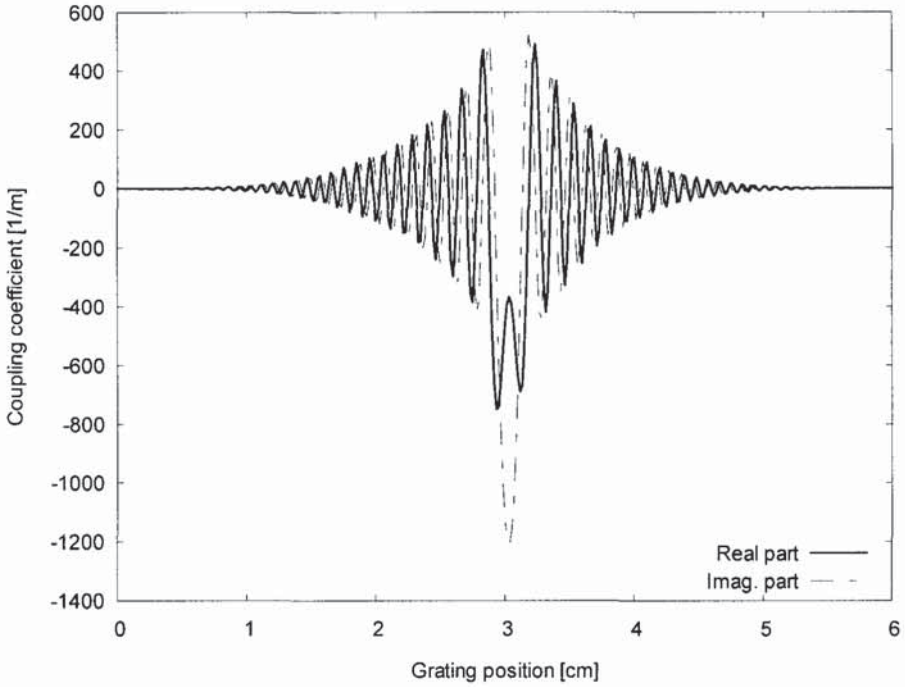

Fig.3.13 Coupling coefficient of the reconstructed grating: solid line- real part, dashed and dotted line-imaginary part.

The refractive index changes for the grating are of the order of 8 x 10^{-4}. As the imaginary part of the coupling coefficient in non-zero, we have to take into account the local period change of the grating (a chirp in other words). The corresponding spectrum of the grating is shown in Fig. 3.15. It is seen that it satisfies the desired spectrum requirements.

Based on this design there were some gratings fabricated at Aston University. It was shown, that using the gratings it's possible to tune the dispersion slope continuously from -650 ps/nm^2 to +650 ps/nm^2 [70].

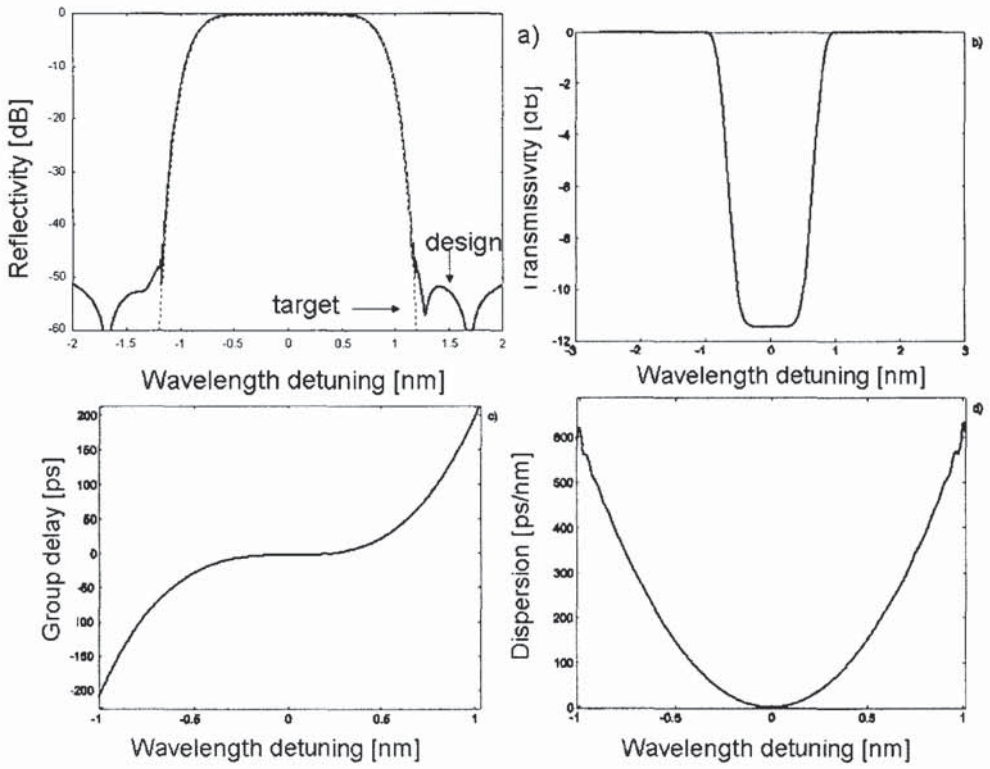

Fig.3.14 Higher-order dispersion compensation grating response: a) reflectivity, b) transmissivity, c) group delay, d) dispersion.

In conclusion, the discrete layer peeling method described in 3.2 and the implemented program (based on this method) are suitable for designing complex gratings that could, for instance, provide tunable dispersion and dispersion slope compensating devices for fibre communication links.

PART III
Applications of Fibre Bragg Gratings

This is the third part of the thesis, containing four chapters in which novel applications using fibre Bragg gratings along with new gratings design are presented. Gratings performance is evaluated in applications to various fibre communication systems.

4 FBGs as ultra-narrow optical filters

This section presents a new approach to ultra-narrow optical filtering based on a specially designed slightly asymmetric filter, which can be fabricated using fibre Bragg gratings.

4.1 Introduction

Ultra-Dense Wavelength Division Multiplexing (UDWDM) is a technology of packing optical communication channels spectrally as closely as physically possible in a single optical fibre. This allows for a dramatic increase in the capacity of fibre communication systems. The UDWDM might also require development of new technologies at the transmitter and receiver, in particular, spectrally efficient modulation formats along with ultra-narrow optical filters. In this approach, new optical modulation formats are desirable because the conventional on-off-keying intensity modulation is spectrally inefficient. High-performance ultra-narrow optical filters are required to separate out the UDWDM channels at the receiver and/or transmitter without adding excessive distortion or crosstalk. It has been demonstrated that the asymmetrically optically pre-filtered carrier-suppressed return-to-zero (CS-RZ) signal had a great potential for ultra-DWDM applications [74-78]. CS-RZ format is an appropriate choice for 40Gbps optical long-haul communication systems because of its robustness to dispersion tolerance and high nonlinearity tolerance compared to conventional RZ modulation format. It has been shown [78] that the CS-RZ DPSK modulation format is another option for extending

the transmission distance and increasing the spectral efficiency when combined with ultra-narrow filtering. However, inter-channel cross phase modulation (XPM) in WDM systems and channel spacing factor have an impact on the maximum distance, which can be obtained with RZ DPSK signals [79, 80].

Conventionally, narrow filtering is realised at the expense of increasing nonlinear penalties due to closer channel spacing and signal waveform distortion. Therefore, to maximize the advantage of spectral filtering, the filtering should be performed synchronously with the optimisation of carrier pulse characteristics in the temporal domain. Ultra-narrow filtering detuned around the carrier frequency exhibits narrow signal bandwidth and partial carrier suppression, in which the transmission passband is filtered to reject either the upper or lower side band. High spectral efficiency with very closely spaced channels increases cross-talk, therefore, we can expect that using sharper filters it would be beneficial to apply filtering more symmetrically across the signal spectrum – in other words, filter detuning from the channel wavelength will not be large. Otherwise removing all the unwanted sidebands may lead to problems of faithfully recovering the signal pulse sequence. This ultra-narrow filtering approach differs from the commonly used VSB filtering technique that can be considered as an ultra-narrow filtering with large detuning.

Here I present a novel method of ultra-narrow optical filtering based on specially designed asymmetric and symmetric FBG-based filters.

4.2 Asymmetric ultra-narrow filter design

Detuning of the narrow passband filter off the carrier enhances the favored side-band, while making an efficient reduction of cross-talk. The best system performance is achieved as a complex trade-off between cross-talk suppression and waveform distortion leading to propagation penalties. Therefore, when designing an advanced ultra-narrow filter for a particular system, it is important to establish an optimal combination of filter bandwidth,

detuning and temporal signal characteristics.

Here we propose a special design of an asymmetric dispersion-free ultra-narrow filter, with a super-Gaussian shape (10^{th} order) on one side (in this case for negative frequencies) and a super-Gaussian (SG) shape of n^{th}-order (n=2,4,6,8,10) on the other side (positive frequencies), as shown in Fig. 4.1.

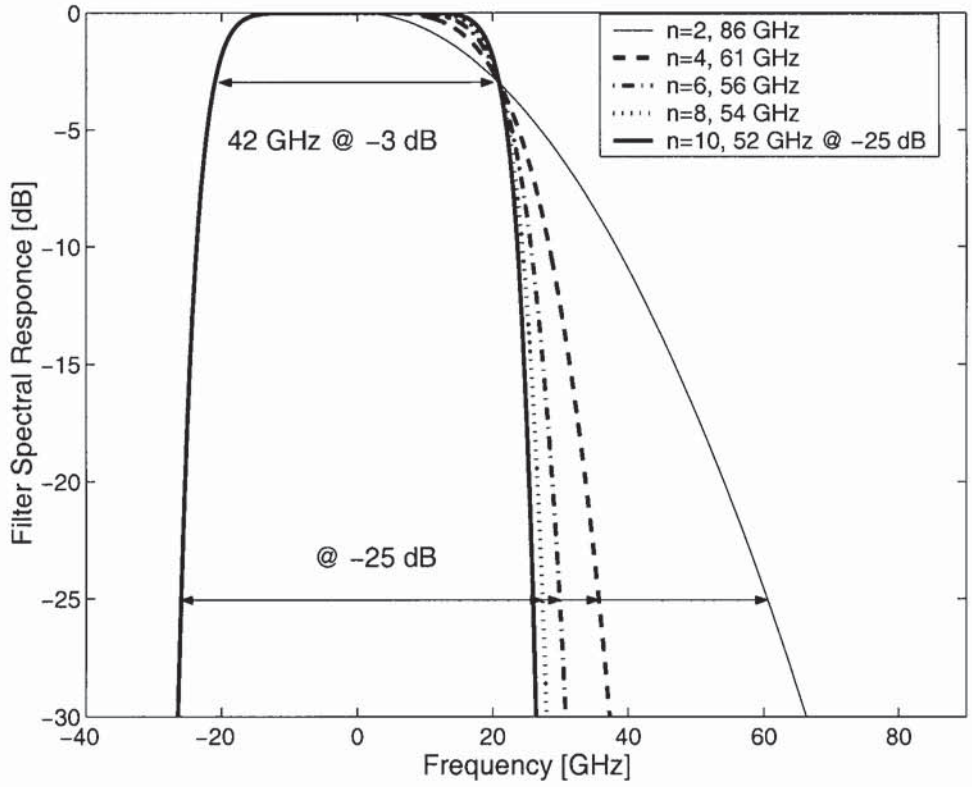

Fig.4.1 Spectral response of the proposed ultra-narrow filters

It is seen from Fig. 4.1, that the considered filters have the same bandwidth of 42 GHz at -3dB level and different bandwidth at -25 dB level: 86GHz for n=2, 61 GHz for n=4, 56 GHz for n=6, 54 GHz for n=8 and 52 GHz for n=10, which is the symmetrical filter.

4.3 Ultra-narrow filter fabrication using fibre Bragg grating

There are different ways to design and fabricate the proposed ultra-narrow filter. Here I present a design of a fibre Bragg grating (Fig.4.2a) that has the required response (reflection) function for an asymmetrical filter (n=8) as described above and the reflectivity of 95%. The grating was designed using the layer-peeling algorithm

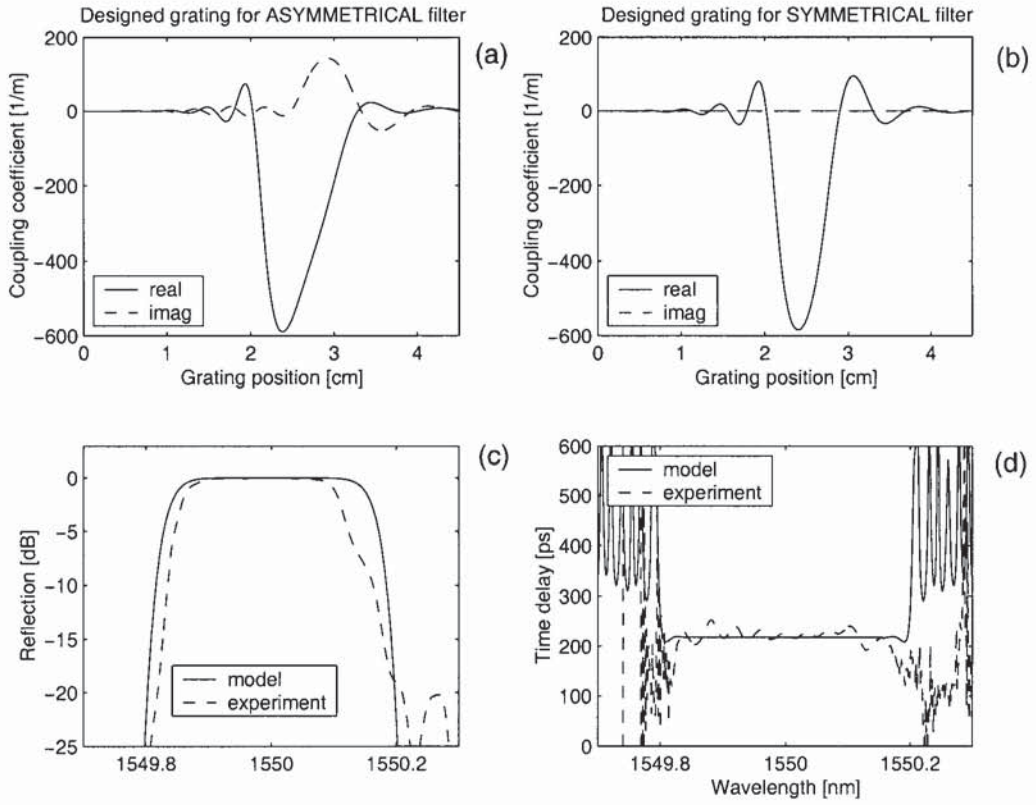

Fig.4.2 Asymmetrical ultra-narrow filter design, using FBG (a), SGF filter design using FBG (b), reflection profile of SGF filter (c) and time delay profile (d) of the designed and fabricated gratings.

It is shown that the imaginary part of the coupling coefficient is non-zero, causing a fabrication technique of the desired FBG to be more complicated than a fabrication of FBG with a zero imaginary part. Figure 4.2b demonstrates the grating profile (with zero imaginary part), which has a response (reflection) function similar to the transfer function of a super-Gaussian filter (SGF) of the 10^{th} order. Figure 4.2 also shows a comparison in reflection and time delay between designed and fabricated gratings (symmetrical SGF of the 10^{th} order). The FBGs were written using a static beam and phase mask whilst translating the fibre [81]. Initially, only these types of grating were fabricated due to simplicity of fabrication, which requires insertions of π shifts and doesn't require any control over the local period variations. Because the agreement between fabricated and designed gratings wasn't as good as expected and due to the lack of people available at that moment (who could fabricate gratings) there were no asymmetric filters

fabricated at all.

4.4 Evaluation of filter performance in a typical transmission system

To illustrate the advantage of the proposed design, without loss of generality we first investigate back-to-back performance in terms of standard Q-factor and employ ultra-narrow filtering with MUX/DEMUX functions in 8x40Gb/s WDM system, using the RZ signal with 80% spectral efficiency (channel spacing of 50 GHz) as shown in Fig. 4.3. Fig. 4.3a demonstrates only the first four channels and the eighth channel (instead of displaying all channels) used in the transmission map to give an idea of the channel density and to avoid the picture being too crowded. For this particular application a bandwidth (at – 3 dB level) of the designed filters has been set to be 42GHz. The filter bandwidth at -25 dB level is different: 86 GHz for n=2; 61 GHz for n=4; 56 GHz for n=6; 54 GHz or n=8 and 52 GHz for n=10.

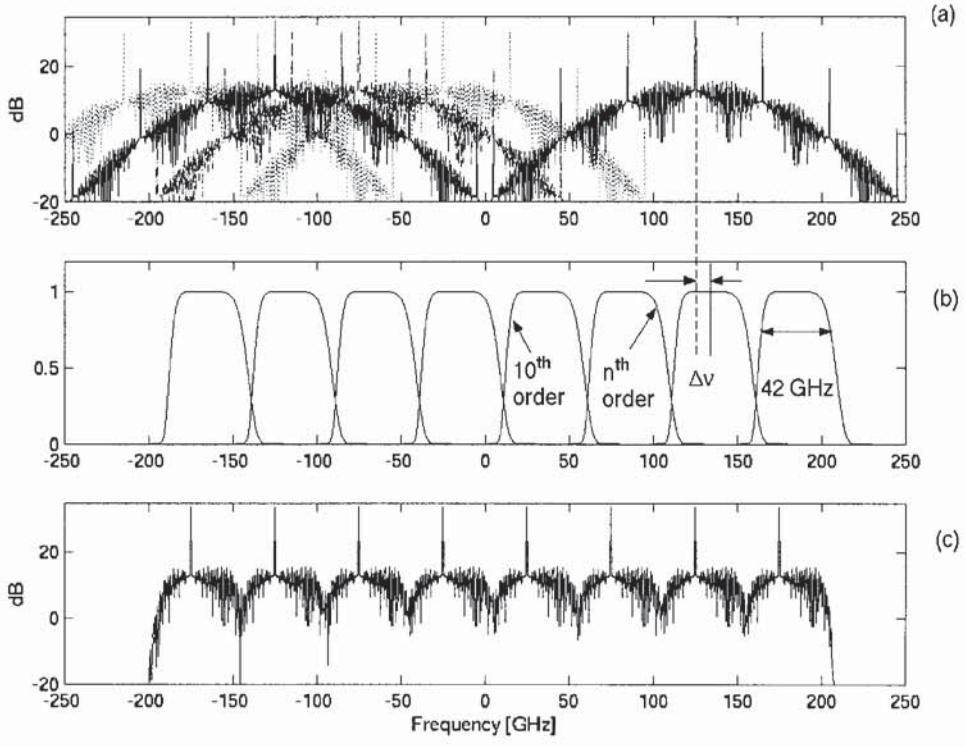

Fig.4.3 Channel spectra of optical signal combined without filtering, on the right:- a single channel before MUX (a); narrow filters shape and location (b); channel spectra after filtering via MUX (c).

By varying the value of *n* while simultaneously optimising the duty cycle and filter detuning, the best result for back-to-back performance was achieved for n=8. It should be stressed that the duty cycle mentioned here is for the input signal *before filtering*. The table below lists the best results for different *n* and the corresponding optimal values of duty cycle and detuning.

N	duty cycle	$\Delta\nu$ [GHz]	Q (linear)
2	0.52	12	6.1
4	0.32	6	12.9
6	0.24	5	22.8
8	0.2	-2	34.3
10	0.2	-3	31.5

Table 4.1 Best optimisation results in terms of Q factor for the order n, duty cycle and filter detuning.

It is seen that with an increase of the filter sharpness (from n=2 to 8) the optimal detuning is decreased (from 6 GHz to -2 GHz) as well as the optimal input pulse width (duty cycle from 0.52 to 0.2). Note, for comparison, that similar optimisation, using the symmetric Gaussian filter (n=10 in Table 4.1) for off-centre narrow filtering, produces inferior results. Back-to-back consideration could be of importance for local area networks, when filtering impairments (due to a cross-talk) dominate over transmission penalties; and the key issue is to achieve maximal spectral efficiency rather than to maximize the transmission distance.

Next I examine the performance of the proposed technique in transmission. A fibre line, as depicted in Fig. 4.4, has been considered without loss of generality.

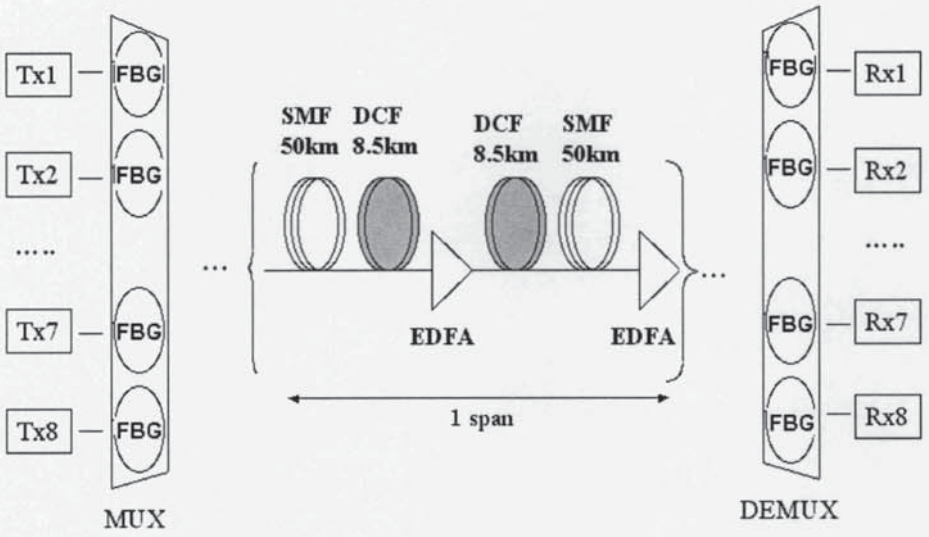

Fig 4.4 Scheme of the 8 x 40 GB/s WDM SMF/DCF transmission system used to evaluate performance of the proposed filtering technique.

A periodic dispersion map consists of 50km standard single mode fibre (SMF) and 8.5 km dispersion compensating fibre (DCF) followed by EDFA (with standard telecom noise figure NF = 4.5 dB) and a similar block with the reverse order of SMF and DCF. Ultra-narrow filtering has been realised at both MUX and DEMUX (see Fig.4.4). Transmission performance of eight channels (8 x 40 Gb/s) spaced by 50 GHz has been modelled using a $2^7 - 1$ pseudorandom binary sequence data signal.

The chosen length of the pattern wasn't too big due to the practical restrictions imposed by computing ifrastructure. It should be pointed out that use of long PRBS of $2^{31} - 1$ that is typical in experiments is not yet technically possible in numerical experiments with existing computing power even using supercomputers. Discussion of the numerical approaches to this problem can be found in [71, 72]. In these works it has been shown that instead of running a long PRBS of a given length it is possible to obtained right estimates of Q-factor by running several times (typically not more than seven) shorter patterns and then averaging obtained results. To run numerical simulations Aston GNLS code has been used. I have implemented an additional module for this code (ReadFilter), which reads data of the reflection function of the grating and applies it as a filter's transfer function.

Error-free transmission distance was defined using the standard requirement (linear Q-factor > 6 or BER < 10^{-9}). By varying a value of the initial peak power of the signals (from 0 dBm up to 15 dBm) and simultaneously optimising the average dispersion of the span (from –0.3 ps/nm/km up to 0.3 ps/nm/km), the best result in terms of Q factor has been achieved for signals with initial peak power of 10dBm and the average span dispersion of 0.1ps/nm/km. The asymmetrical filter performs slightly better than a symmetrical one. In case of applying asymmetrical ultra-narrow filters, the signal can be transmitted over 1400km of SMF/DCF link. Whereas using a 10^{th} order symmetrical super-Gaussian filter for ultra-narrow filtering technique, the signal can perform error-free transmission over 1287km (11spans) of the same link with 0.8 bit/s/Hz spectral efficiency (see Fig. 4.5).

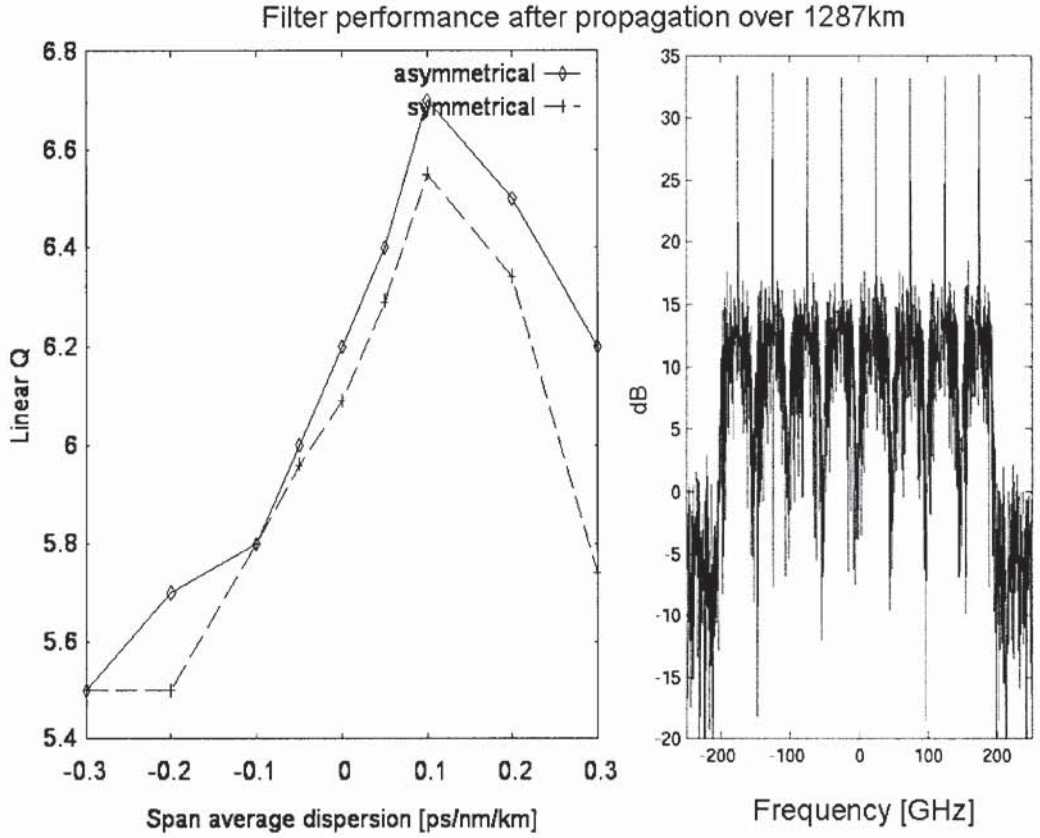

Fig.4.5 Filters performance after propagation over 1287 km of SMF/DCF: Q values versus average span dispersion for symmetric and asymmetrical filters (left) and channel spectra for the symmetrical filter (right).

To account for statistical fluctuations for each point in Fig. 4.5, six numerical runs were performed and the mean value of Q in the worst performed

channel, has been taken. Figure 4.5 also demonstrates the Q value versus the average dispersion of a span; and signal characteristics after propagation over 1287km (signal spectra). A dashed line states for the symmetrical filter and solid line - for the asymmetrical filter, which performs slightly better. Note that existence of a clear maximum at the anomalous average dispersion likely can be attributed to soliton-like effects in single carrier pulse dynamics.

To summarise, another method of ultra-narrow optical filtering, based on specially designed asymmetric and symmetric filters, has been presented and evaluated. A FBG-based device with required spectral response has been designed. A feasibility of 8x40Gbit/s DWDM RZ transmission with 0.8bit/s/Hz spectral efficiency (without polarization multiplexing and FEC) over 1287km of SMF/DCF link has been confirmed by numerical modelling.

5 Filtering with FBGs operating in transmission

This section presents a design of ultra-narrow optical filtering based on a specially designed Fibre Bragg grating (FBG) operating *in transmission regime*.

5.1 Introduction

As it has been mentioned already in Section 4.1, ultra-narrow filtered data format exhibits narrow signal bandwidth and partial carrier suppression, in which the transmission passband is filtered to reject either an upper or lower side band [82-83]. The best system performance is achieved as a complex trade-off between cross-talk suppression and waveform distortion, leading to propagation penalties. Therefore, when designing an advanced ultra-narrow filter, we have to find a compromise between the envelope distortions, power efficiency and filter bandwidth. Performance of such systems critically depends on a design of the corresponding ultra-narrow filters.

Here a novel approach to ultra-narrow optical filtering based on a specially designed FBG operating in transmission has been proposed. The main limitation of the gratings used in commercial application is that they work as reflector filters. A 50:50 fibre coupler is often used to separate the reflected signal from the incident one, which incurs a 6-dB signal loss that adds to other insertion losses. Gratings insertion loses are typically below 1 dB with coupling efficiencies as high as 99%. Using an optical circulator instead of fibre couplers helps to reduce the insertion loss to 1 dB.

FBG operating in *transmission* allows avoiding additional losses at couplers or at an optical circulator that is required while using a *reflection* transfer function of the FBG. It is difficult to estimate insertion loss of the gratings in the proposed design, because the gratings resonance frequencies were not placed at the channel's carrier frequencies. Although we consider here a specific application of the proposed technique, it is important to stress, that actually, a fundamentally new approach of FBGs applications has been introduced here – *by constructing a desirable response function through*

composite action of two or more FBGs operating in transmission. I would like to anticipate that the proposed and demonstrated method might find interesting applications far beyond the area of telecommunication.

5.2 Filter design

Conventionally a VSB filter is adjusted for a transmission of a half at the carrier frequency (the optimal point for VSB generation), though this is not the optimal point for back–to-back OSNR performance. If the transfer function *H(f)* of the VSB filter has an inflection point, there should be an odd symmetry around the inflection point.

Here we propose to generate a VSB-type ultra-narrow filter via a fibre Bragg grating operating in transmission (Fig.5.1). This makes the implementation very simple as such a grating can be written for each WDM channel before signal multiplexing, and involves minimal parts counts in a practical equipment design. We use a right part of the transmission transfer function by shifting it to the left in order to place the inflection point at the carrier frequency (Fig.5.2).

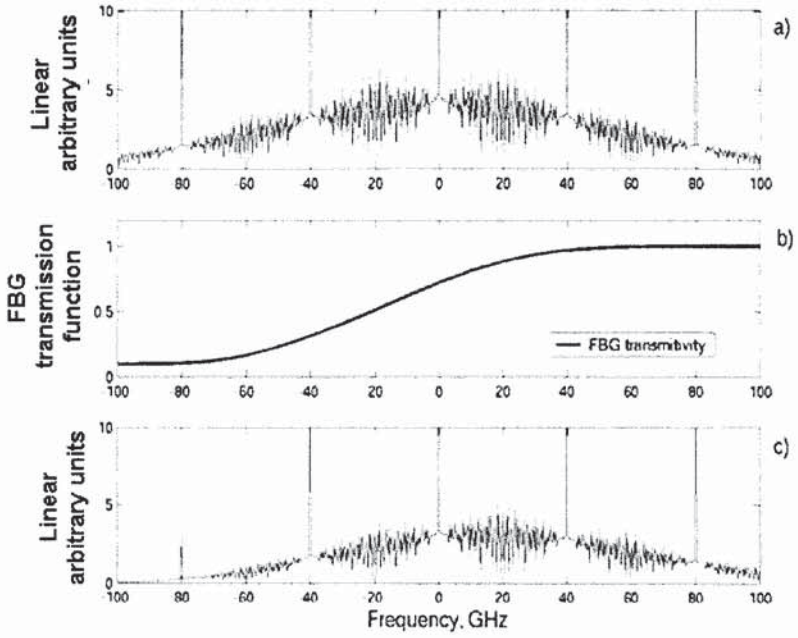

Fig.5.1 VSB-type filtering: a) spectrum of input pulse; b) FBG transfer function; c) filtered pulse.

We would like to find / design a grating with a transmission response, which group delay variations are as little as possible. The important feature of using FBGs in a transmission regime is that the group delay $D_T(\omega)$ in transmission is uniquely determined by the transmissivity $T(\omega)$ of the grating [64] (as I described in Section 2.2.3). Specification of the requirements on the group delay response of the grating imposes some limitations on the amplitude transmission response.

I have examined different shapes of fibre Bragg gratings, including standard apodised gratings with Gaussian and raised cosine profiles, in order to find an optimal transmission profile. Conventional apodised gratings didn't provide required flatness in group delay response. I decided to design dispersionless gratings with Gaussian and Supergaussian reflection profiles with different bandwidth using DLP algorithm and verify their transmission functions performance. It's not real to check all possible variants of gratings profiles. For illustration purpose, without loss of generality, here I use gratings with Gaussian and super Gaussian reflection profile with a varying bandwidth to achieve a compromise between steepness of the transfer function and the group delay response.

Two gratings with Gaussian reflection profile with a bandwidth of 100 and 200GHz, and two gratings with superGaussian (4th order) reflection profile with the same bandwidth of 100 and 200GHz (with reflection 90%) have been designed using the DLP algorithm. Figure 5.2 demonstrates the grating profiles (a), their transmissivity (c), and the group delay response (b).

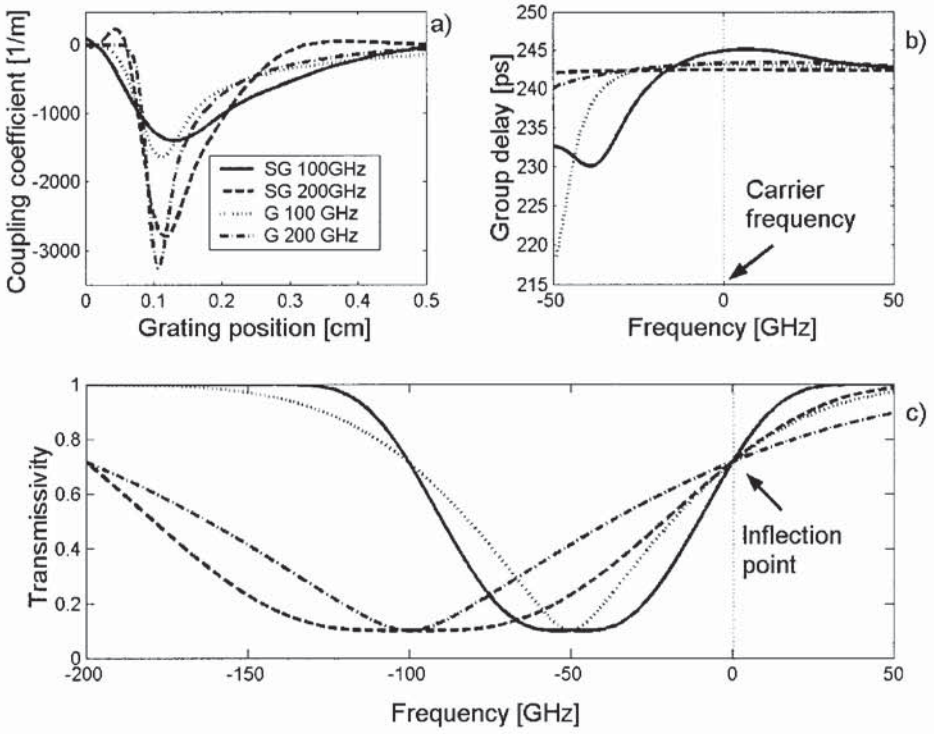

Fig.5.2 Types of gratings considered (a); their time delay profile (b); transmission used for off-centre filtering (c).

5.3. Evaluation of Filter Performance

To illustrate the operation of the proposed filtering technique, without loss of generality, I examine an 8 x 40 Gbit/s DWDM transmission, employing ultra-narrow off-centre FBG filtering along with square MUX/DEMUX filters of 42 GHz bandwidth and using an RZ signal with 80% spectral efficiency (channel spacing of 50 GHz). (See Fig. 5.3-5.5). By a square filter here we mean any filter (for instance, based on arrayed waveguide grating) with a stopband of 42 Ghz, which transition band is more narrow than a transition band of the applied FBG filter. This filter is used to suppress adjacent channels crosstalk. A periodic dispersion map consisting of 50km of a standard single mode fibre (SMF) and 8.5 km of a dispersion compensating fibre (DCF) followed by a EDFA (noise figure NF = 4.5 dB) and a similar block with the reverse order of SMF and DCF has been considered.

The span average dispersion is zero. Error-free transmission distance was defined using a standard requirement (linear Q factor > 6 for BER < 10^{-9}). Transmission performance has been modeled using a 2^7-1 pseudorandom binary sequence data signal.

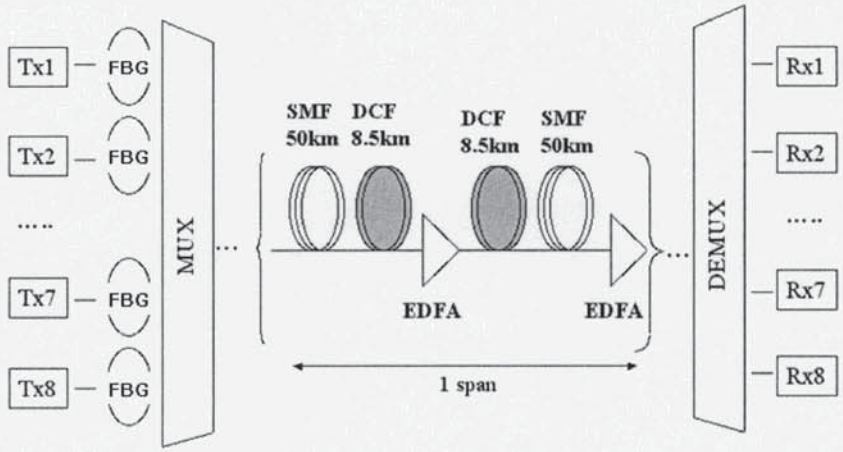

Fig.5.3 Scheme of 8 x 40 Gbit/s WDM SMF/DCF transmission system used to evaluate performance of proposed filtering technique.

By optimising a duty cycle of the input pulses for different types of gratings (described in Section 5.2) I observed the best filter performance whilst using a FBG with Gaussian, linear phase reflection profile with the bandwidth of 100 GHz and the input pulses of 5 ps.

It is shown that the error-free DWDM 8x40Gb/s transmission over 500 km SMF/DCF link with 0.8 bit/s /Hz spectral efficiency is feasible.

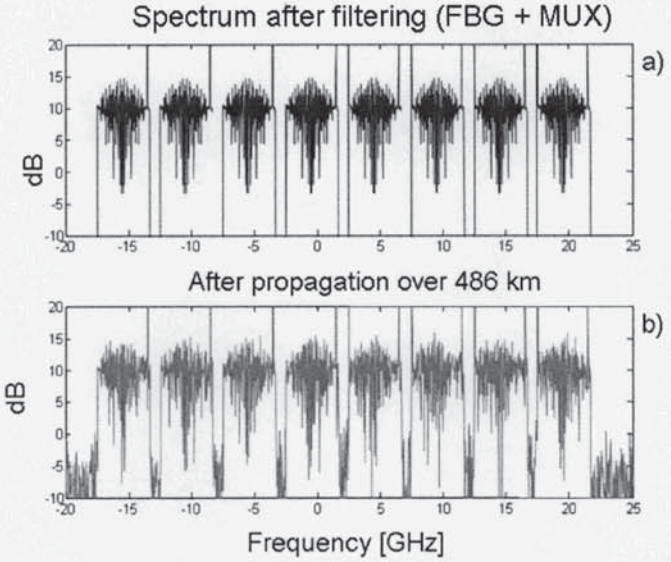

Fig.5.4 Channel spectra of optical spectra after filtering (FBG+MUX) (a); channel spectra after propagation over 486 km (b).

Fig. 5.4 shows WDM channels after filtering before (a) and after (b) transmission over 486 km.

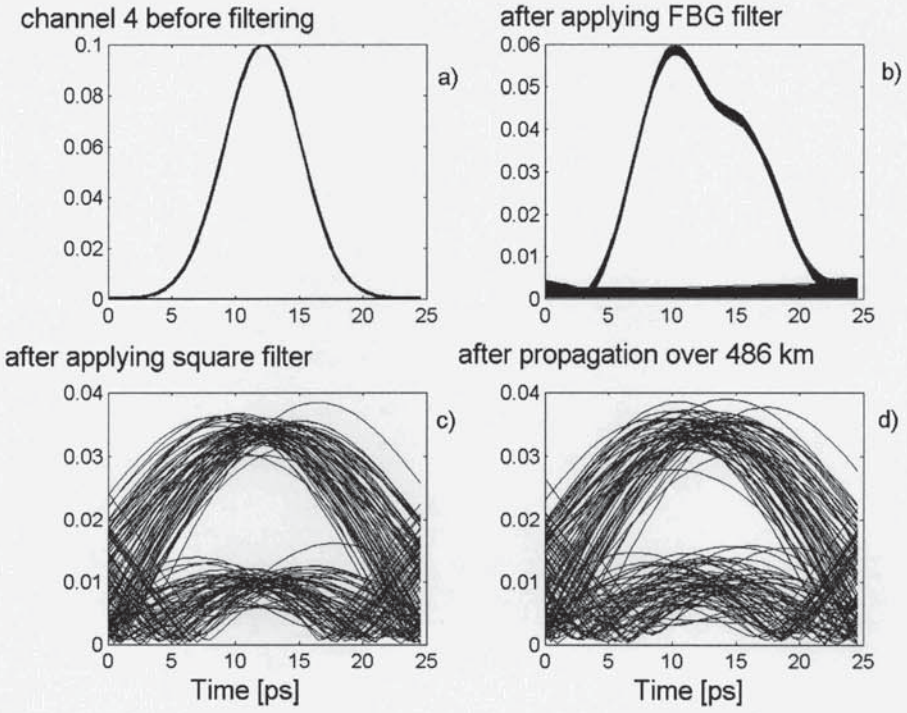

Fig.5.5 Fourth channel eye diagram: a) before filtering; b) after FBG filtering; c) after applying square filter; d) after propagation over 486 km.

5.4 Double-Notch Filter

Design of ultra-narrow filter proposed in Section 5.2 and in [84] included an additional (not FBG-based) specific filtering at MUX. Here we propose to realize narrow filtering using *only* fibre gratings. The proposed design presents a composite narrow filter comprised a pair of FBG's operating in transmission. The technique considered here could be complimentary to methods based on special optical filters with periodic filtering characteristic, such as the optical interleavers used in experiments [85-86]. Such interleavers have the advantage of operating on many WDM channels simultaneously. However, they do not provide sharp enough filtering characteristics, and as a result introduce cross-talk penalties.

5.4.1 Proposed Filtering

This solution has an advantage of a low cost, flexibility and tuneability offered by FBG devices. Such a composite filter comprises a pair of matched FBGs operating in transmission as schematically shown in Fig. 5.6. Note that the multiplexing device shown in Fig. 5.6 and used in simulations is not a conventional filter-based MUX, but a N:1 coupler. The first FBG is used to reject upper or lower sideband and the second is introduced to limit the favored sideband from the opposite side. This design substantially limits inter-channel cross-talk resulting from the overlap between the spectral tails of adjacent channels. A cascade of the two notch filters is effectively equivalent to one pass-band filter in which low and high stop bands are formed by stop bands of respective Bragg gratings.

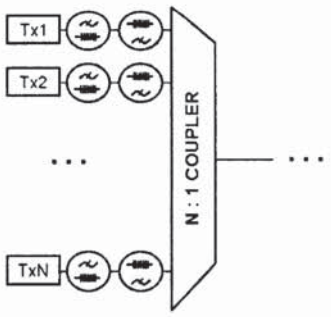

Fig.5.6 Schematic design of the proposed pre-processing filters, based on the cascade of two FBGs operating in transmission.

Note that both Bragg gratings are used in transmission regime, which does not affect the signal-bearing sideband, and evidently, avoids the additional loss that would be required when operating grating in reflection with a circulator. Again, the gratings can be written for each WDM channel before signal multiplexing.

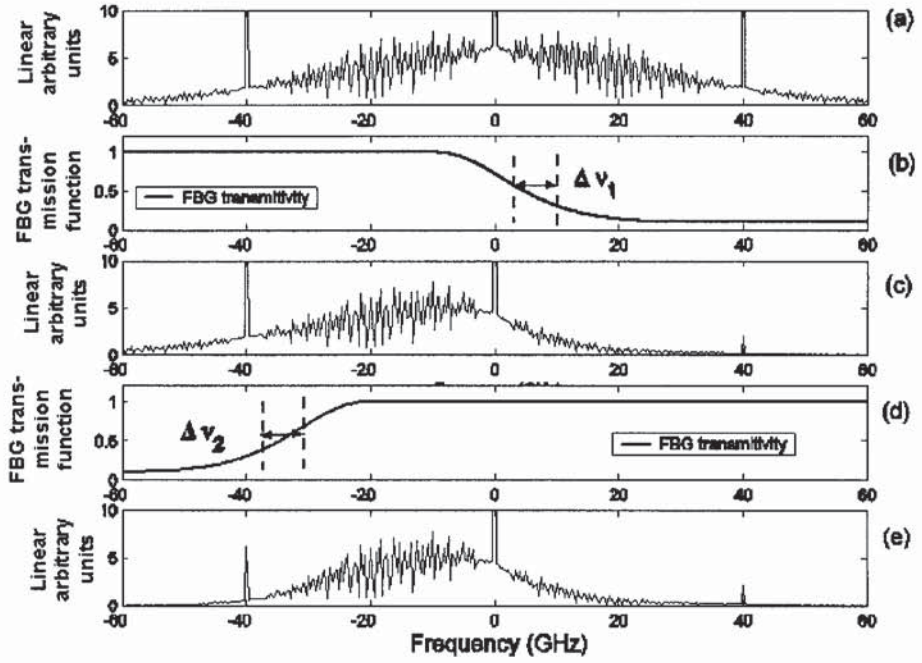

Fig.5.7 Spectral transformation: a) channel spectrum before first FBG;b) amplitude response of the FBG1; c) signal spectrum after FBG1; d) amplitude response of the FBG2, e) signal spectrum after FBG1 and FBG2.

We use a right part of the transmission transfer function by shifting it to the left in order to place the inflection point at the carrier frequency (Fig. 5.7).

Figure 5.7 describes the evolution of the signal spectrum along the cascaded VSB filter and the positioning and response (transmission) of the both FBGs. It is seen that the first grating cuts the right side of the spectrum while retaining the sufficient carrier as required in the VSB format. The second grating can be tuned to optimise the trade-off between narrower filtering and distortion added to the signal waveform.

5.4.2 Filter design using fibre Bragg gratings

Again, I considered different types of gratings with Gaussian, super-Gaussian and raised cosine profiles of the transmission function trying to achieve a compromise between steepness of the transfer function and the group delay response.

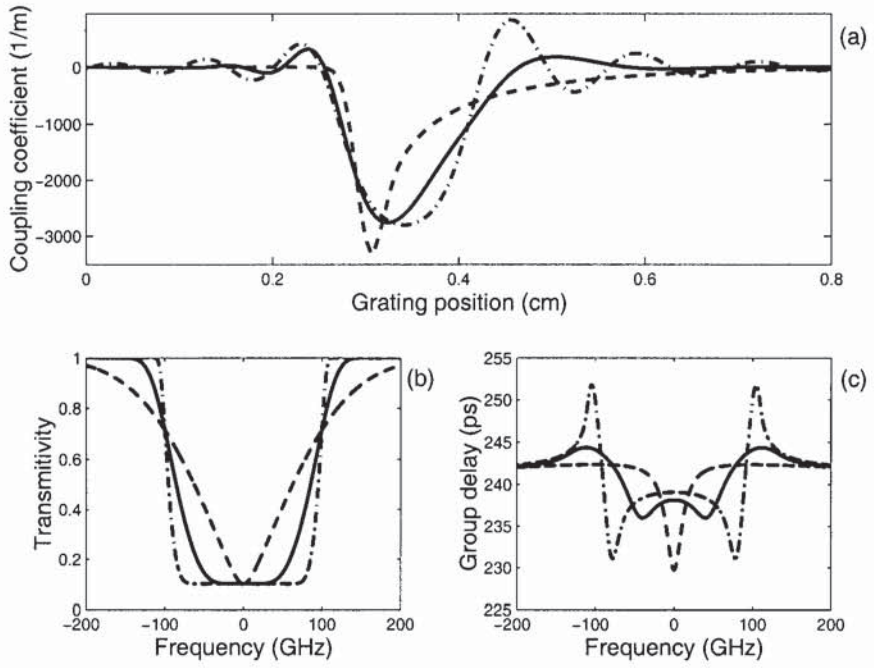

Fig. 5.8 Three types of gratings considered (a); their transmission profile: dashed- Gaussian, solid- super-Gaussian of 6^{th} order, dashed and dotted- super-Gaussian of 10^{th} order (b); time delay profile (c).

Figure 5.8 demonstrates three types of considered gratings (Fig. 5.8a) with Gaussian (dashed line) and super-Gaussian of 6^{th} order (solid line) and super-Gaussian of 10^{th} order (dashed and dotted line) profile of the transmission function (Fig. 5.8b) and the corresponding group delay (Fig. 5.8c).

The bandwidth of the gratings is set to be 200 GHz, to be broad enough to cut the sidebands of the signal spectrum. The gratings were designed using the DLP method.

5.4.3. Evaluation of filter performance

To illustrate the operation of the proposed filtering technique, without loss of

generality, I examine an 8 x 40 Gbit/s DWDM transmission, employing VSB filtering and using an RZ signal with 0.8 bit/s/Hz spectral efficiency (channel spacing of 50 GHz).

Firstly, I investigate back-to-back performance in terms of Q factor. Optimisation was achieved by varying a duty cycle of the input signal, detuning Δv_1 of the right FBG-based filter and Δv_2 of the left FBG-based filter (see Fig. 5.7), and simultaneously detuning and adjusting the bandwidth of the DEMUX filters. I observed the best back-to-back performance with the super-Gaussian 10^{th} order FBG transmission function. A DEMUX using 42GHz bandwidth Super-Gaussian optical filters was found to be optimum.

A system transmission using this configuration was investigated next. A transmission map with zero average dispersion consists of several spans of SMF(50 km) + DCF (8.5 km) + EDFA+ DCF(8.5 km) + SMF(50 km) + EDFA (noise figure *NF* = 4.5 dB). A combination of 100 km of single mode fibre (SMF) and 17 km of dispersion compensating fibre (DCF) is specially designed to compensate both dispersion and dispersion slope from the transmission through SMF. A transmission performance was initially evaluated using a $2^7 - 1$ pseudorandom binary sequence data signal. The optimisation was performed by varying the input signal duty cycle, detuning of the right and left FBG-based filters, whilst also simultaneously optimising the DEMUX filter detuning. Measurements of Q factor values after propagation over 5 spans (585 km) of the SMF/DCF transmission line were made by running numerical simulations.

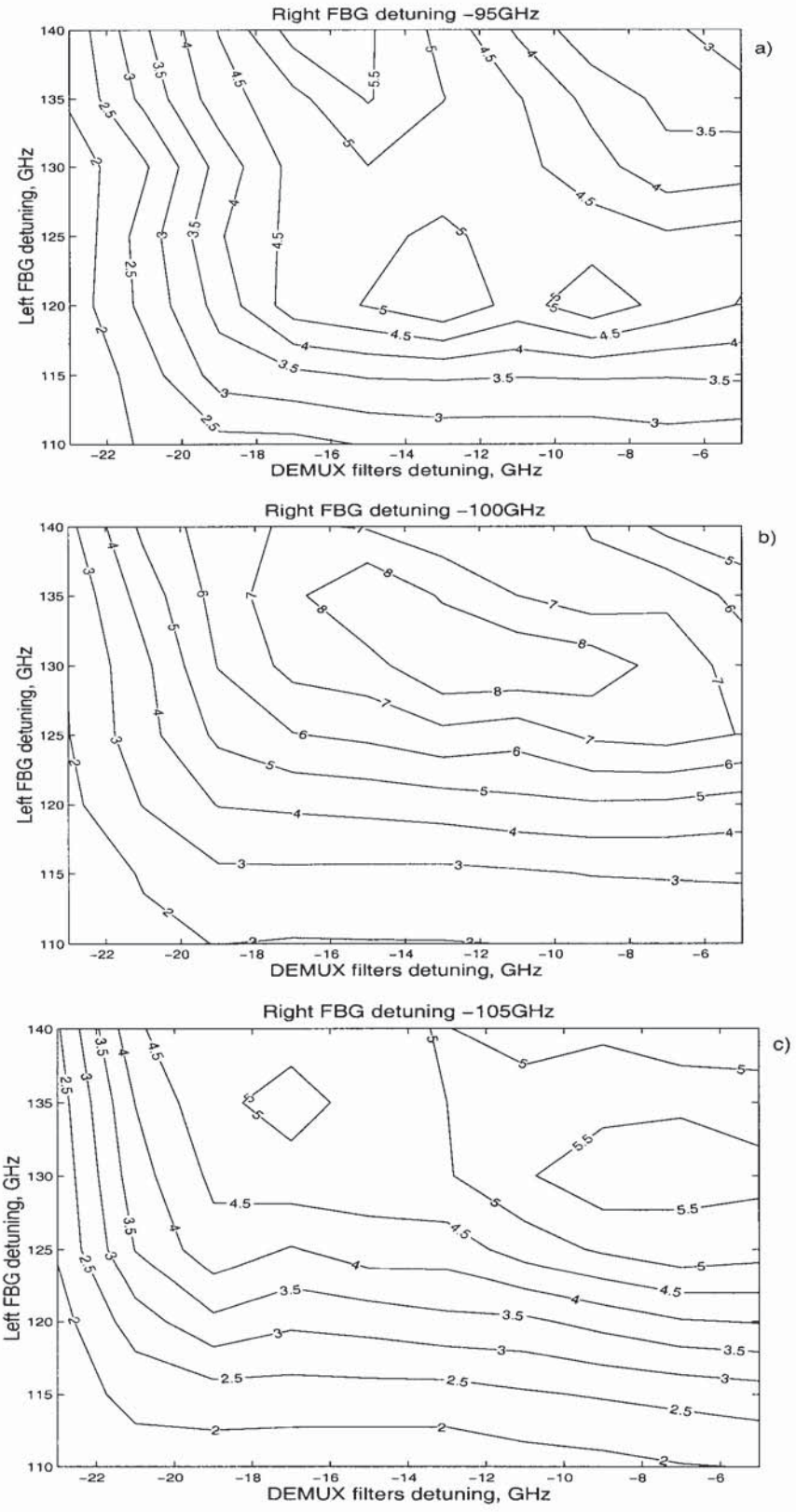

Fig.5.9 Q factor optimisation results after propagation over 585km of the transmission line using a 12 ps FWHM pulse: with the right FBG detuning of -95GHz (a); right FBG detuning -105 GHz (b); right FBG detuning -100 GHz (c).

Figure 5.9 shows that the inflection point of the transfer function for the right FBG has to be placed at the carrier frequency (detuning -100 GHz). The optimal value of the left filter detuning is 130 GHz. The best performance was achieved by -10 GHz detuning of the DEMUX filter.

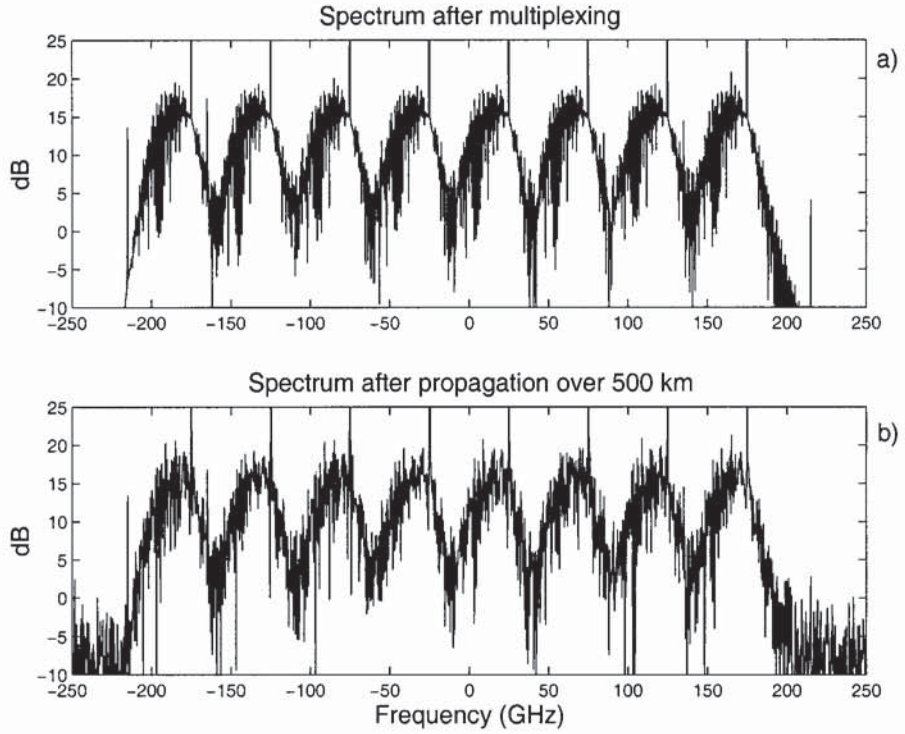

Fig 5.10 Channel spectra of optical signal after filtering (a); channel spectra of optical signal after propagating over 585 km (b).

By varying the value of the average input power of the initial signal, the error free transmission over 500 km is feasible (Figs 5.10, 5.11 and 5.12).

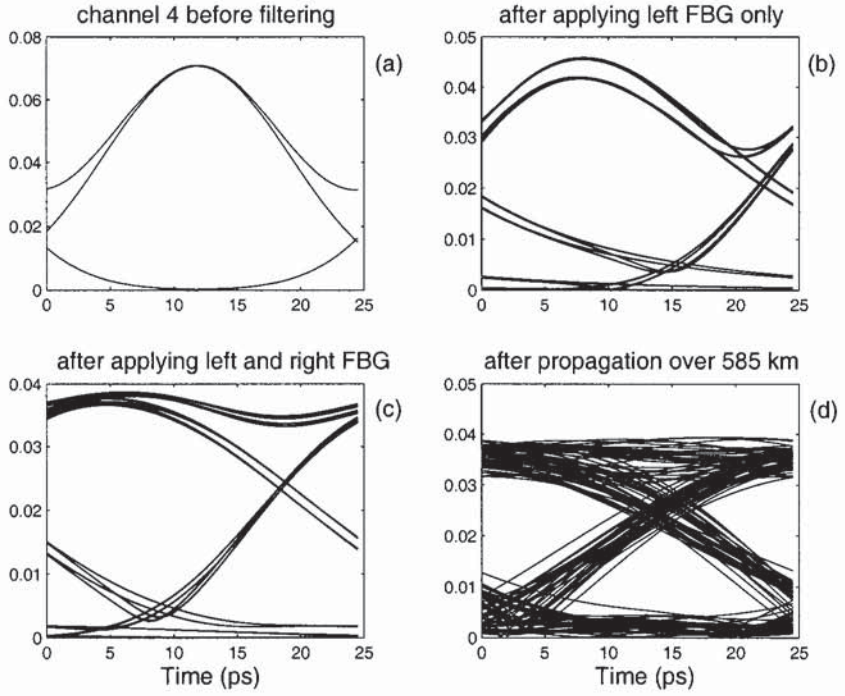

Fig.5.11 Fourth channel eye diagram before filtering (a); after applying left FBG (b); applying left and right FBG (c) and after propagating over 585 km (d).

Error-free transmission distance was defined using the standard requirement (linear Q-factor >6 or BER $<10^{-9}$). The averaging over five numerical runs with different transmission data patterns has also been applied to account for patterning effects. The average Q factor value for the worst channel has been considered.

Figure 5.12 demonstrates how the Q factor of the worst channel after the propagation over 500km depends on the average channel input power (solid line). To illustrate how the dispersive characteristics of the FBGs affect the filter performance I have plotted here for comparison the Q-factor dependence for the "dispersion-free" filters, using only the amplitude profile of the FBGs (dash-dotted line). It is seen that the overall performance of the "real FBG-based filter" is reasonably close to the ideal "dispersion-less" filter and the error-free transmission over 500 km of SMF is feasible even without comprehensive optimisation. Further improvement of the proposed filter performance can be achieved by optimisation of the filter design parameters.

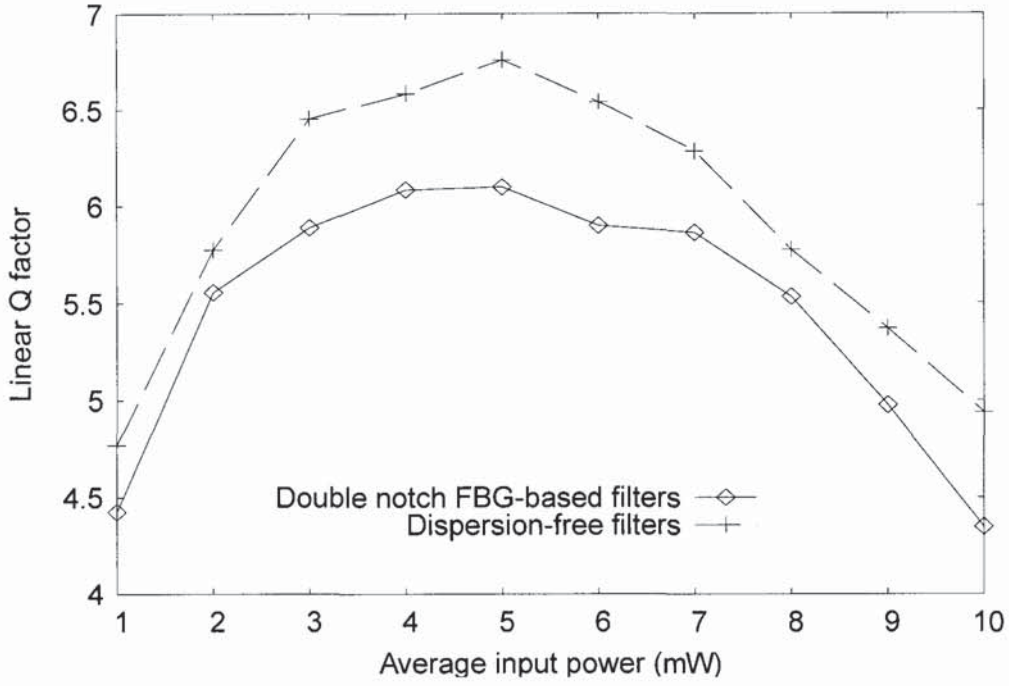

Fig.5.12 Q factor against input channel power after propagation over 500 km for double notch FBG-based filters (solid line) and for dispersion-free filters (dashed line).

To summarise, a novel design of optical filters based on a cascade of the tailored fibre Bragg gratings (FBGs) all operating in the transmission regime has been proposed. I would like to stress that the main goal of this work is not to provide an optimal solution for VSB filters, but to demonstrate a novel approach in designing ones. A new simple and cost-efficient technical solution for VSB channel filtering in DWDM systems has been examined. The proposed design presents a composite VSB filter comprised a pair of FBG's operating in transmission. The filtering method proposed here has an advantage of low cost, and the flexibility of tuneability offered by FBG devices that could be especially important for large channel count DWDM systems. I would like to point out that FBG-based filters can also be used simultaneously for many WDM channels. Using the proposed VSB filter a feasibility of 8 x 40 Gbit/s DWDM RZ transmission with 0.8 bit/s /Hz spectral efficiency (without polarisation multiplexing and FEC) has been demonstrated over 500 km SMF/DCF link.

6 FBG as a single device for filtering and pulse shaping / processing

This chapter presents a design and experimental results of a new type of fibre Bragg grating with a V-shaped dispersion profile. I will demonstrate that such V-shaped FBGs have superior properties for some optical signal manipulation functions compared to conventional FBGs with a constant dispersion.

6.1. Introduction

Fibre Bragg gratings have great, and not yet fully explored potential in optical signal control and processing. Novel fabrication technologies such as, for example, femtosecond radiation inscription, open new practical ways to create sophisticated advanced grating structures. The FBG is a powerful tool for performing optical pulse manipulation. In particular, it is now well known that fibre gratings can be employed as highly dispersive nonlinear elements for pulse compression [23, 88] and for compensation of the second- or third-order dispersions in fibre communication links. Dynamic or tunable operations are possible since the transfer function of FBG-based devices can be made adaptive through temperature or stress control [89]. In telecommunications, recent progress in advanced modulation formats draws attention to techniques that are based on signal pre-distortion to compensate for transmission impairments. For instance, appropriate pre-chirping of a return-to-zero signal can enhance transmission through the effect of pulse compression in an optical fibre [90-92]. Generally, pre-compensation/pre-chirping now plays an important role in the optimisation of the dispersion management of fibre links, helping to suppress nonlinear transmission impairments. The development of simple and cost-efficient solutions for the appropriate optical signal processing functions are of present interest, then, for telecommunications and for other photonics applications, *e.g.* laser technologies.

Commonly, optical signal pre-chirping/post-compensation and filtering functions are realised by using two different devices. A possibility to combine in one passive device both amplitude filtering and phase transform functions is very attractive for applications varying from signal processing/control for optical communications to pulse shaping/manipulation in ultrafast optics. Being inherently of low cost, fibre Bragg gratings are natural candidates to be considered for this purpose. Here a new type of the FBG with V-shaped dispersion (that performs simultaneously the optical filtering and signal chirping functions) is proposed.

There are two essential ideas behind the proposed V-shaped dispersion profile. The first is that such a profile, in combination with tunability of the central wavelength of the FBG, gives freedom of selection between negative or positive dispersion slopes in the device response. This introduces additional flexibility in using such a device for pre-compensation or post-compensation of dispersion and/or dispersion slope. Secondly, using a V-shaped FBG centered at the signal frequency, the left and right parts of the signal spectrum are affected by grating dispersions with opposite slopes, giving new opportunities for signal manipulation. For instance, as will be shown below, in combination with simultaneous signal filtering, this allows for reduction of the signal broadening while creating larger chirp as compared to conventional FBG with constant dispersion. In addition, due to non-parabolic phase response, a V-shaped FBG can act as a pulse shaping device. Note also that V-shaped dispersion response is an elementary cell of the periodic group delay.

I will demonstrate that the V-shaped FBGs possess some interesting properties for optical signal manipulation and chirping that outperform conventional FBGs with linear non-zero slope dispersion, or with constant dispersion slope. In general, signal manipulation functions similar to the described here can be achieved by combination of fibre-based dispersion compensators and optical filters. However, apart from the cost issue, such device combinations generally are less tunable than FBG-based schemes. I compare here only a performance of FBG-based two-in-one devices. Note that the V-shaped FBG can also be used to create a signal with the phase having different (controllable) behavior at the center and at the pulse tails.

This property can be exploited for creating pulses with different temporal behaviors in the central part and tails.

6.2 Chirped Gaussian Pulses

Consider the propagation of Gaussian input pulses in optical fibres using the basic propagation equation

$$\frac{\partial A}{\partial z}+\frac{i}{2}\beta_2\frac{\partial^2 A}{\partial t^2}-\frac{1}{6}\beta_3\frac{\partial^3 A}{\partial t^3}=0 \tag{6.1}$$

where the coefficient β_2 is related to the dispersion parameter, whereas β_3 is related to the dispersion slope. The Gaussian pulse is described as

$$A(0,t)=\sqrt{P_{in}}\exp\left[-iCt^2-\frac{1}{2}\left(\frac{t}{T_o}\right)^2\right] \tag{6.2}$$

Here the standard notation as in [1] is used: P_{in} is the average input power, C is the chirp of the pulse, T_0 is related to the full half-width at half maximum (FWHM) by the relation $T_{FWHM}=2(\ln 2)^{1/2}T_0$. From (6.2) we can see that the chirp is related to phase ϕ of the pulse as $C=-\frac{1}{2}\frac{\partial^2\phi}{\partial t^2}$.

If we consider an unchirped pulse ($C=0$) and propagate it through a fibre with negligible β_3 term, the solution of the pulse-propagation equation (6.1) can be easily found:

$$A(z,t)=\frac{\sqrt{P_{in}}T_0}{\left[T_0^4+\beta_2^2z^2\right]^{1/2}}\exp\left[-\frac{t^2(T_0^2+i\beta_2 z)}{2\left[T_0^4+\beta_2^2z^2\right]}\right] \tag{6.3}$$

It is easy to show from (7.3) that the chirp of the output pulse is $C(z)=\frac{\beta_2 z}{2\left[T_0^4+\beta_2^2z^2\right]}$. It means that the chirp value of the unchirped initial Gaussian pulse propagated through a fibre with zero third-order dispersion coefficient satisfies the following: $-\frac{1}{4T_0^2}\le C\le\frac{1}{4T_0^2}$.

Figure 6.1 shows the chirp area covered with Gaussian pulse propagation though a fibre.

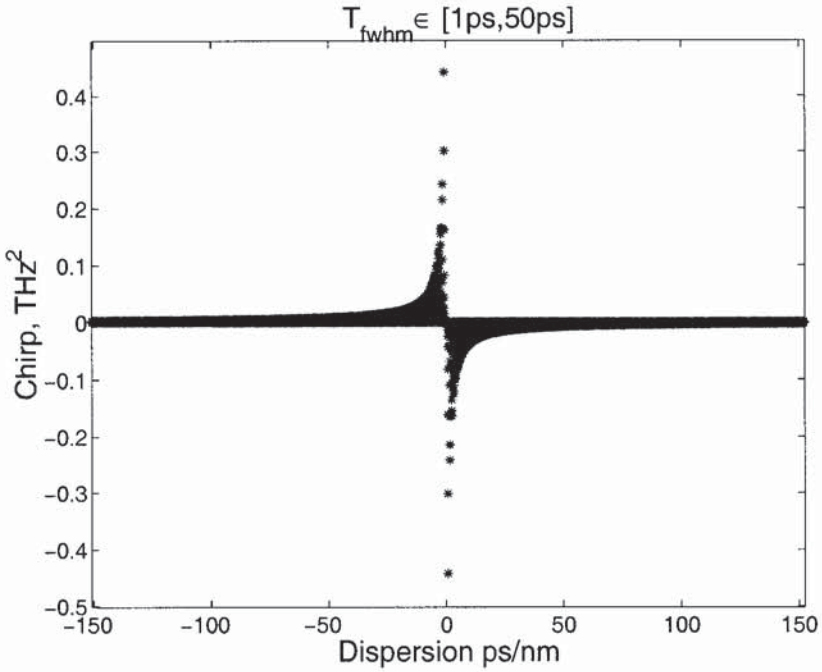

Fig.6.1 Chirp area covered after propagation of Gaussian pulses of different width through fibres with negligible third-order dispersion coefficient.

We can see that the output pulse remains Gaussian with the width $T_{out} = T_0 [1+(\beta_2 z / T_0)^2]^{1/2}$.

6.3 FBGs as filters and chirping devices

Consider an FBG that acts simultaneously as a bandpass Gaussian filter and as a linear dispersive element of the second- and third-order with the transfer function $T(\omega) = \exp[-\omega^2/(2\Omega_f^2) + i\, 0.5\, \alpha_{FBG}\, \omega^2]$, where Ω_f is a bandwidth of the FBG and α_{FBG} relates to the second-order dispersion coefficient. Such a two-in-one device produces a pulse with the output chirp as $C_{out} = 0.5\alpha_{FBG} / [(T_{in}^2 + \Omega_f^{-2})^2 + \alpha_{FBG^2}]$ and the pulse width as $T_{out}^2 = T_{in}^2 + \Omega_f^{-2} + \alpha_{FBG^2} / (T_{in}^2 + \Omega_f^{-2})$. Assuming equal output chirps, the ratio between the widths of the output pulses FBG and fibre is given by

$$\frac{T_{out_{FBG}}^2}{T_{out_f}^2} = \frac{\alpha_{FBG}}{\alpha_f} \frac{T_{in}^2}{T_{in}^2 + \Omega_f^{-2}}. \tag{6.4}$$

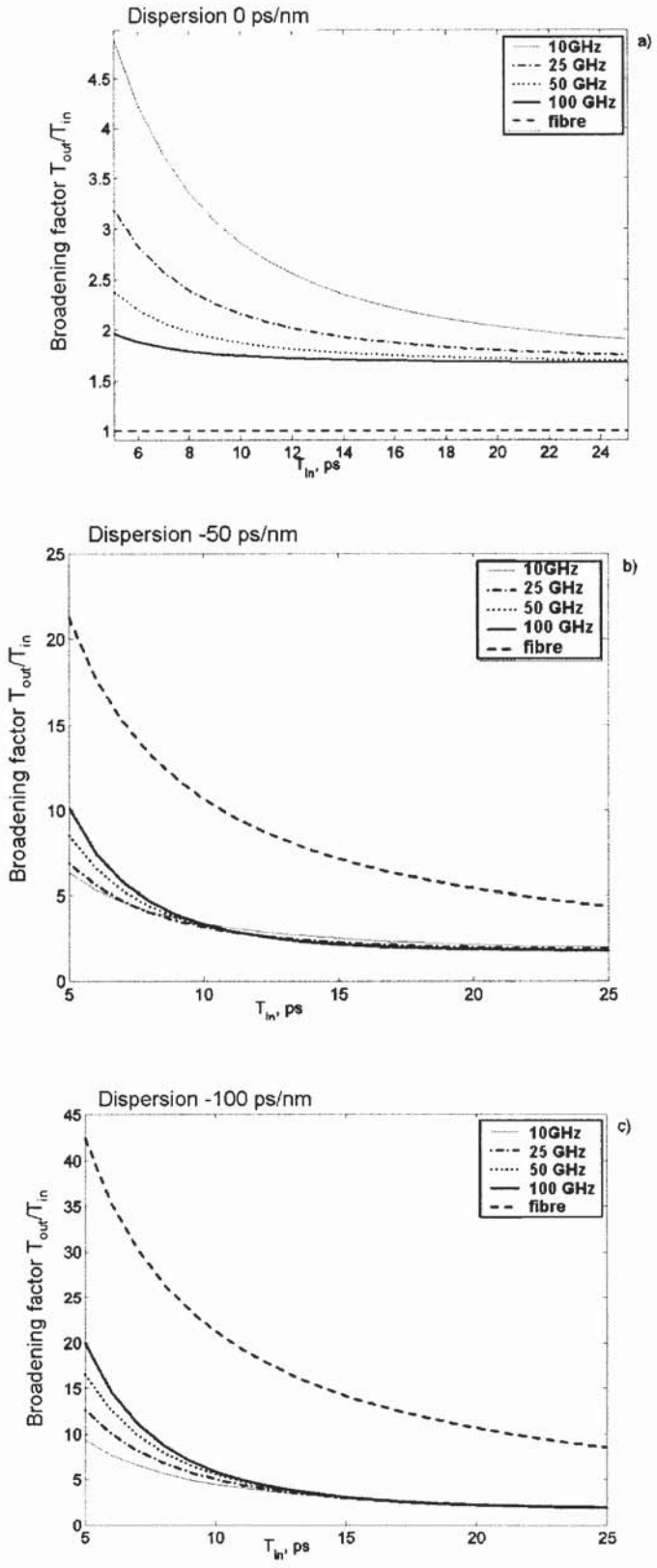

Fig.6.2 Broadening factor (T_{out}/T_{in} at FWHM) for different grating bandwidths versus FWHM of input pulse: a) dispersion 0 ps/nm, b) -50 ps/nm, c) -100 ps/nm.

Figure 6.2 shows how the broadening factor (the ratio between the FWHM of the output and input pulses) depends on the grating bandwidth and the dispersion coefficient. It is seen that for large enough dispersion, the use of a fibre with the same dispersion leads to a larger broadening. The pulse chirping using an FBG could be an attractive solution when it is desirable to chirp the signal without significant broadening.

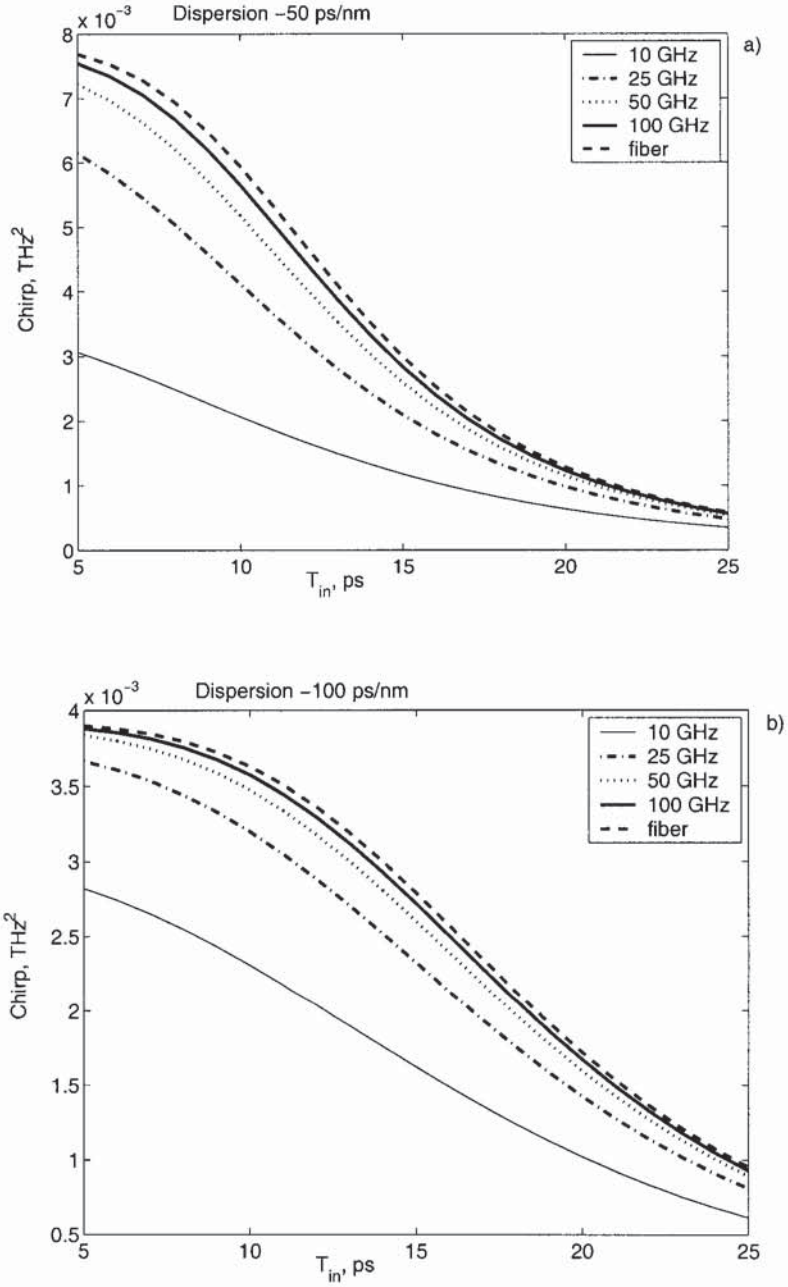

Fig.6.3 Chirp for different grating bandwidths versus FWHM of input pulse.
a) dispersion -50 ps/nm, b) -100 ps/nm.

Figure 6.3 shows the chirp of the output pulse. It is seen e.g., that FBG with the bandwidth of 100 GHz compared to a fibre with the same dispersion produces pulses with a similar chirp, but narrower output pulse width (Fig. 6.2).

6.4 Design and characteristics of FBG with V-shaped dispersion profile

Powerful design methods [26, 28], like the inverse-scattering algorithm make it possible to synthesize FBGs with a desired reflection response and phase control. Our target grating response would be:

$$H_R(\delta) = \sqrt{0.95}\exp(-(\delta/\delta_B)^4)\times\exp(-j(\beta''/2!)L((c/n_{eff})\delta)^2))\times \exp(-j(\beta'''/3!)L((c/n_{eff})\delta)^3)) \quad (6.5)$$

where δ is the detuning parameter between the wave-number of counter-propagating waves and the reference Bragg wave number, δ_B corresponds to the grating bandwidth (here 100 GHz at -3 dB), β'' and β''' are the second- and third-order dispersion coefficients for the fibre, L is the link length, c is the speed of light in vacuum and n_{eff} is the average effective refractive index. By varying the values of β'' and β''' it is possible to achieve different dispersion profiles of the grating response spectrum, including the desired V-shaped or Λ-shaped profile. The β''' coefficient is responsible for the dispersion slope; and the β'' coefficient- for the V or Λ peak positions. To achieve V or Λ dispersion shapes we just use $+\beta'''$ and $-\beta'''$ values correspondingly for positive and negative values of the detuning parameter δ. Figure 6.4 shows the reflection profile (a), group delay response (b) and the dispersion profile (c) of the designed grating. Fig. 6.4d presents the distributed coupling coefficient of the grating.

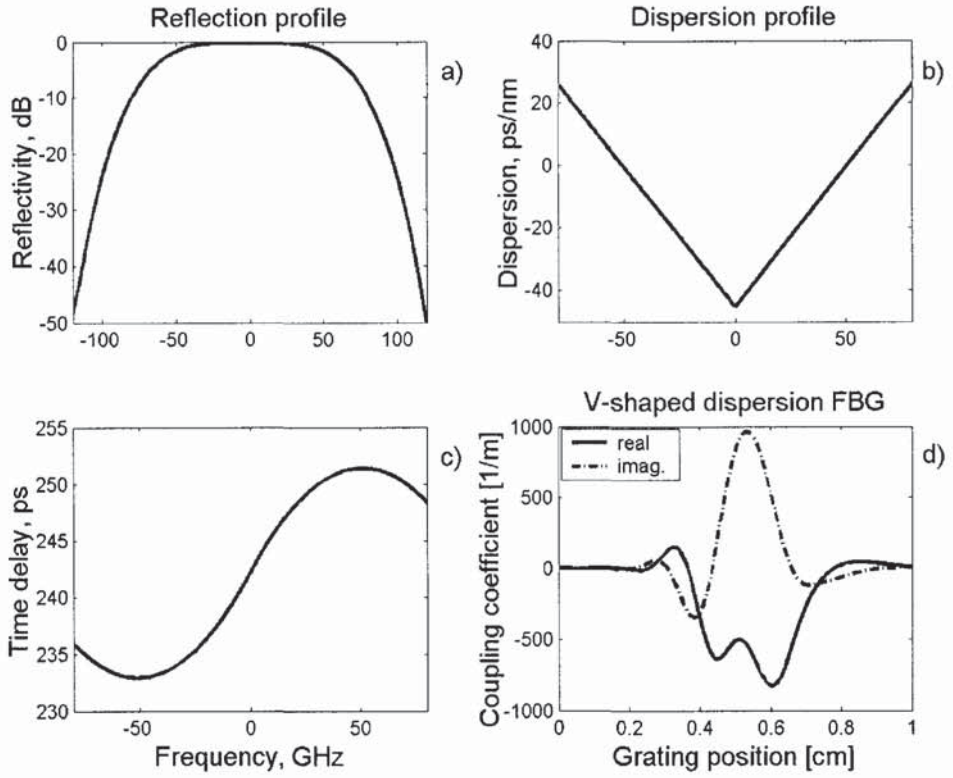

Fig.6.4 FBG with V-shaped dispersion: a) reflection profile b) dispersion; c) group delay; d) coupling coefficient of the FBG (solid-real part, dashed- imaginary part).

6.4.1 V-shaped grating performance in signal processing

Now I examine the performance of the FBG with a V-shaped dispersion in a pre-chirping of transform limited pulses. Here I compare four types of FBGs having exactly the same reflection profile (super-Gaussian, with a bandwidth of 100 GHz at -3 dB as shown in Fig.6.4a), but with different types of dispersion characteristic: constant (two different values), linear dispersion slope (dashed line) and V-shaped as explained in Fig.6.5a (solid line).

Two values of the constant dispersion have been chosen for comparison as shown in Fig. 6.5a: first, with the dispersion corresponding to the dispersion of the V-shape FBG at the bending point (dashed and dotted line, FBG CD1), and the second – with the dispersion value close to the average dispersion of the V-shaped FBG over the grating bandwidth (FBG CD2). Group delays of the considered set of gratings are shown in Fig. 6.5b.

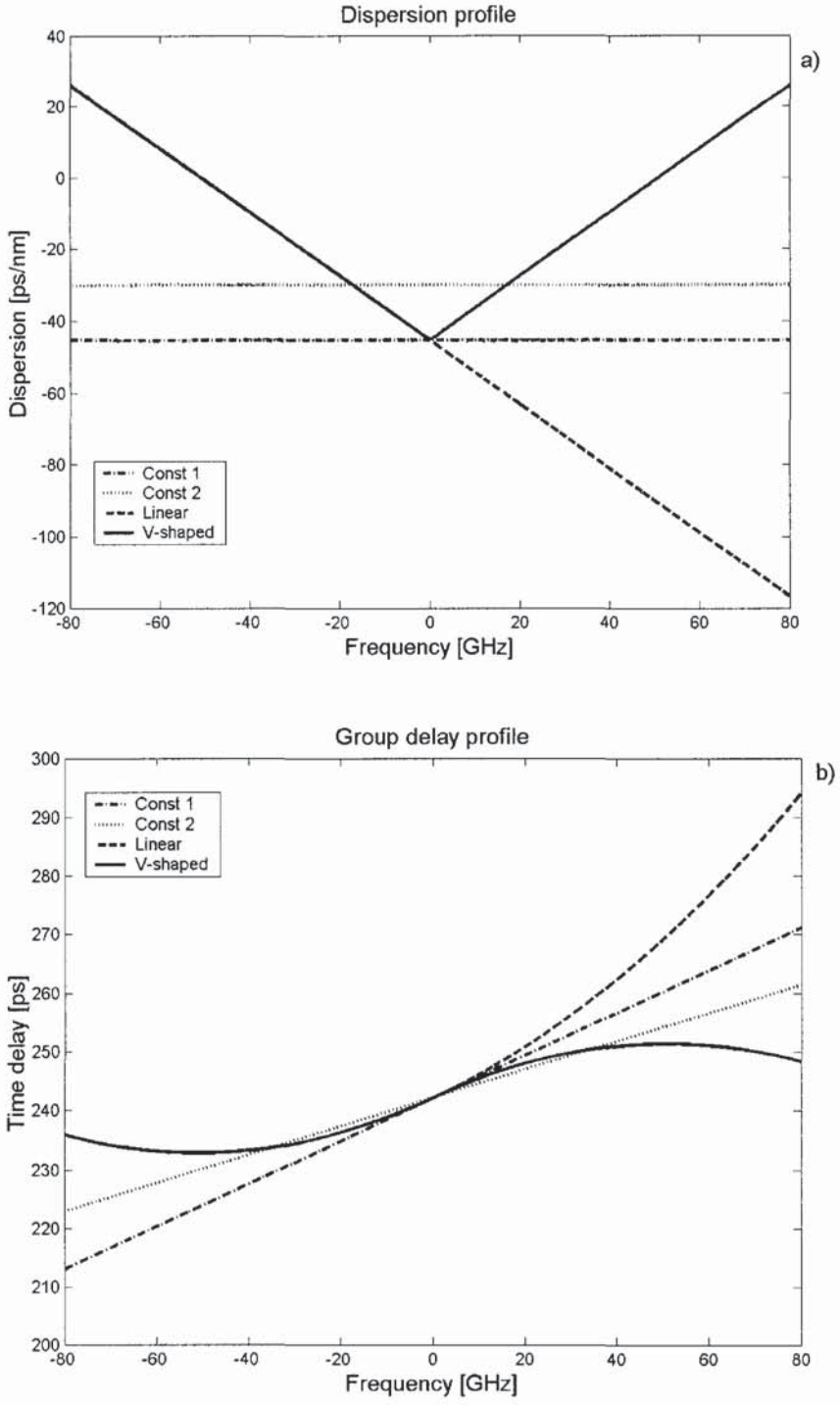

Fig 6.5 Four types of FBGs considered: a) dispersion profile; b) group delay.

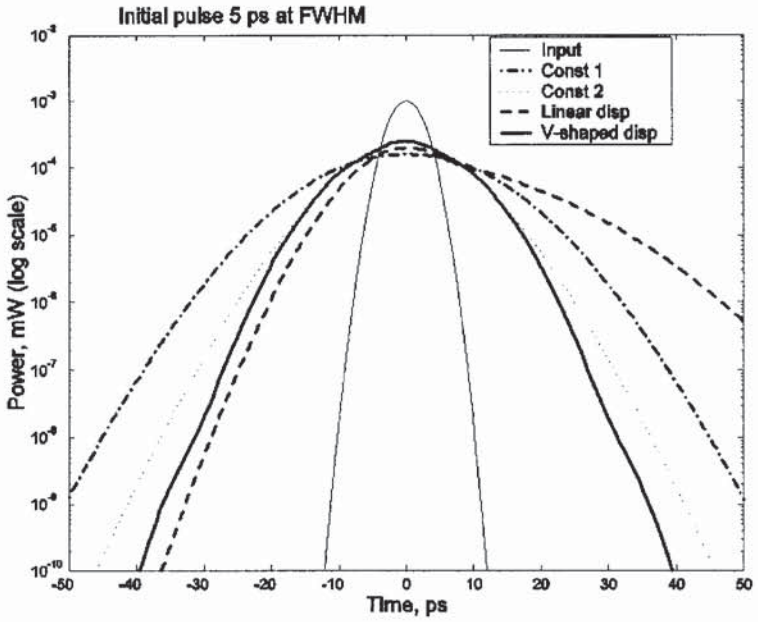

Fig. 6.6 Comparison of pulses transmitted through four types of FBGs.

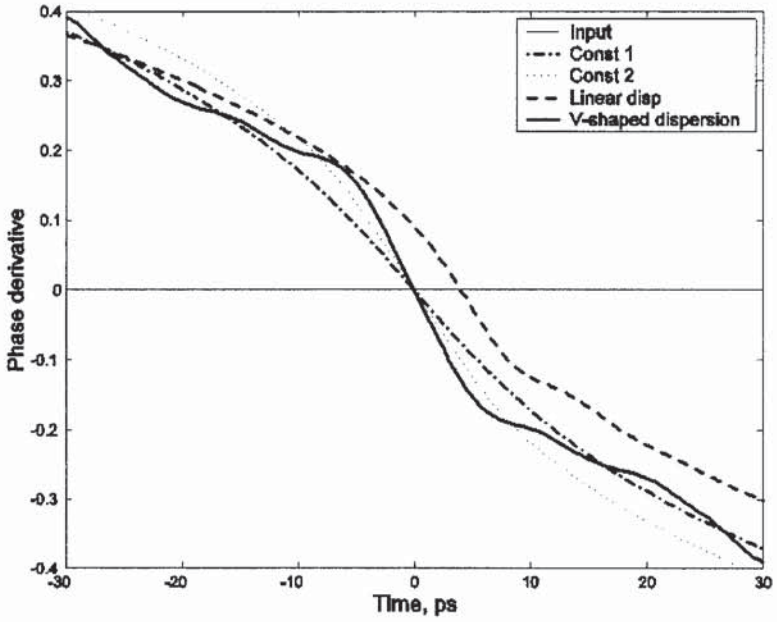

Fig 6.7 Phase derivative of pulses transmitted through different types of FBGs.

Fig. 6.6 shows power distributions, and Fig. 6.7 shows phase derivative of an initially un-chirped pulse at the outputs of the four FBGs described above. Firstly, note that, as expected, the FBG with linear dispersion (non-zero dispersion slope) introduces an asymmetry into the signal evolution (dashed

line), whilst those with constant (dotted, and dashed and dotted lines) and V-shaped dispersions (solid line) preserve pulse symmetry.

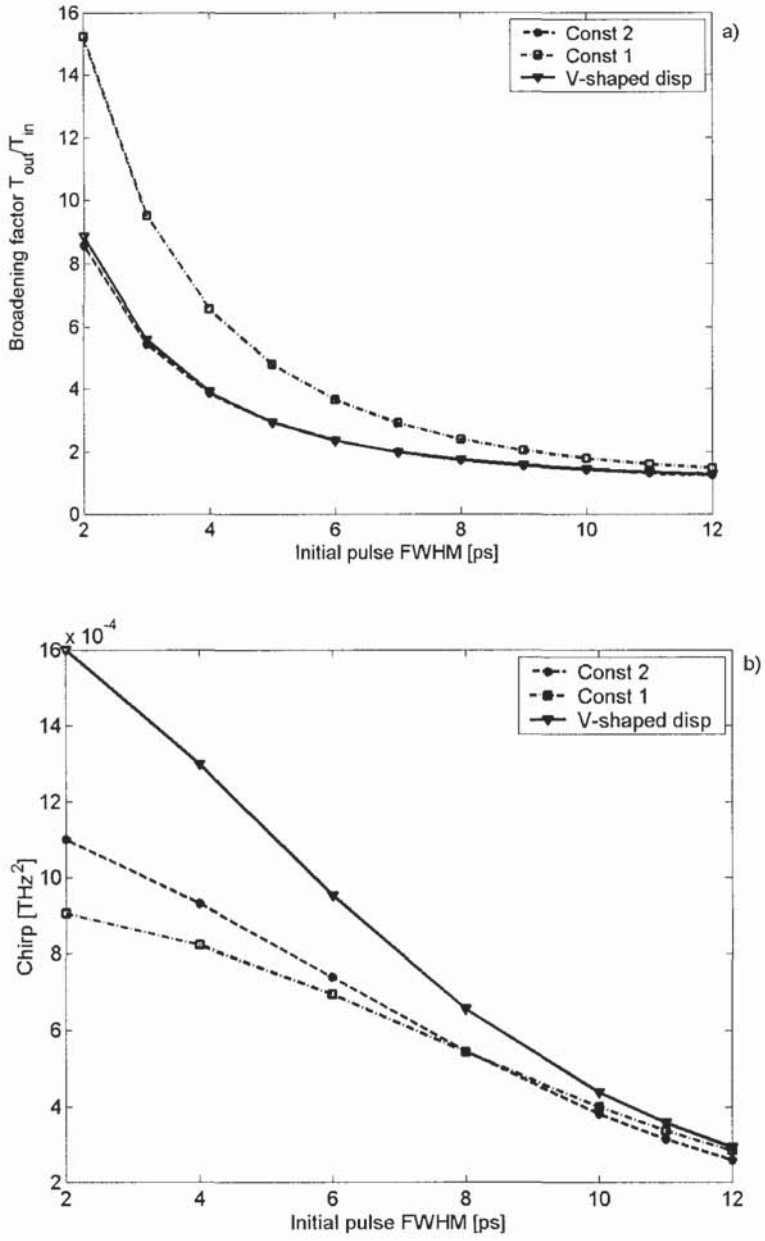

Fig.6.8 Comparison of the broadening factors for pulses propagated through different FBGs (a) and chirps acquired (b).

Secondly, it may be seen from Fig. 6.8 that the V-shaped FBG produces a larger chirp on the signal whilst keeping the pulse width (FWHM) at the same level, or even below it, compared to the FBGs with constant dispersion.

Figure 6.8 quantifies this comparison for various input pulse widths. It can be seen from Fig.6.8 that the FBG with V-shaped dispersion outperforms gratings

with constant dispersions. Namely, FBG with V-shaped dispersion produces a larger chirp of the output pulse, while having the similar (compared to FBG CD2) or even less (compared to FBG CD1) pulse width broadening factor compared to the grating with constant dispersion. This effect is more pronounced for shorter pulses.

6.4.2 *V-shaped gratings as pre-chirping elements*

To evaluate the performance of V-shaped FBGs as pre-chirping elements, without loss of generality, consider a single channel SMF/DCF transmission line shown in Fig.6.9. Here the V-shaped FBG and constant dispersion FBG are used as optical pre-chirping elements.

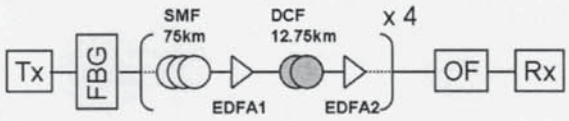

Fig.6.9 Transmission system used for evaluation of FBGs' performance.

A transmission map consists of four spans of SMF(75 km) + EDFA(15 dB, noise figure *NF* = 4.5 dB)+DCF (12.75 km) + EDFA (8.2875 dB, a noise figure *NF* = 4.5 dB). The combination of 75 km of single mode fibre (SMF with dispersion 17ps/(km-nm), dispersion slope 0.07 ps / (km-nm$^{2)}$ and the fibre loss 0.2 dB/km in the wavelength region near 1.55 μm) and 12.75 km of dispersion compensating fibre (DCF with dispersion -100ps/(km-nm), dispersion slope -0.41 ps/(km-nm$^{2)}$) and the fibre loss 0.65 dB/km in the wavelength region near 1.55 μm) is specially designed to slightly compensate both dispersion and dispersion slope from the transmission through SMF. The cumulative dispersion of the line is 280ps/nm. Different FBGs (with constant dispersion of -270 and -280 ps/nm or (for comparison) V-shaped with steep dispersion slope and average dispersion about -280 ps/nm) are placed at the beginning of the line as dispersion pre-compensation elements. Optical filter with 100 GHz bandwidth is used at the receiver. Figure 6.10 shows that V-shaped grating operates not only as a signal pre-chirping element, but also as a pulse shaper. The V-shaped grating flattens the carrier waveform while produce the same chirp as the conventional FBG.

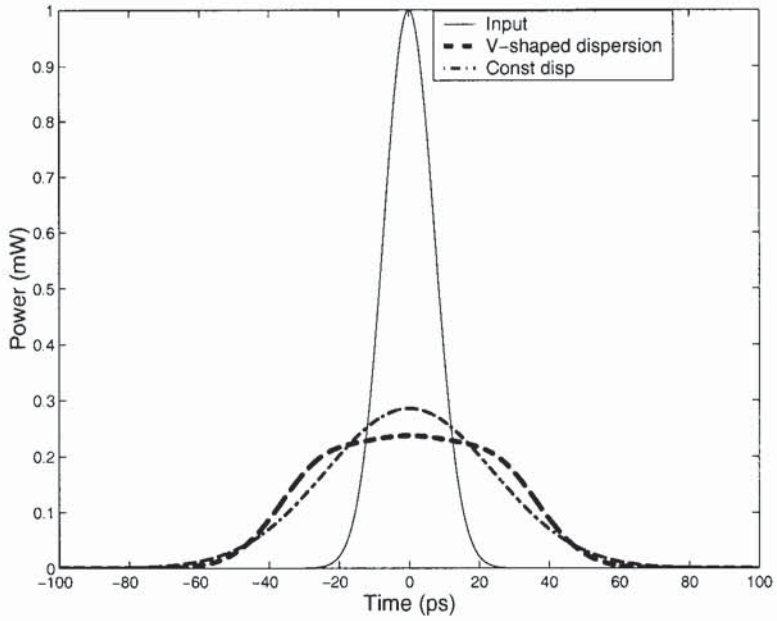

Fig.6.10 Gaussian pulse of 17 ps (solid line) propagated through V-shaped FBG (dashed line) and through FBG with constant dispersion (dashed and dotted line).

Without any loss of generality, consider the transmission of an RZ signal at 40Gbit/s channel rate. A transmission performance was evaluated using a standard Q-factor technique based on $2^{10} - 1$ pseudorandom binary sequence data signal. Measurements of Q factor values after the propagation over 4 spans (300 km) of the SMF fibre are used for evaluation of the grating performance.

Figure 6.11 demonstrates the Q factor values versus the cumulative dispersion of the line after the propagation of the Gaussian pulse (with the FWHM of 17ps and 0.5mW (-3 dBm) input power) through the transmission line. I used a low pulse input power to avoid nonlinear effects of the considered transmission system. It is seen that for this particular link, the V-shaped FBG (solid line) performs slightly better than FBGs with constant dispersion (dashed and dotted line).

Due to a few number of parameters used in designing FBGs with V-shaped dispersion profile, (like a dispersion slope, a peak position, bandwidth), it is impossible to state which is the best one for a particular application. Evidently, there are many situations when V-shaped gratings performance will be not that different from the performance of conventional FBGs. The

goal of this work is to demonstrate that for some applications V-shaped gratings could be rather beneficial.

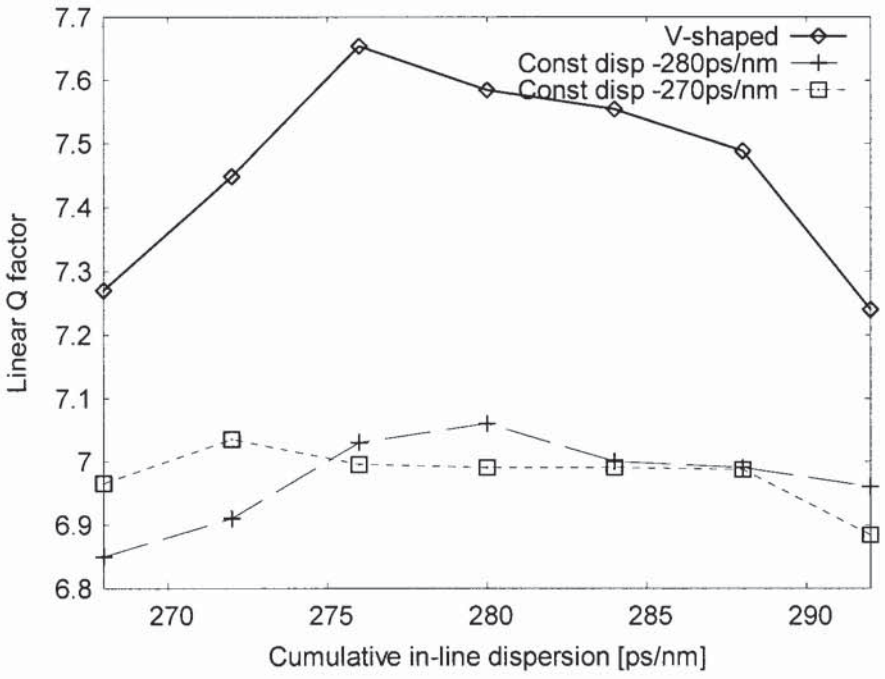

Fig.6.11 Q factor versus cumulative in-line dispersion for V-shaped FBG (solid line) and FBGs with constant dispersion (dashed and dotted lines).

Considering an application of V-shaped FBGs as optical filters for multiplexing / demultiplexing it is easy to observe some advantages of such devices over the filters based on FBG with constant dispersion or linear (with non-zero slope) dispersion. By detuning V-shaped FBGs filters around the carrier frequency, one can change the dispersion compensation value (like linear dispersion filters) without worrying too much about the sign of the detuning (as opposite to the case of the constant dispersion filters). This property of the FBGs with V-shaped dispersion profile can be widely used in WDM transmission systems. For instance, as it has been demonstrated in [93], using dense wavelength-division multiplexing at 10 Gbit/s channel rate complemented by periodic-group-delay dispersion compensation it is feasible to achieve distances of 9000 km with uncorrected (no forward error correction) bit error rates of 10^{-8}. Potentially, the proposed V-shaped gratings implemented in a multi-channel version can serve as such periodic group-delay compensators.

6.5 Experimental results

For the fabrication of the FBG (as described in Fig.6.4), the coupling coefficients $q(z)$ of the grating have been used for rewriting the refractive index profile in terms of apodisation $h(z)$ and period change $\Lambda(z)$, where the grating period is introduced in a way $2\pi / \Lambda(z) = 2\pi / \Lambda_0 + d\arg(q(z))/dz$. The apodisation of the grating is $h(z)=|q(z)|\lambda_B/(2\pi\eta)$.

The proposed V-shaped dispersion fibre Bragg grating was fabricated with a UV direct writing system at Aston University [94]. The structure was written in hydrogen loaded photosensitive SMF-28 fibre with a writing speed of 0.125 mm/s. The grating was finally characterised with the Agilent Chromatics Dispersion Test Set (86073C). The wavelength resolution and the modulation frequency in the measurement were set at 2.5 pm and 250 MHz, respectively. The dispersion has been averaged over the 240 pm window, and the group delay average window was 10 pm.

Figure 6.12 shows the reflection profile (a), the time delay response (b) and the dispersion (c) of the fabricated and designed gratings. It demonstrates a reasonably good agreement between theoretical design and experimental fabrication results.

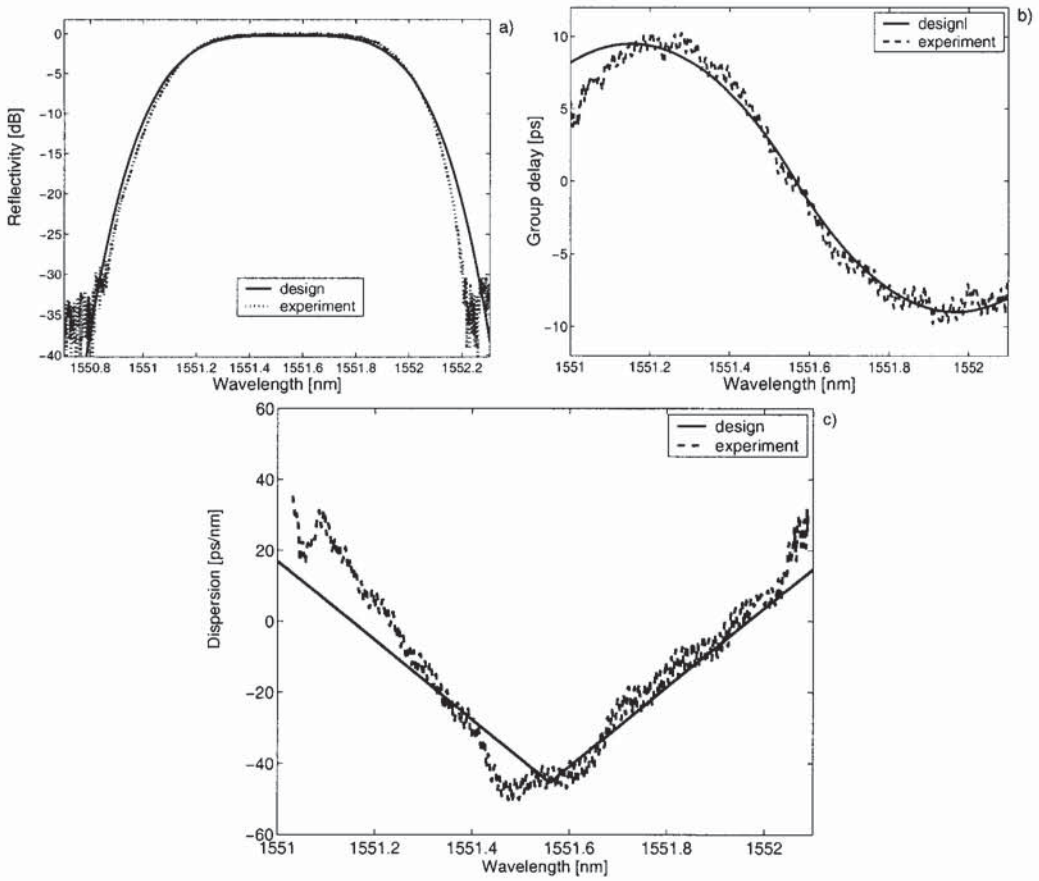

Fig.6.12 Comparison between designed and fabricated FBGs: a) reflection profile, b) group delay, c) dispersion (solid line-design, dashed- experiment).

We have proposed and have fabricated a new type of the fibre Bragg gratings with V-shaped dispersion. It has been demonstrated that the V-shaped FBGs have superior properties for optical signal manipulation and chirping compared to conventional FBGs with constant dispersion or with the dispersion slope. Application of the proposed V-shaped FBGs for signal pre-chirping in fibre transmission has been examined. We have observed an operational regime in which a V-shaped grating performs slightly better than a conventional FBG with constant dispersion.

7 Multi-channel dispersion compensation FBGs

This chapter presents design and fabrication of a novel design FBG for multi-channel dispersion compensation in communication links.

7.1 Introduction

Since 1980s, when WDM systems were introduced, there is a continuing demand for increasing system capacity by transmitting multiple channels over fibre links. This approach, however, has its limitations as an implementation of too many WDM channels (at low channel rates) might require a complex terminal equipment and might be a less competitive solution compare to fewer channels operating at higher bit rates. Therefore, an increase of system capacity by increasing a channel rate is an important direction in building cost-efficient high-capacity systems. The usage of higher bit rates, however, requires shorter pulses and a more accurate control of the dispersion in such systems. Therefore, the generation of fibre optic communication systems using high (40 Gbit/s and higher) channel rates is concerned with control of the fibre-dispersion. I discuss here an application of FBG in WDM systems for multi-channel dispersion compensation.

The multi-channel FBGs have recently attracted great deal of interest in WDM systems as dispersion and dispersion-slope compensators [12, 43] for tuneable post-processing at the receiver or in-line application as in [82]. Originally there was a sampling method proposed for fabrication of multi-channel FBGs [94], when a single-channel ("seeding") FBG has been sampled. In this method the amplitude and/or phase of the seeding grating is periodically modulated. There have been introduced different types of advanced sampling functions, which lead to periodic modulations in amplitude [28, 49], in phase [97-98] or in both amplitude and phase [55]. However, the designs based on the sampling methods have some disadvantages, like they can not provide an accurate channel presentation for strong gratings, also it is impossible to create different complex channel spectrum for different channels. Conventionally, sampled fibre Bragg gratings have both a

channelised reflection band (*i.e.* multiple reflection bands) and channelised dispersion spectrum. Although channelised reflection bands can add a filtering function, in some cases their presence also reduces the efficiency of the usage of the spectrum [99].

Here we present a novel design of advanced FBGs with multi-channel dispersion and dispersion-slope compensation (see an example in Fig. 7.3) but with a single reflection band.

7.2 Design and fabrication of multi-channel "zigzag" dispersion FBG

Consider an FBG with 400 GHz bandwidth (at -3 dB level) with reflectivity 95%. The dispersion profile of the grating is divided into 8x50 GHz channels with dispersion variation over 500 ps/nm throughout each channel (see Fig.7.1). The desired reflection profile for *2N* channels (*N=4* in our case) is:

$$H_R(\beta) = \sqrt{0.95}\exp(-(\beta/\beta_T)^4)\times \sum_{m=0}^{N-1}\left[\begin{array}{l}\delta(\beta_m)\exp(-j(\beta''/2!)L((c/n_{eff})\beta_m)^2))\times \\ \exp(-j(\beta'''/3!)L((c/n_{eff})\beta_m)^3))\end{array}\right] \quad (7.1)$$

Here β is a detuning parameter between the wave-number of counter-propagating waves and the reference Bragg wave-number, β_T corresponds to the grating reflection bandwidth (here 400 GHz at -3 dB), $\beta_m = \beta - \beta_S * (m - N + 0.5)$ for $m = 0 \ldots N-1$, β_S corresponds to a single channel bandwidth (here 50 GHz), $\delta(\beta_m)$ is a delta function, β'' and β''' are the second- and third-order dispersion coefficients for the fibre, L is the link length, c is the speed of light in vacuum and n_{eff} is the average effective refractive index. The coefficients β''' and β'' determine a dispersion slope and zigzag peak positions correspondingly. To obtain a zigzag dispersion profile of the grating response we just use different signs of β''' coefficient for negative and positive values of detuning parameters β_m, (e.g. $+\beta'''$ for positive β_m and $-\beta'''$ for negative β_m). By varying β''' third-order dispersion coefficient, it is possible achieve different steepness of the dispersion slope, but there are restrictions on β'' second-order dispersion coefficient values as we want to obtain a smooth line for the group delay response.

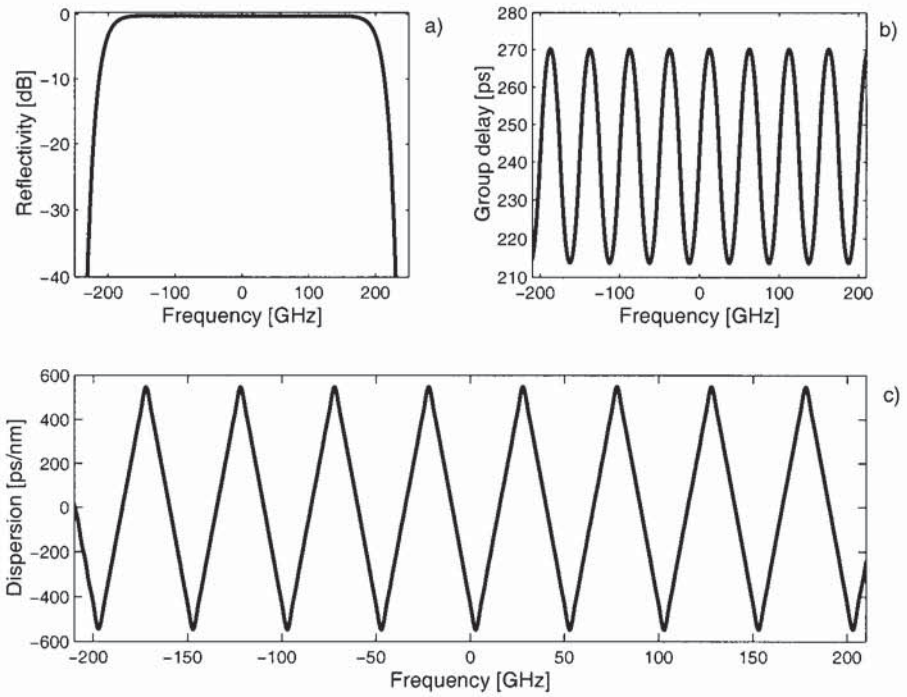

Fig.7.1 Spectrum response of 8-channel FBG.

Figure 7.2 demonstrates the grating profile, which was designed using the layer peeling algorithm with the target reflection described in (7.1); its response is shown in Fig.7.1.

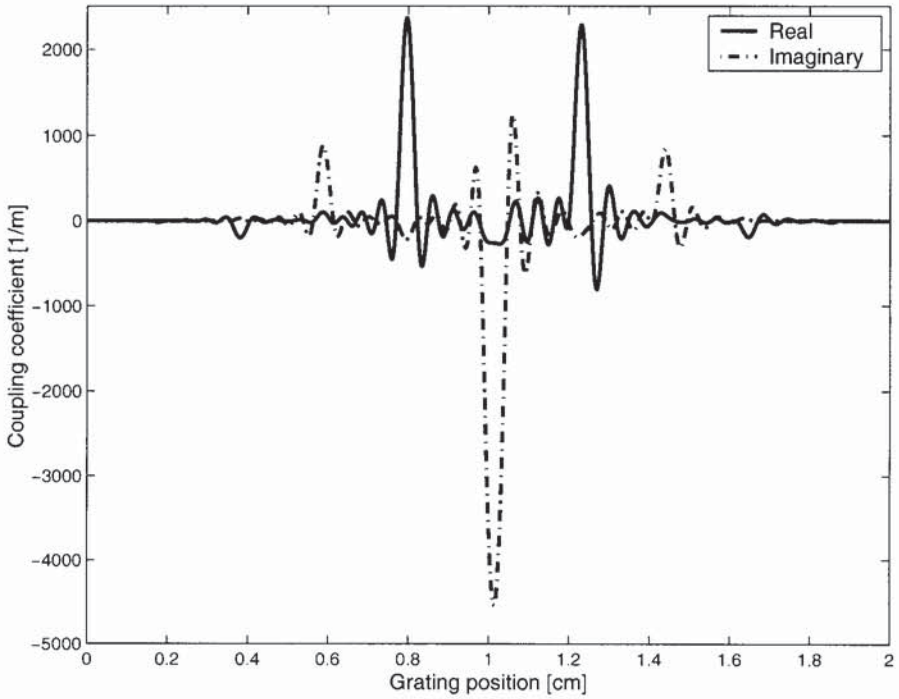

Fig.7.2 FBG with 8-channel symmetric dispersion compensation (solid line-real part, dashed and dotted line- imaginary part of the coupling coefficient).

The designed grating is non-trivial and rather challenging for fabrication, so for an experimental test we decided to reduce the number of channels to four. The corresponding designed grating looks less complex, but still not simple (see Fig. 7.3).

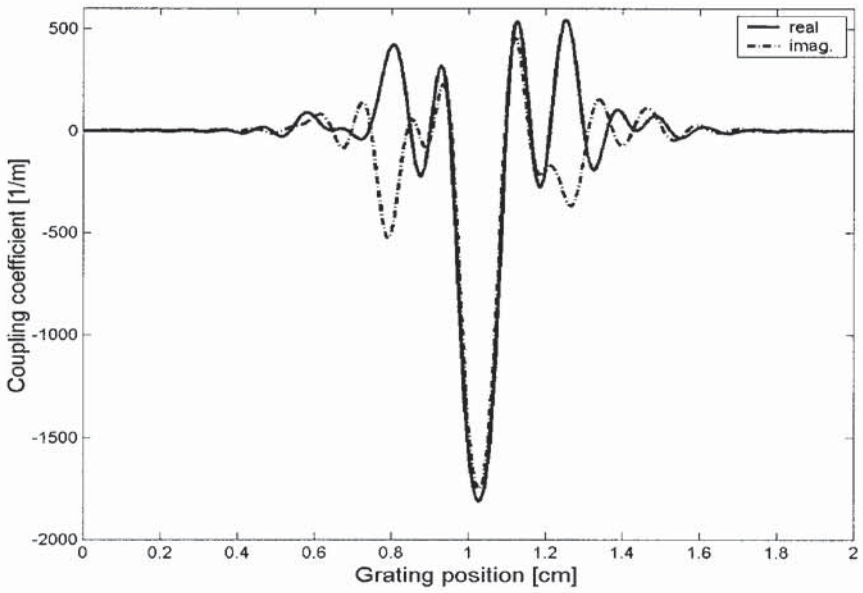

Fig.7.3 FBG with four-channel dispersion compensation: (solid line - real part, dashed - imaginary part of the distributed coupling coefficient).

The target grating response is a super-Gaussian 4^{th} order profile with the bandwidth 200 GHz at -3 dB and a central wavelength 1550 nm (see Fig. 7.4a solid line), with reflectivity of 95% (to have a strength of approx. 13 dB). Grating's group-delay (dispersion) profile is divided into 4x50 GHz channels with the dispersion variation range about 500 ps/nm throughout each channel (Fig. 7.4c, solid line).

However, a good agreement between designed and first samples of fabricated FBGs has been achieved (see Fig 7.4).

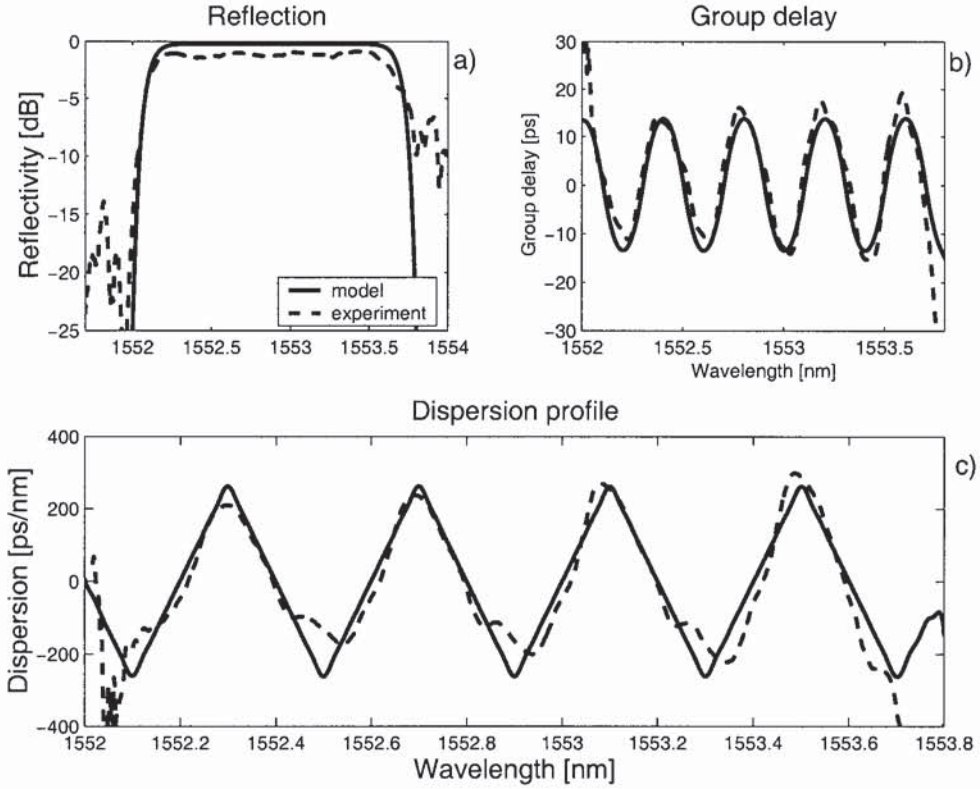

Fig.7.4 Spectra comparison of the designed and fabricated FBGs: a) reflection, b) group delay, c) dispersion profile (solid-design , dashed- experiment).

7.3 Design of FBG with multi-channel asymmetric dispersion compensation

The next stage was to try to design and fabricate an asymmetric dispersion compensation multi-channel FBG with the following target profile (Fig. 7.5). These kind of grating can be used in 10 Gb/s WDM transmission systems for dispersion compensation.

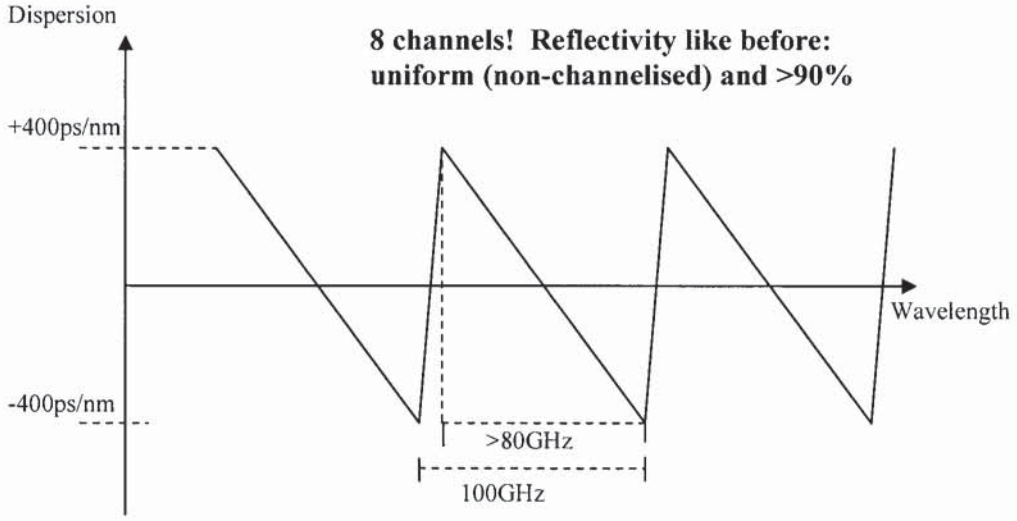

Fig.7.5 Target profile of asymmetric multi-channel dispersion.

To achieve this dispersion profile I use different values of β''' coefficient for two different dispersion slopes. According to Fig.7.5, the coefficients β''' used for steeper slope (lets call it β'''_{left}) must be four times larger than the other one (β'''_{right}) and the peak positions of the dispersion variation are shifted from the channel carrier frequency. It also imposes more restrictions on the corresponding value of β'' coefficient as it is even more difficult to achieve smoothness in the group delay and dispersion profile. Simple calculations show that the value of β'' coefficient depends on the value of β'''_{left} as $\beta'' = 6 * (100GHz - 80GHz) * \beta'''_{left}$.

The FBG designed using the DLP algorithm looks even more complex and challenging to fabricate (Fig. 7.6), but its spectrum profile (Fig. 7.7) satisfies all the requirements described in Fig. 7.5.

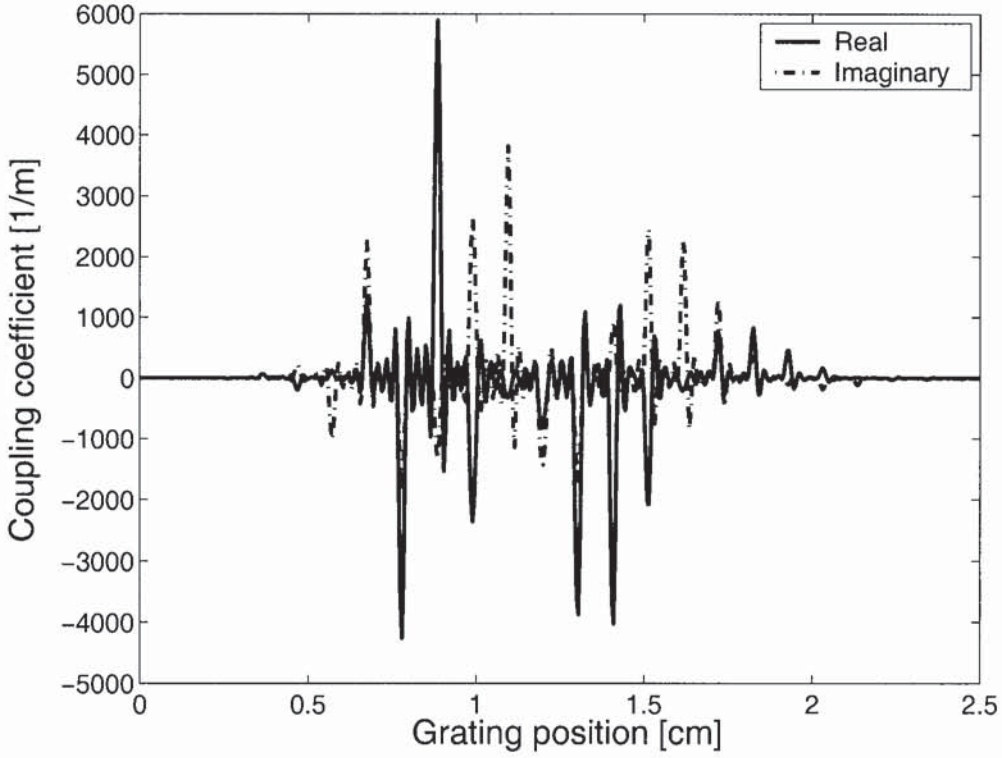

Fig.7.6 Coupling coefficient of an asymmetric dispersion compensation 8-channel FBG.

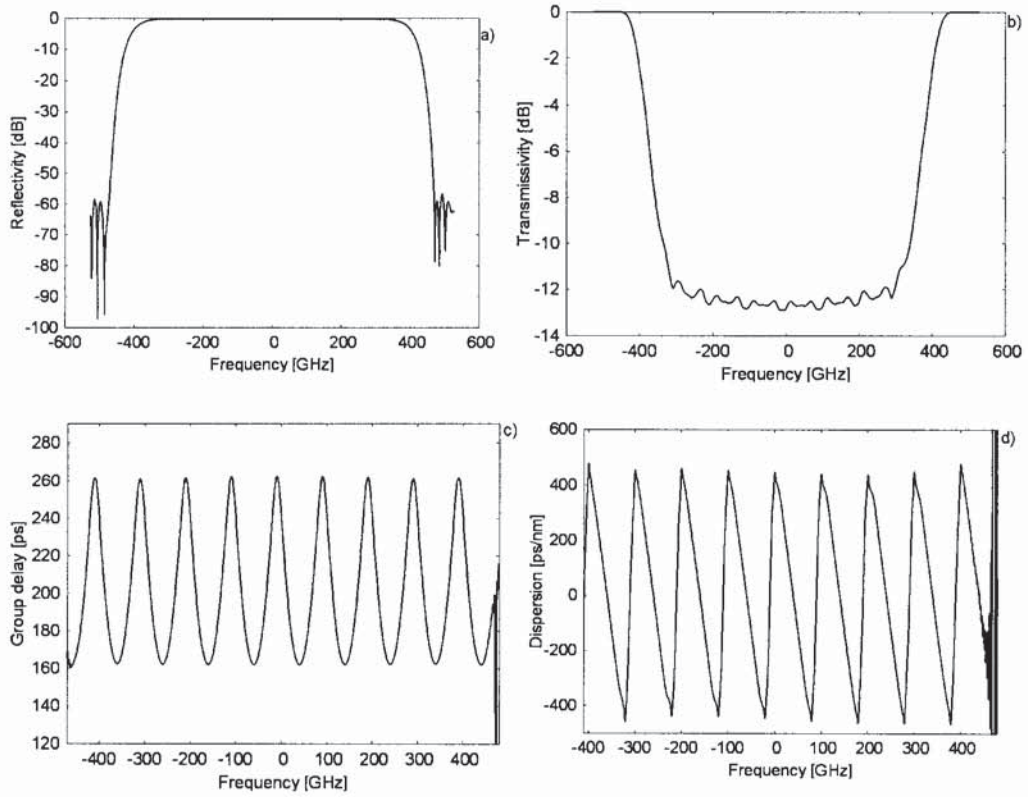

Fig. 7.7 Spectrum of asymmetric dispersion compensation multi-channel FBG: a) reflectivity; b) transmissivity; c) group delay; d) dispersion profile.

Again, for an experimental test we used a 4-channel asymmetrical FBG, which structure is less complex (Fig.7.8)

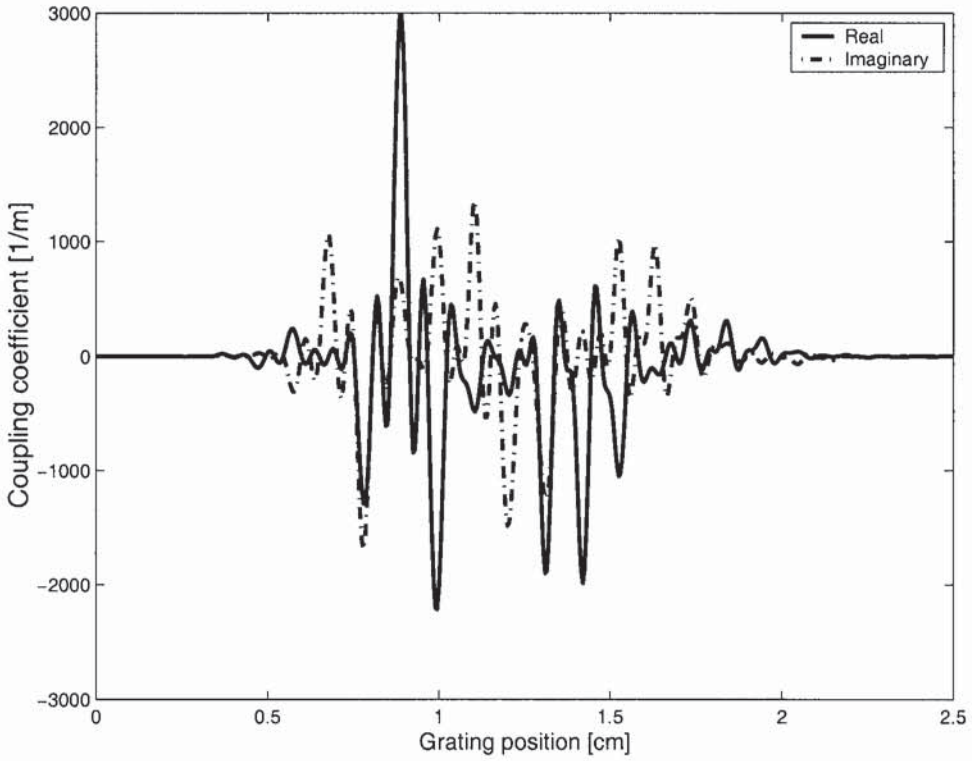

Fig. 7.8 Coupling coefficient of FBG with 4-channel asymmetric dispersion compensation.

Figure 7.9 shows the reflection profile (top), the dispersion (bottom) of the fabricated and designed gratings [100]. The resulted broadband grating has four channels with a channel spacing of 100 GHz. For each channel, the grating has a quadratic group delay and a linear dispersion with average slope of about -1450 ps/nm^2. Though the ripples in the experiment for both the reflectivity and dispersion are worse than in the theoretical model, the agreement between them is still reasonably good.

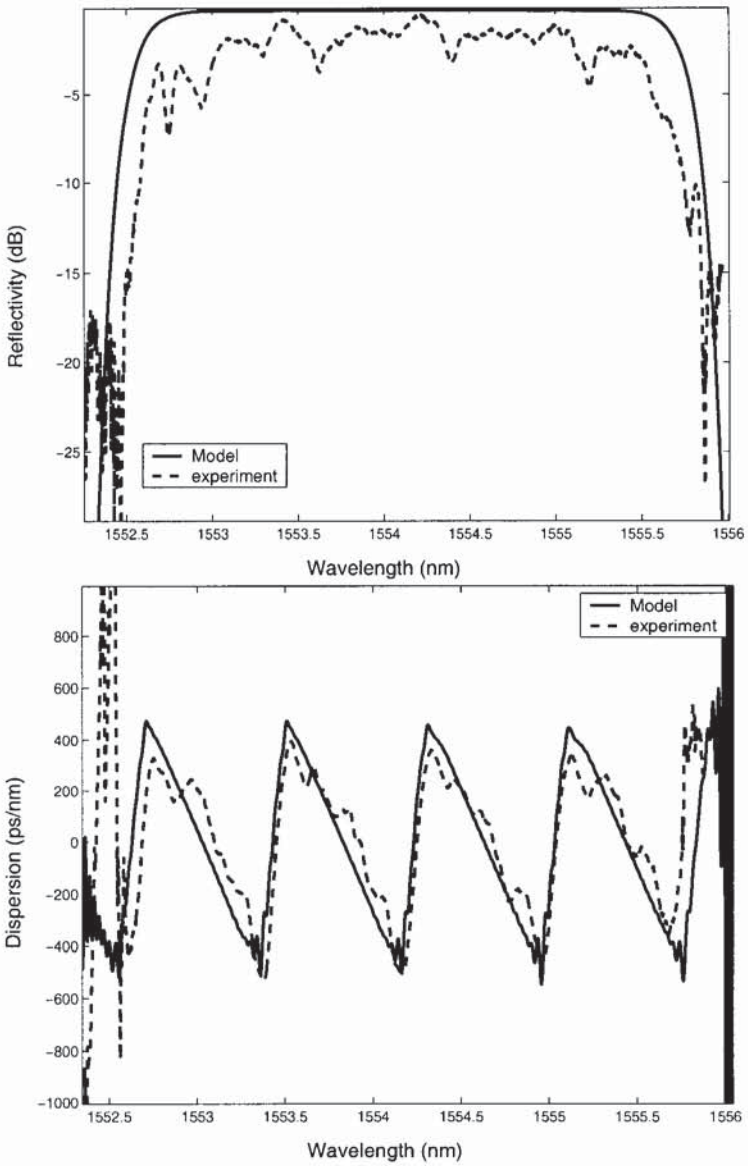

Fig.7.9 Reflection (top) and dispersion (bottom) comparison between designed and fabricated FBGs (solid line-design, dashed- experiment).

The demonstrated gratings were fabricated using a continuous-writing system developed at Aston University similar to [101]. This system allows one to write FBG plane by plane and to control the apodisation and period of the FBG continuously along the grating length. The UV writing beam (244 nm) was generated from a frequency-doubled Argon ion laser. The beam size was reduced to tens of micrometers and a small portion of a uniform phase mask was used to generate interference fringes in the experiment. The fibre (SMF-28) was mounted on an air-bearing translation stage moving at constant speed with good stability and accuracy. The apodisation profile and the varied

period were realised by appropriately controlling the ON/OFF of an acousto-optic modulator and synchronically moving the fibre. The structure was written in hydrogen loaded photosensitive fibre with the writing speed of 0.01 mm/s. The grating was finally characterised with the Agilent Chromatics Dispersion Test Set (86073C). The wavelength resolution and the modulation frequency in the measurement were set at 2.5 pm and 250 MHz, respectively. The dispersion data were averaged over 200 pm window, whereas the group delay average window was 80 pm. Due to the system constrains, local period variations of the gratings can't exceed +/- 3 nm. In order to keep the period variations within required range, I had to reduce the number of points in the designed coupling coefficients profiles. However it affects the quality of fabricated gratings.

In summary, a novel class of broadband fibre Bragg gratings with channelised dispersion but a single reflection band has been presented. The gratings of this type have advantage over the gratings with both channelised reflection and dispersion. Even when channelised reflection bands can add a filtering function, in some cases their presence also reduces the efficiency of the usage of the spectrum. Moreover, the dispersion may exhibit sharp changes near the band edges, which limits the overall device performance, especially when combined with the inevitable insertion loss. The designed gratings can be used for tunable dispersion compensation [99], 2R regeneration (pulse reamplification and reshaping) [102], and collision-induced timing jittering reduction [103].

8 Conclusions and future work suggestions

8.1 Conclusions

This thesis has presented a study of advanced fibre Bragg gratings. Starting with the coupled-mode theory I described a fibre Bragg grating model, methods of synthesis and the characterisation of FBGs. Several novel applications of FBGs along with the new types of specifically designed FBGs have been presented in this thesis.

The main achievements and results of the presented work are:

1) The numerical codes based on the layer-peeling algorithm and the transfer matrix method, capable of designing advanced fibre Bragg gratings with the desirable grating's reflection and transmission spectrum has been developed and implemented.

2) I have investigated the impact of a simplified grating structure on the performance of the flat-top dispersionless FBG-based filter, when a different number of sections of the grating structure. New designs of advanced FBGs for compensation of the third and fourth-order dispersion have been demonstrated.

3) A new design of asymmetric FBG-based filters for ultra-narrow filtering in DWDM systems has been proposed and demonstrated. The performance of the designed filters in a typical fibre link has been investigated. I carried out the optimisation of the system parameters, such as filter detuning, duty cycle, and steepness of the filter reflection function; then I compared the performance of the symmetrical Gaussian profile filter and specially designed asymmetrical filter. A feasibility of 8x40Gbit/s DWDM RZ transmission with 0.8 bit/s/Hz spectral efficiency (without polarization multiplexing and FEC) over 1287km of SMF/DCF link has been confirmed by numerical modelling.

4) A fundamentally new approach of designing FBG-based filters using a combination of two gratings operating in transmission has been proposed. We proposed a new ultra-narrow VSB filtering technique based on the double-notch filter, which presents a composite VSB filter that comprised of a pair of FBG's operating in transmission. The proposed filtering method has an advantage of low cost, together with the tuneability offered by FBG devices that could be especially important for large channel count DWDM systems. Using the proposed VSB filter a feasibility of 8 x 40 Gbit/s DWDM RZ transmission with 0.8 bit/s GHz spectral efficiency (without polarisation multiplexing and FEC (forward error correction)) has been demonstrated over 500 km of SMF/DCF link.

5) A new type of fibre Bragg grating with a V-shaped dispersion profile, which can produce a signal with a phase having different (controllable) behaviors at the center and at the pulse tails has been proposed. It has been demonstrated that the V-shaped FBGs have superior properties for optical signal manipulation and chirping compared to conventional FBGs with a constant dispersion or with a non-zero dispersion slope. The operational regime in which a V-shaped grating outperforms a conventional FBG with constant dispersion has been presented; when the proposed V-shaped FBGs were used for a signal pre-chirping in fibre transmission.

6) We proposed a novel design of multi-channel gratings with a "zigzag" (channelised) dispersion (with as symmetric as asymmetric profiles) and single (non-chanelised) reflection band. To design this type of grating a "synthesis" programming code has been substantially modified. The grating with multi-channel dispersion and single reflection band presents an advantage over the multi-channel sampled fibre Bragg gratings, which have both channelised reflection and dispersion, because for sampled FBGs dispersion may exhibit sharp changes near the band edges. It is the first time that such a grating has been designed and fabricated.

8.2 Future work suggestion

Fabrication of complex superstructured gratings requires a writing system, which allows a precise control of grating apodisation and phase along the length of the grating. It has been shown throughout the thesis that it is possible to write very complex FBGs using the direct writing technique. However, it is difficult to fabricate gratings, whose design requires large local period variations over a short grating length, like with multi-channel FBGs. One of the problems in designing multi-channel FBGs is how to achieve the highest quality spectrum response of the grating, including reflection profile, group delay and dispersion profile, without sacrificing the grating's strength. We have observed that by increasing the number of layers in the grating structure we improve the quality of grating spectrum response, but this simultaneously increases the period change variation, which affects the fabrication process. It would be interesting to implement a code capable of automatically determining an optimised grating profile with the period change variation remaining within a reasonable range, whilst providing a high quality spectrum response of the grating. Also it is useful to modify the existing program by including parameters, which are a part of the experimental system constrains (like a noise for example), and which play a significant role in the fabrication process of the gratings always affecting their quality.

Another interesting direction of research is the design of long period gratings (LPGs). LPGs are fibre grating devices in which the guided core mode is coupled to the forward propagating cladding modes through the periodic photo-induced index grating. During recent years LPGs have found important applications as gain-flattering filters, mode-converters, codirectional couplers and high-sensitivity sensors. There is a number of works devoted to the synthesis of long period gratings [104,105], including the layer peeling algorithm [106, 107]. It would be interesting to convert the existing program, which I use for designing fibre Bragg gratings, to the new one, suitable for the design and characterisation of long period gratings.

I believe that the proposed technique of fabrication composite filters using two FBGs operating in a transmission regime has a great technical and commercial potential. Using the technique proposed and developed in this thesis it is possible to overcome one of the key disadvantages of FBG-based devices additional loss introduced by optical circulators that are required to operate gratings in a reflection regime. I believe that the technique proposed in my thesis can form a background for a new generation of FBG-based devices.

References

[1] Agrawal G. P., *Nonlinear Fiber Optics*, 2nd ed., Academnic Press, San Diego, CA, 1995.

[2] R. J. Mears, L. Reekie, I. M. Janucey, and D. N. Payne, *"Low noise erbium-doped fibre amplifier operating at 1.54 μm"*, Electron. Lett., vol. **15**, pp.106, 1987.

[3] M.I. Hayee and A.E. Willner, *"NRZ vs. RZ in 10-40 Gb/s Dispersion-Managed WDM Transmission Systems,"* IEEE Photonics Technology Letters, vol. **11**, pp. 991-993, 1999.

[4] Lemaire J., Atkins R. M., Mizrahi V., and Reeed W. A., *"High pressure H2 loading as a technique for achieving ultrahigh UV photosensitivity and thermal sensitivity in GeO2 doped optical fibers,"* Electron. Lett., vol. **29**, pp.1191-1193, 1993.

[5] Hill K. O., Fujii Y., Johnson D. C. and Kawassaki B. S., *"Photosencitivity in optical waveguides: Application to reflection filter application,"* Appl. Phys. Lett., vol. **32** (10), pp. 647, 1978.

[6] Meltz G., Morey W. W., and Glenn W. H., *"Formation of Bragg gratings in optical fibres by transverse holographic method,"* Opt. Lett., vol. **14** (15), p. 823, 1989.

[7] Stubbe R., Sahlgren B., Sandgren S., and Asseh A., *"Photosensitivity and Quadratic Nonlinearity in Glass Waveguides (Fundamentals and Applications)"*, (Postdeadline papers, Portland, OR), p. PD1, 1995

[8] Asseh A., Storøy H., Sahlgren B. E., Sandgren S., and Stubbe R., *"A writing technique for long fiber Bragg gratings with complex reflectivity profiles,"* J. Lightwave Tech., vol. **15**, pp.1419-1423, 1997.

[9] Hill K. O. and Meltz G., *"Fiber Bragg Grating Technology: Fundamentals and Overview,"* J. Lightwave Technol., vol. **15**, pp. 1263-1276, 1997.

[10] Baumann I., Seifert J., Nowak W., and Sauer M., *"Compact all-fiber add-drop multiplexer using fiber Bragg gratings,"* IEEE Photon. Technol. Lett., vol. **8**, pp.1331-1333, 1996.

[11] Chen Y. K., Hu C. J., Lee C. C., Feng K. M., Lu M. K., Chang C. H., Tu Y. K., and Tzeng S. L., *"Low-Crosstalk and Compact Optical Add–Drop*

Multiplexer Using a Multiport Circulator and Fiber Bragg Gratings", J. Photon. Technol. Lett., vol. **12**, pp. 1394-1396, 2000.

[12] Ouellette F., *"Dispersion cancellation using linearly chirped Bragg grating filters in optical waveguides,"* Opt. Lett., vol. 12, pp.847-849, 1987.

[13] Williams J. A. R., Bennion I., and Doran N. J., *"Fiber dispersion compensation using a chirped in-fibre Bragg grating,"* Electron. Lett., vol. **30**, pp. 985-987, 1997.

[14] Miyagi M, and Nishida S., *"Pulse spreading in a single-mode fiber due to third-order dispersion,"* Appl. Opt., vol. **16**, pp. 678-682, 1979.

[15] Amemiya M., *"Pulse Broadening due to Higher Order Dispersion and its Transmission Limit,"* J. Lightwave Technol., vol. **20**, pp. 5910-597, 2002.

[16] Nuyt R. G., Park Y. K. and Gallion P., *"Dispersion equalization of a 10 Gb/s repeated transmission system using dispersion compensating fiber",* J. Lightwave Technol., vol. **15**, pp. 31-42, 1997.

[17] Agrawal G. P., *Lightwave Technology*, John Wiley & Sons, Hoboken, 2005.

[18] Kringlebotn J. T., Archambault J. L., Reekie L., and Payne D. N., *"Er^{3+}:Yb^{3+}- codoped fiber distributed-feedback laser,"* Opt. Lett., vol. **19**, pp. 2101-2103, 1994.

[19] Reekie, L., Mears, R.J., Poole, S.B., Payne, D.N.. *"Tunable single-mode fiber lasers"*, J. Lightwave Technol., vol. LT**4**, pp. 956-957, 1986.

[20] Ball, G. A., Morey, W. W., and Waters, J. P., *"Nd fiber laser utilizing intra-core Bragg reflectors"*, Electronics Letters, vol. **26**, pp.1829 -1830, 1990.

[21] Ball, G. A. and Glenn, W. H., *"Design of a single-mode linear cavity erbium fiber laser utilizing Bragg reflector"*, J. Lightwave Technol., vol.**10**, pp. 1338-1343, 1992.

[22] Kersey A. D., Davis M. A., Patrick H. J., LeBlanc M., Koo K. P., Askins C. G., Putnam M. A., and Friebele E. J., *"Fiber grating sensors,"* J. Lightwave Technol., vol. **15**, pp.1442-1463, 1997.

[23] Sipe J., Poladian L., and de Sterke C., *"Propagation through nonuniform grating structures,"* J. Opt. Soc. Am. A, vol. **11**, pp. 1307-1320, 1994.

[24] Erdogan T., *"Fiber grating spectra,"* J. Lightwave Technol., vol. **15**, pp. 1277-1294, 1997.

[25] Othonos A., and Kalli K., *Fiber Bragg Gratings,* (Artech House, London), 1999.

[26] Longhi S., Marano M., Laporta P., Svelto O., and Belmonte M., *"Propagation, manipulation, and control of picosecond optical pulses at 1.5 mm in fiber Bragg gratings",* JOSA B, vol. **19**, pp. 2742-2757, 2002

[27] Asseh A., Storoy H., Sahlgren B., and Stubbe R., *"A writing technique for long fiber Bragg gratings with complex reflectivity profiles,"* J. Lightwave Technol. **15**, 1419–1423 (1997).

[28] Ibsen M., Durkin M., Cole M., and Laming R., *"Sinc-sampled fiber Bragg gratings for identical multiple wavelength operation,"* IEEE Photon. Technol. Lett., vol. **10**, pp. 842-844, 1998.

[29] Ibsen M., Durkin M., Cole M., Zervas M., and Laming R., *Recent Advances in Long Dispersion Compensating Fibre Bragg Gratings* (Institution of Electrical Engineers, London, UK), 1999.

[30] Song G.-H., and Shin S.-Y., *"Design of corrugated waveguide filters by the Gel'fand–Levitan–Marchenko inverse scattering methods,"* J. Opt. Soc. Am. A, vol. **2**, pp. 1905-1915, 1985.

[31] Peral E., Capmany J., and Marti J., *"Iterative solution to the Gel'Fand–Levitan–Marchenko coupled equations and application to synthesis of fiber gratings,"* IEEE J. Quantum Electron., vol. **32**, pp. 2078-2084, 1996.

[32] Feced R., Zervas M., and Muriel M., *"An efficient inverse scattering algorithm for the design of nonuniform fiber Bragg gratings,"* IEEE J. Quantum Electron., vol. **35**, pp.1105-1115, 1999.

[33] Poladian L., *"Simple grating synthesis algorithm,"* Opt. Lett., vol. **25**, pp. 787–789, 2000.

[34] Skaar J., Wang L., and Erdogan T., *"On the synthesis of fiber Bragg gratings by layer peeling,"* IEEE J. Quantum Electron., vol. **37**, pp. 165-173, 2001.

[35] Bruckstein A. M., Levy B. C., and Kailath T, *"Differential methods in inverse scattering* algorithm for the design of nonuniform fibre Bragg gratings," IEEE J. Quantum. Electron, vol. **45**, pp. 312-335, 1995.

[36] Michielssen E., Ranjithan S., and Mittra R., *"Optimal multilayer design using real coded genetic algorithms,"* IEE Proc.-Optoelectronics, vol. **139**, pp. 413-420, 1992.

[37] Skaar J., and Risvik K. M., *"A genetic algorithm for the inverse problem in synthesis of fiber gratings,"* J. Lightwave Techn., vol. **16**, pp. 1928-1932, 1998.

[38] Cormier G., Boundreau R., and Thériault S., *"Real-coded genetic algorithm for Bragg grating parameter sythesis,"* J. Opt. Soc. Amer. A, vol. **18**, pp. 1771-1776, 2001

[39] Ibsen M., Feced R., Petropoulos P, and Zervas M., *"99.9% reflectivity dispersion-less square-filter fibre Bragg gratings for high speed DWDM networks,"* in OFC, OSA Technical Digest, vol. **4,** pp.230-232, 2000, paper PD21.

[40] Liu Y., Dong L., Pan J. J., and Gu C., *"Strong phase-controlled fiber Bragg gratings for dispersion compensation,"* Opt. Lett., vol. **28**, pp. 786-788, 2003.

[41] Durkin M. K., Feced R., Ramirez C., and Zervas M. N., *"Advanced fibre Bragg gratings for high performance dispersion compensation in DWDM systems,"* OFC, OSA Technical Digest, 2000, paper TuH4.

[42] Ibsen M., Petroupoulos P., Zervas M. N., and Feced R., *"Dispersion-free fibre Bragg gratings, "* OFC, OSA Technical digest, 2001, paper MC1.

[43] Ibsen M., and Feced R., *"Fibre Bragg gratings for pure dispersion-slope compensation,"* Opt. Lett. , vol. **28**, pp. 980-982, 2003.

[44] Petropoulos P., Ibsen M., Ellis A. D., and Richardson D. J., *"Rectangular pulse generation based on pulse shaping using a superstructured fiber Bragg grating,"* J. Lightwave Techn., vol. **19**, pp.746-752, 2001

[45] Longhi, S., Marano M., Laporta P., Belmonte M., and Crespi P., *"Experimental observation of superluminal pulse reflection in a double-Lorentzian photonic band gap,"* Phys. Rev. E, vol. **65**, 2002.

[46] Eggleton B., Krug P. A., Poladian L., and Oullette F., *"Long periodic superstructure Bragg gratings in optical fibres,"* Electron. Lett., vol. **30**, pp. 1620-1622, 1994.

[47] Ouellette F., Krug P. A., Stephens T., Dhosi G., and Eggleton B., *"Broadband and WDM dispersion compensation using chirped sampled fibre Bragg gratings,"* Electron. Lett., vol. **31**, pp. 899-901, 1995.

[48] Feng K.-M., Cai J.-X., Grubsky V., Starodubov D. S., Hayee M. I., Lee S., Jiang X., Willner A. E., and Feinberg J., *"Dynamic dispersion compensation in a 10-Gb/s optical system using a novel voltage tuned nonlinearly-chirped fiber Bragg grating,"* IEEE Photon. Technol. Lett., vol. **11**, pp. 373-375, 1999.

[49] Loh W. H., Zhou F. Q., and Pan J. J., *"Sampled fiber grating based-dispersion slope compensator,"* IEEE Photon. Technol. Lett., vol. **11**, pp. 1280-1282, 1999.

[50] Cai J.-X., Feng K.-M., Willner A. E., Grubsky V., Starodubov D. S.,and Feinberg J., *"Simultaneous tunable dispersion compensation of many WDM channels using a sampled nonlinear chirped fiber Bragg grating,"* IEEE Photon. Technol. Lett., vol. **11**, pp. 1455–1457, 1999.

[51] Painchaud Y., Mailoux A., Chotard H., Pelletier E., and Guy M., *"Multi-channel fiber Bragg gratings for dispersion and slope compensation,"* in *OFC*, vol. **70** of OSA Trends in Optics and Photonics Series (Optical Society of America, Washington, D.C., 2002), paper THAA5, 2002.

[52] Pan Z., Song Y. W., Yu C., Wang Y., Yu Q., Poplek J., Li H., Li Y., and Willner A. E., *"Tunable chromatic dispersion compensation in 40-Gb/s systems using nonlinearly chirped fiber Bragg gratings,"* J. Lightwave Technol., vol. **12**, pp.2239-2245, 2002.

[53] Song W., Motaghian Nezam S. M. R., Starodubov D., Rothenberg J. E., Pan X., Li H., Wilcox R., Poplek J., Caldwell R., Grubsky V., and Willner A. E., *"Tunable interchannel broadband dispersion-slope compensation for 10-Gb/s WDM systems using a nonchannelized third-order chirped FBG,"* IEEE Photon. Technol. Lett., vol. **15**, pp. 144-146, 2003.

[54] Shu X., Gwandu B. A. L., Liu Y., Zhang L., and Bennion I.,*"Sampled fiber Bragg grating for simultaneous refractive index and temperature measurement,"* Opt. Lett., vol. **26**, pp. 774-776, 2001.

[55] Li H., Kumagai T., Ogusu K., and Sheng Y. "*Advanced design of multuchannel fiber Bragg grating based on layer-peeling method*", JOSA B, vol. **21,** pp. 1929-1938, 2004.

[56] Kashyap R., *Fiber Bragg Gratings*, (San Diego, CA: Academic Press), 1999.

[57] Snyder A. W., and Love J. D., *Optical Waveguide Theory,* (Chapman & Hall), 1983.

[58] Kogelnik H., *"Filter response of nonuniform almost-periodic structures,"* Bell Sys. Tech. J., vol. **55**, pp. 109-126, 1976.

[59] Marcuse D., *Theory of Dielectric Optical Waveguides*, (New York: Academic), 1991.

[60] Poladian L., *"Resonance Mode Expansions and Exact Solutions for Nonuniform Gratings,"* Phys. Rev. E, **vol**. 54, pp. 2963-2975, 1996.

[61] J. Skaar, "Synthesis and characterization of fiber Bragg gratings", Ph. D Thesis, The Norwegian University of Science and Technology, (2000).

[62] Pierce J. R., *"Coupling of modes of propagation,"* J. Appl. Phys., vol. **25**, p. 179, 1954

[63] Yariv A., *"Coupled-mode theory for guided-wave optics,"* IEEE J. Quantum Electron., vol. **9,** pp. 919-933, 1973.

[64] Poladian L., *"Group delay reconstruction for fiber Bragg gratings in reflection and transmission,"* Opt. Lett., vol. **22,** pp.1571-1573, 1997.

[65] Brinkmeyer E., "*Simple algorithm for reconstructing fiber gratings from reflectometric data",* Opt.Lett., vol. **20,** pp.810–812, 1995.

[66] M. A. Muriel, J. Azana, A. Carballar, *"Fiber grating synthesis by use of time-frequency* representations*"*, Opt. Lett. , vol. **23**, pp. 1526-1528, 1998.

[67] Turitsyna E. G., Ania-Castanon J. D., Turitsyn S. K., Kennedy L., Sugden K., *"Impact of design of sharp non-uniform fibre Bragg gratings on system performance",* El. Letters, vol. **39**, p. 351-353, 2003.

[68] W.H. Loh, F.Q. Zhou and J.J. Pan, *"Sampled fiber grating based-dispersion slope compensator,"* IEEE Photon. Technol. Lett. vol.**11**, no.10, pp.1280-1282, 1999.

[69] Song W., Pan Z., Nezam S. M. R. M., Yu C., Wang Y., Starodubov D., Grubsky V., Rothenberg J. E., Popelek J., Li H., Li Y., Caldwell R., Wilcox R., and Willner A.E., *"Tunable dispersion slope compensation for 40-Gb/s*

WDM systems using broadband nonchannelized third-order chirped fiber Bragg gratings," J. Lightwave Tech., vol. **20**, 2259-2266, 2002.

[70] Shu X, Turitsyna E. G., Sugden K. and Bennion I., *"Tunable pure dispersion slope compensators realized with novel complex gratings"*, accepted for BGPP, Canada, June, 2007.

[71] Breuer D., Kueppers F., Mattheus A., Shapiro E. G., Gabitov I., and Turitsyn S. K. , *"Symmetrical dispersion compensation for standard monomode-fiber-based communication systems with large amplifier spacing"*, Optics Letters, vol. **22**, p.982-984, 1997.

[72] Shapiro E. G., Fedoruk, M. P., and Turitsyn S. K., *"Numerical estimate of BER in optical systems with strong patterning effects"*, Electron. Lett. vol. **37,** no. 19, p 1179-1181, 2001.

[73] Laedke E. W., Goder N., Schaefer T. Y., Spatschek K. H. and Turitsyn S. K, *Improvement of optical fibre sytems performance by optimisation of receiver filter bandwidth and use of numerical methods to evaluate Q-factor*, Electron. Lett. vol. **35,** no. 24 , pp. 2131-2133, 1999.

[74] Bigo S., and Frignac Y., "*5.12Tbit/s (128x40Gbit/s WDM) transmission over 3x100km of Teralight™ fiber ,"* in proc. ECOC 2000, Munich, paper PD1.2, 2000.

[75] Morita I., "*100% spectral-efficient 25x42.7Gbit/s transmission using asymmetrically filtered CS-RZ signal and a novel crosstalk suppression,"* in Proc. ECOC2002, Copenhagen, paper PD4.7, 2002

[76] Agata A., Morita I., Tsuritani T., and Edagawa N., *"Characteristics of asymmetrically filtered 40Gbit/s CS-RZ signals,"* in Proc. OFC 2003, paper MF787, 2003.

[77] Tsuritani T., Agata A., Morita I., and Edagawa N., *"Ultra-long haul 40Gbit/s-based DWDM transmission using optically prefiltered CS-RZ signals,"* IEEE J. Select. Top. Quantum Electron., vol. **10**, pp. 403-410, 2004.

[78] Yoshikane N., Morita I., Agata A., Tsuritani T., and Edagawa N., *"50GHz-spaced 55x42.7Gbit/s transmission over 2500km using a SPM-based all-optical reshaper,"* in proc. OAA 2002, paper PD6, 2002.

[79] B. Zhu, L. E. Nelson, S. Stulz, A. H. Gnauck, C. Doerr, J. Leuthold, L. Grüner-Nielsen, M. O. Pedersen, J. Kim, R. Lingle Jr., Y. Emori, Y. Ohki,

N. Tsukiji, A. Oguri, and S. Namiki, *"6.4-Tb/s (160 x 42.7 Gb/s) transmission with 0.8 bit/s/Hz spectral efficiency over 32 x 100 km of fiber using CSRZ-DPSK format,"* in OFC2003, Atlanta, GA, 2003, paper PD19.

[80] A. S. Lenihan, G. E. Tudury, W. Astar, and G. M. Carter, *"XPM-Induced Impairments in RZ-DPSK Transmission in a Multi-Modulation Format WDM System"*, Proceedings CLEO' 2005, CW05, 2005.

[81] Turitsyna E. G., Bhamber R., Mezentsev V. K., Gillooly A., Mitchell J., and Turitsyn S. K., *"Design of FBG-based ultra-narrow asymmetric filter for transmission wih 0.8 bit/s/Hz spectral efficiency without polarization multiplexing"*, Opt. Fiber Techn., vol. **11,** pp. 202-208, 2005.

[82] Lee J., Kim S., Kim Y., Oh Y. J., Hwang S. and Jeong J., *"Optically preamplified receiver performance due to VSB filtering for 40 Gb/s optical signals modulated with various formats," J. Lightwave Technology,* vol. **21**, pp. 521-528 , 2003.

[83] Morita I., Tsuritani T., and Edagawa N., *"Experimental study on optical band-limited 40 Gb/s RZ signals with optically time-devision demultiplexing receiver", J. Lightwave Technology,* vol. **20**, pp. 2182-2189, 2002.

[84] Turitsyna E. G., and Webb S., *"Simple design of FBG-based VSB filters for ultra-dense WDM transmission",* Electron. Lett., vol. **41**, pp.86-88, 2005.

[85] Yann Frignac, et al., *"Transmission of 256wavelength-division and polarization-division-multiplexed channels at 42.7Gb/s(10.2Tb/s capacity) over 3x100km of TeraLight fiber"*, OFC2002, PD FC5-1.

[86] Takehiro Tsuritani, et al., *"Study on optimum optical pre-filtering condition for highly spectral-efficient ultralong-haul transmission using 40Gbit/s CS-RZ signal and all-Raman repeaters"* OFC2003, FE4, pp660-662, vol.**2**, 2003.

[87] Yamada M., and Sakuda K., *"Analysis of almost-periodic distributed feedback slab waveguides via a fundamental matrix approach,"* Appl. Opt., vol. **26**, pp. 3474-3478, 1987.

[88] Lenz G., Eggleton B. J., Litchinitser N., and Eggleton B. J.," *Pulse compression using fiber gratings as highly dispersive nonlinear elements",* JOSA B , vol. **15**, pp. 715-721, 1998.

[89] Shu X., Sugden K., Bennion I., "*Optically tunable chromatic dispersion controller with coupled-cavity etalon structure",* Opt. Lett., vol. **30,** no. 12, 1440-1442, 2005.

[90] Favre F., Le Guen D., Moulinard M. L., Henry M., Michaud G., Devaux F., Legros E., Charbonnier B., and Georges T., *"Demonstration of soliton transmission at 20 Gbit/s over 2200 km of standard fibre with dispersion compensation and pre-chirping",* Electronics Lett., vol. **33**, pp. 511-512, 1997.

[91] Sano A., Miyamoto Y., Kuwahara S., and Toba H., *"A 40-Gb/s/ch WDM Transmission with SPM/XPM Suppression Through Prechirping and Dispersion Management,"* J. Lightwave Technol., vol. **18**, pp. 1519-1526, 2000.

[92] Cundiff S., Collins B., Boivin L., Nuss M., Bergman K., Knox W., and Evangelides S., *"Propagation of highly chirped pulses in fiber-optic communication systems",* J. Lightwave Technol., vol. **17**, pp. 811-816, 1999.

[93] Mollenauer L., Grant A., Liu X., Wei X., Xie C., Kang I., *"Experimental test of dense wavelength-division multiplexing using novel, periodic-group-delay-complemented dispersion compensation and dispersion-managed solitons "*, Opt. Lett., vol. **28,** pp. 2043-2045, 2003.

[94] Turitsyna E. G., Shu X., Bennion I, *"Design and Fabrication of Fibre Bragg Gratings with V-shaped Dispersion Profile for Multi-Channel Signal Processing",* accepted for European Conference of Optical Communications (ECOC), Th3.3.4 (Cannes, September 2006).

[95] G. P. Agraval, "Fiber-Optic Communication Systems", John Wiley & Sons Inc,Toronto, 1997.

[96] Jayaraman V., Durkin M. K., Cole M. J., and Laming R. I., *"Theory, design, and performance of extended tuning semiconductor lasers with sampled gratings,"* IEEE J. Quantum Electron., vol. **29**, pp. 1824-1834, 1993.

[97] Rothenberg J, E., Li H., Li Y., Popelek J., Wang Y., Wilcox R. B., and Zweiback J., *"Dammann fiber Bragg gratings and phase-only sampling for high channel counts, "* IEEE Photon. Technol. Lett., vol. **14**, pp. 1309-1311, 2002.

[98] Li H., Sheng Y., Li Y., and Rothenberg J. E., *"Phased-only sampled fiber Bragg g*ratings for high-channel-count chromatic dispersion compensation," J. Lightwave Technol., vol. **13**, pp. 2074-2083, 2003.

[99] Cai J.X., Feng K.-M., Willner A. E., Grubsky V., Starodubov D. S., and Feinberg J., *"Simultaneous tunable dispersion compensation of many WDM channels using a sampled nonlinear chirped fiber Bragg grating,"* IEEE Photon. Technol. Lett. , vol. **11**, pp.1455-1457, 1999.

[100] Shu X., Turitsyna E. G., and Bennion I., *"Novel broadband fiber Bragg grating with channelized dispersion,"* submitted to Optics Express, (May 2007).

[101] Loh W. H., Cole M. J., Zervas M. N., Barcelos S., and Laming R. I., *"Complex grating structures with uniform phase masks based on the moving fiber-exposurening beam technique,"* Opt. Lett. vol. **20**, pp. 2051–2053, 1995.

[102] Vasilyev M., and Lakoba T.I., *"All-optical multichannel 2R regeneration in a fiber-based device,"* Opt. Lett., vol. **30**, pp.1458-1460, 2005.

[103] Wei X., Liu X., Xie C., and Mollenauer, L. F., *"Reduction of collision-induced timing jitter in dense wavelength-division multiplexing by the use of periodic-group-delay dispersion compensators,"* Opt. Lett., vol. **28**, pp.983-985, 2003.

[104] Lee C. L., and Lai Y., *"Evolutionary Programming Synthesis of Optimal Long-Period Fiber Grating Filters for EDFA Gain Flattening,"* IEEE Photon. Technol. Lett., vol. **14**, pp. 1557-1559, 2002.

[105] Lee C. L., and Lai Y., *"Long-Period Fiber Grating Filter Synthesis Using Evolutionary Programming,"* Fiber and Integrated Optics, vol. **24**, pp. 249-261, 2004

[106] Wang L., and Erdogan T., *"Layer peeling algorithm for reconstruction of long-period fibre gratings,"* Electron. Lett., vol. **37**, 2001.

[107] Brenne J. K., and Skaar J., *"Design of Grating-Assisted Codirectional Couplers with Discrete Inverse-Scattering Algorithms,"* J. Lightwave Technol., vol. **21**, pp. 254-263, 2003.

Appendix

A1 Publications

Journal articles

1. X. Shu, E. G. Turitsyna, and I. Bennion, *"Novel broadband fiber Bragg grating with channelized dispersion,"* submitted to Optics Express, (May 2007).
2. E. G. Turitsyna, X. Shu, S. K. Turitsyn, I. Bennion, *"Design and Fabrication of FBGs with V-shaped Dispersion Profile",* J. Lightwave Technol., vol. 25 (2), pp. 606-611, 2007
3. E.G.Turitsyna, S. Webb, V. Mezentsev, S.K. Turitsyn, *"Novel Design of FBG-Based Composite Double Notch VSB Filter for DWDM Systems"*, J. Lightwave Technol., vol. **24** (9), pp.3547-3552, 2006
4. E. G. Turitsyna, R. Bhamber, V. K. Mezentsev, A. Gillooly, J. Mitchell, S. K. Turitsyn, *"Design of FBG-based ultra-narrow asymmetric filter for transmission wih 0.8 bit/s/Hz spectral efficiency without polarization multiplexing"*, Opt. Fiber Techn., vol. 11, p.202-208, 2005.
5. E. G. Turitsyna, S. Webb, *"Simple design of FBG-based VSB filters for ultra-dense WDM transmission",* El. Letters, vol. **41**(2), p.89-91, 2005.
6. E. G. Turitsyna, J. D. Ania-Castanon, S. K. Turitsyn, L. Kennedy, K. Sugden, *"Impact of design of sharp non-uniform fibre Bragg gratings on system performance",* El. Letters, vol. **39** (4), p. 351-353, 2003
7. S. K. Turitsyn, M. P. Fedoruk, V. K. Mezentsev, E. G. Turitsyna, *"Theory of optimal power budget in quasi-linear dispersion-managed fibre links",* El. Letters, vol. **39**, p. 29-30, 2003.
8. S. B. Medvedev, E. G. Shapiro, M. P. Fedoruk, E. G. Turitsyna, "*The theory of optical communication lines with a short-scale dispersion management",* JETF, vol. **94** (5), (2002), p.892-900.
9. S. K. Turitsyn, M. P. Fedoruk, E. G. Shapiro, V. K. Mezentsev, E. G. Turitsyna, "*Novel approaches to numerical modeling of periodic*

dispersion-managed fiber communication systems", JSQE, IEEE Journal Quantum Electron., vol. **6** (2), (2000) p. 263-268.

10. S. K. Turitsyn, M. P. Fedoruk, S. Medvedev, E. G. Turitsyna, *"Averaged model and integrable limits in nonlinear double-periodic Hamiltonian systems*", Phys. Rev. E, vol. **61** (3), (2000), p. 3127-3134..
11. N. F. Smyth, S. K. Turitsyn, E. G. Turitsyna, *"Solitary waves in nonlinear dispersive systems with zero average dispersion"*, Phys. Rev. E, vol. **58** (1) July 1 (1998), 44R.

Conference proceedings

C1. X. Shu, E. G. Turitsyna, I Bennion, "*Single-Reflection-Band Fiber Bragg Gratings with Channelized Linear and Nonlinear Dispersion and Their Applications",* Proceedings of Optical Fiber Communication Conference (OFC/NFOEC' 2007), JThA17, (Anaheim, USA, March 2007).

C2. E. G. Turitsyna, X. Shu, I Bennion, ***"Design and Fabrication of Fibre Bragg Gratings with V-shaped Dispersion Profile for Multi-Channel Signal Processing",*** Proceedings of European Conference of Optical Communications (ECOC), Th3.3.4 (Cannes, September 2006).

C3. E. G. Turitsyna, S. K. Turitsyn, *"Two examples of fibre Bragg gratings designed for optical pulse manipulation and processing*", Proceedings of Conference on Lasers and Electro-Optics Europe (CLEO/Europe-EQEC 2005), Munich, Germany, pp. CI-5-TUE (June 2005).

C4. E. G. Turitsyna, S. Webb, *"Design of ultra-narrow WDM filters using the transmission response function of fiber Bragg gratings",* Proceedings of Conference on Lasers and Electro-Optics Europe (CLEO/Europe-EQEC 2005), Munich, Germany, pp. CF-21-TUE (June 2005).

C5. E. G. Turitsyna, R. Bhamber, V. K. Mezentsev, A. Gillooly, J. Mitchell, and S. K. Turitsyn, "*Ultra-Narrow Asymmetric Filter for Transmission with 0.8 bit/s/Hz Spectral Efficiency"* , Conference on Lasers and Electro-Optics (CLEO 2005), Baltimore, USA, JThE54, (May 2005).

C6. E. G. Turitsyna, J. D. Ania-Castanon, S. K. Turitsyn, L. Kennedy, K. Sugden, *"Simple design of non-uniform fiber Bragg grating with sharp*

reflection", CLEO Europe '2003, CJ1-2-MON , Munich, Germany (Jun 2003).

C7. S. K. Turitsyn, M. P. Fedoruk, V. K. Mezentsev, E. G. Turitsyna, "*Optimal power budget in quasi-linear dispersion-managed fiber links",* Proc. of IEEE/LEOS '2002, (Glasgow, UK), 2, (2002), p. 701-702.

C8. S. K. Turitsyn, M. P. Fedoruk, E. G. Turitsyna, "*Path-average theory of intra-channel four-wave mixing*", Conference of Lasers and Electro-Optics, Technical Digest, CLEO'2000, (San Francisco, California USA), CMF1, p.27.

C9. S. K. Turitsyn, N. J. Doran, E. G. Turitsyna, E. G. Shapiro, M. P. Fedoruk, "*Soliton interaction in optical communication systems, with short-scale dispersion management*", Technical Digest CLEO'2000, (San Francisco, California USA), CMF5, (2000), p.30-31.

C10. S K Turitsyn, M P Fedoruk, E G Shapiro, N J Doran, E G Turitsyna, *"Dispersion-managed transmission systems with short-scale dispersion management"*, in "Massive WDM and TDM Soliton Transmission Systems", Kluwer Academic Publishers, Dordrecht, The Netherlands, (2000), pp. 235-251.

C11. N. J. Doran, M. P. Fedoruk, S. K. Turitsyn, E. G. Shapiro, E. G. Turitsyna, *"Dispersion-managed transmission systems with short-scale dispersion management"*, in Proc. of III International Symposium on Physics and Applications of Optical Solitons in Fibers, Kyoto, (1999), edited by M. Shinomiya and A. Hasegawa.

C12. S. K. Turitsyn, V. K. Mezentsev, E. G. Turitsyna, "*Nonlinear mapping and path-averaged theory of dispersion-managed fiber communication systems",* Technical digest, Quantum Electronics and Photonics Conference, (Manchester, 1999, Institute of Physics), P 2-38, p. 217.

A2 List of programmes

C++ programs

- "Direct" program based of the transfer matrix method to solve coupled-mode equation using data of the modelled grating.
- "Inverse" (synthesis) program based on the discrete layer peeling algorithm for finding the coupling coefficient of the grating using the desired reflection function.
- Program that reads data containing grating reflection function and converts data to a form of complete grating response: reflection, transmission, group delay and dispersion.
- Programs for preparing data of reflection function for the "direct program".
- Programs ReadFilter.cc and ReadFilter.h as additional modules for GNLS code (Aston code for optical transmission lines numerical simulation).
- Modification of the "inverse" program for multi-channel gratings with "zigzag" dispersion profile.

MATLAB and Perl scripts:

- Numerous scripts for reading data from files and for plotting the corresponding graphs.
- Scripts for optimisation tasks using different set of parameters selected for optimisation.
- Scripts, that read data from files saved during the optimisation processes, sort them and save in the form convenient to work with or to plot.